Dynamics and Control of a Spacecraft-Mounted Robot Capturing a Spinning Satellite

by

Gilbert J. Jaar

Department of Mechanical Engineering

McGill University, Montréal

May 1993

This thesis was submitted to the Faculty of Graduate Studies and Research in partial fulfilment of the requirements for the Master of Engineering degree.

©Gilbert Jaar, 1993.

Dynamics of a Spacecraft-Mounted Robot Capturing a Satellite.

To my parents Jacob and Liliane.

Abstract

Issues associated with dynamical modelling and control of a spacecraft-mounted robotic manipulator capturing a spinning satellite are investigated in this research. The formulation of the post-capture dynamical equations of the system was carried out by writing the individual Lagrange's equation for the mother spacecraft, the two-link robotic manipulator, and the captured payload. These equations were then assembled to obtain the constrained dynamical equations of the system as a whole. This method, however, introduces the non-working constraint forces and moments which substantially complicate the dynamical analysis and therefore have to be eliminated. A novel technique that involves the use of the *natural orthogonal complement* of the velocity-constraint matrix was used in order to obtain a set of unconstrained independent equations. A computer code was written using FORTRAN and the IMSL subroutine DIVPAG was used to integrate the equations of motion. The pitch angle of the mother spacecraft, the joint angles of the manipulator, and their rates just after capture were calculated by solving the inverse kinematics problem and using impact dynamics principles. These were then used as initial conditions for the post-capture dynamics. A dynamical simulation of the system for the uncontrolled case was carried out to study the effect of the disturbance, resulting from the capture of the satellite, on the spacecraft/manipulator system. In light of the results corresponding to the uncontrolled system, a control algorithm, whose objective is to produce a set of feedback-linearized, homogeneous, and uncoupled equations, was designed and implemented. The effect of structural flexibility in the robot links on the response of the system was also investigated for both the uncontrolled and controlled cases.

Résumé

La présente recherche a trait aux problèmes que posent la modélisation et le contrôle d'un robot manipulateur, porté par un véhicule spatial, utilisé pour la saisie d'un satellite en rotation. La formulation des équations dynamiques du système après la saisie a été effectuée en établissant séparément les équations de Lagrange correspondant au véhicule porteur, au robot manipulateur à deux éléments articulés et à la charge payante. Ces équations ont été, par la suite, assemblées afin d'obtenir les équations dynamiques de contrainte du système dans son ensemble. Cette méthode introduit des forces et des moments de contrainte passifs qui compliquent considérablement l'analyse dynamique, raison pour laquelle elles ont été éliminées. Une nouvelle technique, qui consiste à appliquer le *complément orthogonal naturel* de la matrice vitesse-contrainte, a été utilisée afin d'obtenir une série d'équations indépendantes non contraintes. Un code informatique a été élaboré avec FORTRAN et le sous-programme DIVPAG d'IMSL afin d'intégrer les équations de mouvement. L'angle de tangage du véhicule porteur, les angles d'articulation du manipulateur et leur régime immédiatement à la suite de la saisie ont été calculés après avoir résolu le problème de cinématique inverse et appliqué des principes de la dynamique des chocs. Ces données ont été retenues à titre de conditions initiales pour la dynamique applicable après la saisie. La simulation par ordinateur du système hors-contrôle a permis d'évaluer l'effet de la saisie du satellite sur le système véhicule spatial/manipulateur. Vu les résultats non contrôlés obtenus, un algorithme de contrôle a été conçu et adopté en vue d'obtenir une série d'équations rétrolinéaires, homogènes et découplées. L'effet de la flexibilité structurelle des articulations du robot sur la performance du système a également été examiné dans les cas tant non-contrôlés que contrôlés.

Acknowledgements

I would like to thank my research supervisor Professor A. K. Misra from the department of mechanical engineering at McGill University for his invaluable assistance and continued guidance throughout the Master's program. Working in conjunction with him was a very enriching experience. Special thanks to Dr. Xavier Cyril from CAE Electronics Ltd. for his support and enthusiasm throughout the duration of the thesis. Also, I would like to thank Victor Jaar for translating the abstract into French.

I would like to express my gratitude to the Institute of Robotic and Intelligent Systems Network (IRIS) and the National Sciences and Engineering Research Council of Canada (NSERC) for providing the necessary funding for this research.

Contents

List of Figures

List of Tables

Nomenclature

All bold-face, lower-case, Latin and Greek letters used in this thesis denote vectors; all bold-face, upper-case, Latin and Greek letters denote matrices; and all calligraphic letters denote points. The term *extended* refers to quantities associated with each body; the term *generalized* refers to those quantities associated with the overall system.

A_i : cross sectional area of link i.

$\mathbf{b}_i$: generalized coordinates associated with the bending of link i.

$\mathbf{B}_i$: shape functions associated with the bending of link i.

$\mathcal{C}_s$: spacecraft's centre of mass.

$\mathcal{C}_p$: payload's centre of mass.

E_i : modulus of elasticity of body i.

$\mathbf{f}$: generalized external forces of the system.

G_i : shear modulus for body i.

I_i : area moment of inertia of body i.

$\mathbf{I}_{Hi}$: inertia tensor corresponding to the hub of body i.

K_i : shear constant of body i.

M_i : concentrated mass at the tip of link i.

$\mathbf{M}_i$: extended mass matrix of body i.

$\mathbf{M}$: generalized extended mass matrix of the system.

$\mathcal{N}$: natural orthogonal complement.

$\mathbf{p}_i$: position vector of a point $\mathcal{P}$ on body i measured from the origin of (X_O, Y_O, Z_O) .

$\tilde{\mathbf{p}}_i$: position vector of the origin of (X_i, Y_i, Z_i) as measured from the origin of (X_O, Y_O, Z_O) .

$\mathbf{p}_{c_i}$: position vector of the centre of mass of body i as measured from the origin of (X_O, Y_O, Z_O) .

$\mathbf{q}_i$: extended position vector of body i.

$\hat{\mathbf{q}}_i$: quaternion formed by either the Euler parameters or the linear invariants.

$\mathbf{Q}_i$: tensor defining the orientation of (X_i, Y_i, Z_i) coordinate frame with respect to (X_O, Y_O, Z_O) .

$\mathbf{r}_i$: position vector of a point $\mathcal{P}$ on body i measured from the origin of (X_i, Y_i, Z_i) .

$\mathbf{R}_i$: tensor defining the orientation of (X_i, Y_i, Z_i) coordinate frame with respect to $(X_{i-1}, Y_{i-1}, Z_{i-1})$.

T_i : kinetic energy of link i.

U_i : potential energy of body i.

$\mathbf{U}_i$: cross product tensor of $\boldsymbol{\mu}_i$.

$\mathbf{v}_i$: position vector of a point $\mathcal{P}$ on body i measured from the origin of (X_O, Y_O, Z_O) .

$\tilde{\mathbf{v}}_i$: velocity vector of the origin of (X_i, Y_i, Z_i) as measured from the origin of (X_O, Y_O, Z_O).

$\mathbf{v}_{c_i}$: velocity vector of the centre of mass of body i as measured from the origin of (X_O, Y_O, Z_O).

$\mathbf{w}_i$: extended velocity vector of body i.

X_i : axis perpendicular to Z_i and Z_{i+1}, and directed from the former to the latter.

X_O : axis along the local vertical.

$\mathbf{x}_i$: unit vector along X_i.

$\mathbf{X}_i$: cross product tensor of $\mathbf{x}_i$.

x_i : x-coordinate of a point on the X_i axis.

Y_i : axis perpendicular to X_i and Z_i.

Y_O : axis along the flight direction.

$\mathbf{y}_i$: unit vector along Y_i.

y_i : y-coordinate of a point on the Y_i axis.

Z_i : axis oriented along the axis of rotation of joint i.

Z_O : axis along the orbit normal.

$\mathbf{z}_i$: unit vector along Z_i.

z_i : z-coordinate of a point on the Z_i axis.

α : angular rotation about the positive Z_O direction (pitch).

β : angular rotation about the positive X_O direction (yaw).

γ : angular rotation about the positive Y_O direction (roll).

δ_i : total angular rotation vector of link i about the X_i, Y_i, and Z_i axes due to both bending and shear.

η_i : angular rotation vector of link i about the X_i, Y_i, and Z_i axes due to shear.

θ_i : joint rotation of body i due to the actuator measured along the positive direction of Z_i axis.

κ_i : radius of gyration of body i's cross-section.

μ_i : deflection of link i due to bending, shear, and centrifugal stiffening.

ξ_i : angular rotation vector of link i about the X_i, Y_i, and Z_i axes due to bending.

ρ_i : mass per unit length of body i.

τ_i : applied joint torque to body i.

ϕ_{ij} : shape function of link i corresponding to the jth mode of the flexibility model.

ϕ_i^C : extended constraint forces and moments associated with body i.

ϕ_i^E : extended external forces associated with body i.

ϕ_i^S : extended system forces associated with body i.

ψ_i : generalized coordinates of body i.

ψ : generalized coordinates of the system.

ω_i : angular velocity of (X_i, Y_i, Z_i) with respect to (X_O, Y_O, Z_O).

Ω : angular velocity of the orbital frame.

$\mathbf{1}_{nn}$: nxn identity tensor.

$\otimes$: denotes the tensor product of two vectors.

Chapter 1

Introduction

1.1 Space Robots

In recent years there has been an increasing interest in space as a new application field of robotics. Space robots are expected to play an increasingly significant role in future space operations. They will be used for the assembly and fabrication of space structures required for the construction of the proposed Space Station and a multitude of other tasks in space.

Extensive research is currently being conducted to further improve and develop new technologies in the area of space robotics. The objective is to minimize the need for astronaut Extra Vehicular Activity (EVA), which would greatly reduce both mission costs and hazards to the astronauts involved.

Space robotic systems are typically comprised of one or two cooperating robot manipulators and can either be mounted on a free-flying spacecraft such as the space Shuttle or on a Space Station's platform. The Canadian Remote Manipulator System better known as CANADARM shown in Figure 1.1, is frequently used in conjunction with the Space Shuttle, and represents the only operational space manipulator system

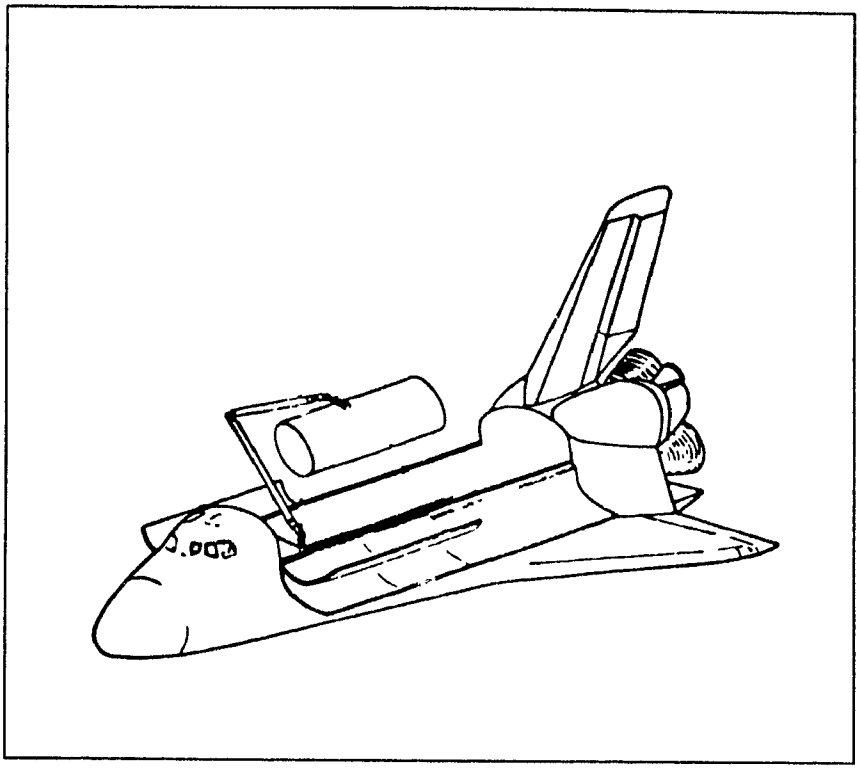

Figure 1.1: Schematic of CANADARM mounted on the Space Shuttle

available. Other advanced space manipulators currently being developed are the European Hermes Robot Arm (HERA) and the Japanese Experiment Module Remote Manipulator System (JEMRMS) as outlined by van Woerkom and de Boer (1992).

A more advanced version of CANADARM is the projected Mobile Servicing System (MSS) which is currently being designed to be the Canadian contribution to the international Space Station, Freedom, whose construction is scheduled to commence in 1995. The Space Station project is the largest of its kind and is designed to be a permanent inhabited orbiting laboratory, where observations of Earth and space will be done and experiments, which can only be performed in a microgravity environment, will be conducted. The proposed MSS is projected to include a large manipulator arm which will be known as the Space Station Remote Manipulator System (SSRMS), a smaller, two-armed, dexterous robot known as the Special Purpose

Dextrous Manipulator (SPDM), as well as sensors, controls, artificial intelligence and other technologies which make up the fully integrated system.

Due to the microgravity environment in space, space robots are able to manipulate a payload whose mass is substantial compared to the mass of the spacecraft on which the manipulator is mounted. For example, the CANADARM which has a mass less than 480 kilogram is rated to manipulate payload masses of up to 30,000 kilogram in space. However, it cannot lift its own weight on Earth. The proposed more advanced SSRMS will be able to lift more than 100,000 kilograms in space, manipulating even the Space Shuttle itself when it berths at the orbiting station and could still handle valuable small loads with care and high precision.

1.2 Dynamics

Space robots have different kinematic and dynamic features than their counterparts on Earth and consequently the dynamical analysis is far more complex. One major characteristic of space robots, which distinguishes them from ground-fixed ones, is the lack of a fixed base in a space environment. That signifies that the modelling techniques used for Earth robots have to be modified in order to account for the moving platform on which the robot is mounted.

1.2.1 Rigid Robots

The lack of a fixed-base for space robots causes the internal dynamics, i.e., the dynamic coupling between the system's components, to become quite significant and must be properly accounted for in order to achieve some favourable results. In a space environment, the commanded motion of the robot manipulator set to per-

form a specific task produces reaction forces and reaction moments on the Shuttle (platform) through the robot's base. These induced forces and moments produce a translation of the centre of mass of the platform and a rotation about its centre of mass. As a result of those same forces and moments, the robot joint angles that would normally be commanded to produce a prescribed robot end-effector position and orientation will cause the end-effector to miss the target. Thus, the tip positioning of the manipulator will affect the motion and control of the platform. Likewise, the motion of the platform will affect the manipulator control. Such interactions have been recently investigated by several researchers such as Umetani and Yoshida (1989a). These movements, which could be large depending on the relative masses of the system's components, are undesirable since they may involve a large end-effector motion and an attitude drift of the spacecraft. It was found by Vafa and Dubowsky (1990) that the manipulator's workspace will be reduced as well.

1.2.2 Flexible Robots

There is a large number of literature available on flexible manipulators. However, only those considered to be most relevant to this work will be cited in the following sections.

1.2.2.1 Link Flexibility

One of the major problems facing ground-based industrial robots is their excessive weight. Heavy links require large actuators to move them which will in turn consume more power. As a result both the manipulated payload capacity and the speed of operation will be adversely affected. Also, the transportation of heavy robots from one location to another would be more difficult and very costly.

In a space environment, the excess in weight becomes critical and space robots should be designed as light as possible in order to cut down on the costs of launching them into space. This could be achieved by using aluminum alloys and composite materials to construct the robot's links. This would result in lightweight links that are strong in compression, but relatively weaker than industrial robots in bending. Space robots are also designed to be very long and slender in order to improve the efficiency, enlarge the workspace, and extend the reach. However, the large spatial dimensions and the large manipulated payload associated with space robots make the flexibility, which results in substantial structural vibrations, an issue of concern even if the manipulator is operating at a low speed.

The structural flexibility inherent in such manipulators introduces a noticeable and undesirable modification of the traditional rigid-body manipulator dynamics. This is a result of the strong coupling between the non-linear *rigid* body motions and the linear elastic displacements of the links during the manipulator's motion. Flexibility of the robot links has been a topic of investigation in the robotics field since the 1970's, by such researchers such as Gevarter (1970) and Hughes (1979). It was found that its effect becomes significant when manipulating large payloads, and/or operating at high speeds and neglecting flexibility will result in gross inaccuracies in the positioning of the end-effector. Consequently, the induced vibrations resulting from the flexibility could be so substantial that they might tumble the spacecraft on which the manipulator is mounted, as suggested by Longman (1990a). The incorporation of structural flexibility of the links in the dynamical model poses a challenge to researchers. Therefore, many researchers have simply ignored the flexibility of the robot's links entirely and treated the system as *rigid*. However, this will lead to a substantial deterioration in tracking accuracy, especially as the flexibility becomes more

significant. Other researchers such as Baruh and Tadikonda (1987) treated the flexibility effect as a deterministic disturbance on the *rigid* body motion. Consequently, the *flexible* motion could be treated similarly to the way gravitational, Coriolis, and centrifugal effects are treated.

1.2.2.2 Joint flexibility

Another equally important concern is the flexibility in the joints of the manipulator. As far as the overall dynamical stability of the system, recent studies, such as those done by Chiou and Shahimpoor (1984), have shown that the joint flexibility has a similar contribution as the link flexibility. The inclusion of the flexibility in both the joints and links in the model complicates the dynamical equations of motion substantially. Therefore, very few researchers have addressed the effect of including both flexibilities on the behaviour of the system. It was found by Yang and Donath (1988) that the inclusion of both joint and link flexibility cuts down on the total deflections, but increases the oscillatory behaviour of the links. They have shown that both the flexibility in the joints and the links, are sources of trajectory tracking errors and undesirable oscillations of the end effector.

1.2.3 Flexible Payload and Platform

Some researchers have investigated the possibility of either having a flexible platform or a flexible payload. Chan and Modi (1991) concluded that the vibrational response of the *flexible* platform is substantially affected by the location of the manipulator and the time history of the slewing manoeuvres, which, in turn, could have a significant influence on the microgravity environment at the Space Station. Flexibility of the payload was also addressed by Carton and Chrétien (1989) where they have considered

payloads with *flexible* appendages.

1.2.4 Cooperating Robots

The dynamics associated with two cooperating robots have been addressed by a few researchers. Murphy et al. (1991) simulated the dynamics of two cooperating robots mounted on a moving platform which forms a closed kinematic chain. They have concluded that the equations of motion are identical in structure to the fixed-platform cooperative manipulator dynamics. A good example of cooperating robots is the proposed SPDM discussed earlier which will be equipped with two manipulator arms, each two metres long. The two arms are designed to cooperate in performing delicate tasks such as replacing components and working on the Space Stations's electrical connections.

1.3 Control Schemes

Control of space manipulators has been investigated by many researchers, but most of them assumed that the manipulator's base is stationary, i.e., the conventional control schemes for ground-fixed manipulators could be directly implemented. However, if the translation and rotation of the platform is to be considered, then a modified scheme that estimates the platform's position and attitude has to be designed and implemented in order to achieve effective control. With the above-mentioned condition and by avoiding singularities, Papadopoulos (1991) suggests that nearly any control algorithm that can be used for fixed-based manipulators can also be implemented to free-floating space robots.

1.3.1 Control of the Spacecraft

Several schemes for the control of the mother spacecraft have been proposed and can be classified in three major categories. In the *first* category, reaction wheels and/or jet thrusters, as suggested by Dubowsky et al. (1989), are used to control the spacecraft's *attitude* and *position* by compensating for the forces and moments exerted on the robot base (spacecraft) as a result of its motion. However, reaction jets may consume large amounts of expensive attitude control fuel and hence limiting the useful life of the system (Torres and Dubowsky, 1991). On the other hand, thanks to the inertially-fixed base, a solution to the relatively simple inverse kinematics problem is only needed and control laws designed for Earth robots could be directly implemented to systems in this category. The *second* category addressed by Longman et al. (1987) proposes an active attitude control system (ACS) that maintains the spacecraft's *attitude* relative to its orbital frame, which is achieved by applying appropriate corrective torques. The spacecraft's centre of mass however, is still free to translate in response to the force disturbances of the robot and its payload. The control of these systems is considerably more complicated than those of the first category. However, the control could be simplified by using a technique called the virtual manipulator (VM) developed by Vafa and Dubowsky (1990). The *third* category, which involves free-flying spacecraft, has been proposed in order to conserve expensive fuel and to avoid possible collision of the robot's end-effector with the payload about to be captured. However, since the Attitude Control System is off for systems in this category, this mode is only feasible when no external forces and torques affect the system and when its total angular momentum is negligible (Papadopoulos 1991). The control of such systems is the most complicated of all the aforementioned categories due to the fact that the platform is floating and therefore the inverse kinetics rather than

kinematics problem has to be reckoned with. Longman (1990b) introduced a method that obtains one feasible solution among an infinite number of solutions to the inverse kinetics problem. The virtual manipulator (VM) method, which only applies to rigid manipulators, could be used as well in order to generate a more practical numerical approach to solving the inverse kinetics problem. Umetani and Yoshida (1989b) introduced the Generalized Jacobian matrix (GJM) concept and suggested that its use will enable the implementation of the conventional control method for ground-fixed manipulators to space robots.

1.3.2 Position Control of the End-Effector

The control of space manipulator systems is complicated by the non-linear nature of its equations of motion. In the absence of vibrations of the manipulator's links due to structural flexibility, i.e., when the system could be treated as *rigid*, satisfactory accuracy of the end-effector positioning could be achieved. However, in the case of a *flexible* system the control is further complicated by the strong coupling between the *rigid* and *flexible* degrees of freedom. Therefore, accuracy in the positioning of the end-effector of the *flexible* manipulator and the avoidance of its oscillations due the structural flexibility pose a big challenge to the control designer.

The complexity of the control scheme used for the positioning of the robot's end-effector is highly dependent on whether the spacecraft control system is turned on or off. In the case when it is off, it was shown by Lindberg et al. (1990) that the position of the robot end-effector is no longer just a function of the present robot joint angles, but rather a function of the whole history of the joint angles. On the other hand, in situations where the ACS is on, the end-effector position is purely a function of the final robot joint rates.

In the case of a single link robot manipulator the control could be simplified by treating the *flexible* manipulator as a linear system. Cannon and Schnitz (1984) used a series of feedback control schemes with sophisticated sensor systems. Sakawa et al. (1985) presented another closed-loop control algorithm based on a detailed analytical model of the link and an alternative sensor system.

In a multi-link case however, neglecting the nonlinear terms may lead to substantial errors in the response of the system. Many researchers have used feedback-linearization techniques in order to control such systems and achieve an accurate end-effector position. Baruh and Tadikonda (1987) treat the flexibility effects as a deterministic disturbance and implement the feedback-linearization control law by means of spatially distributed sensors that measure the elastic motion. Bayo (1988) developed a procedure to calculate the torques required to move the end-effector of a multi-link robot through a specified trajectory while avoiding tip oscillations.

Experimental studies are also being conducted to study the effects of flexibility on the positioning of the end-effector using *Radius* (Buchan et al. 1989). Carusone and D'Eleuterio (1991) have shown that the implementation of a trajectory tracking controller is vastly superior to a **PID** controller; the manipulator end-point followed the desired path more closely without any large oscillations.

1.4 Payload Capturing

There is very little work done on the collision and capture dynamics of a robot manipulator. Umetani and Yoshida (1989b) through experimental studies have shown that a spacecraft-mounted manipulator is capable of properly chasing and capturing both a standing and a moving target (satellite). This is in spite of the complex space-

craft/manipulator dynamical interactions. Yoshida et al. (1992) used the Extended Generalized Inertia tensor (Ex-GIT) and the virtual mass concepts to formulate the collision problem by focusing on the velocity relationship just before and after the collision without an actual sensing of the impact force, but considering the momentum conservation law. However, they have not presented any simulation results that reveal the effects of impact on the system. Chapnik and Heppler (1991) have studied the effect of impact on a single link *flexible* manipulator and concluded that the deflection of the beam after impact is very small and could be ignored, however the deflection rate is significant and cannot be neglected.

Capturing a payload in space is a complicated procedure because dynamics and control issues of the different phases that constitute this particular task have to be dealt with. The phases could be summed up as follows:

1) *Chase* and *approach* of the target which involve the application of appropriate joint torques that will lead to the desired approach trajectory.

2) *Impact* between the payload and the robot's end effector. This phase is highly sensitive to the initial conditions of the payload and the configuration of the spacecraft/manipulator system just before impact.

3) *Grasp* of the payload by the manipulator's end effector.

4) *Suppression* of any residual motion of the payload by applying appropriate joint torques.

1.5 Objective and Motivation

The primary objective of this research is to develop a methodology for the formulation of the dynamical equations of motion of a spacecraft/manipulator system capturing a satellite and to study the impact dynamics. A simulation of the post-capture dynamics will be carried out in order to evaluate the effect of such a task on the system's various degrees of freedom, i.e., spacecraft attitude, joint angles, and the orientation and position of the captured payload, and their rates. Of great interest in the proposed research is to evaluate the effect of the inertial properties (mass and inertia) and the pre-capture dynamical properties (initial velocity and spin rate) of the impacting body on the post-impact behaviour of the system. Hence, cases involving both smooth and hard impacts resulting from the berthing of the spacecraft/manipulator system and the payload will be investigated. Structural flexibility in the robot's links is of great concern as well, and an appropriate modelling technique has to be implemented. Control of the system just after impact is also of importance. The objective of a control scheme is to suppress any residual motion of the payload and maintain stability of the system's components, i.e., the spacecraft, robot manipulator, and payload.

The motivation behind this research is the lack of analyses that address the effect of an impacting body on the behaviour of the spacecraft/manipulator system. Most of the previous research conducted in the area of robot manipulators mounted on a free-flying spacecraft investigated the effect of the dynamic coupling between a robot and its base on the positioning of the end-effector as it performs a certain task. A very small number of researchers actually investigated the effects of capturing a satellite and those who did were only concerned with the approach dynamics associated with capturing a payload; collision was briefly considered by Yoshida et al. (1992), but the post-impact dynamics was not simulated.

1.6 Thesis Organization

In **Chapter 2**, the research problem is clearly stated and a schematic of the spacecraft/manipulator system under study is presented. The generalized coordinates of the system are defined and the extended position and velocity vectors are introduced. Definitions of rotation matrices and recursive relations of the joint position vector and the angular velocity and their rates are also derived. **Chapter 3** starts with expressions for the kinetic and potential energies for each one of the individual bodies constituting the system. Next, the *individual* equations of motion are derived using the Lagrangian formulation. The unconstrained equations of motion of the system are then derived using the *Natural Orthogonal Complement*, whose objective is to cancel the non-working constraint forces. In **Chapter 4** the collision dynamics resulting from the capture of a payload by the spacecraft-mounted manipulator is derived, and a methodology to determine the post-capture numerical values of the generalized velocities is outlined. In **Chapter 5** various control schemes used for space manipulators are briefly introduced. The control method used in the thesis for both the *rigid* and *flexible* cases is then laid out in details. In **Chapter 6** the dynamical simulation results, after solving the equations of motion of the system, are presented and discussed in length. The method used to calculate the post-impact initial conditions of the system is also presented. Finally, **Chapter 7** concludes the thesis by summarizing all the results obtained and outlining some recommendations for future work.

Chapter 2

Kinematics of the System

2.1 Introduction

The system under study is illustrated in Figure 2.1. It is composed of a main body (hereafter referred to as mother spacecraft) that serves as a platform on which a two-link robotic manipulator is mounted, and a payload. It is important to point out that, although the manipulator shown in the figure consists of two links, the formulation developed in this thesis is applicable to the general case, i.e., for a multi-link manipulator. By definition, the orbital frame shown in the Figure rotates about Earth while the system frame, sometimes referred to as the body-fixed frame, is engraved on the spacecraft and rotates and translates with it. At a given instant in time, the orientation of the system frame (X_1, Y_1, Z_1) relative to the orbital frame (X_O, Y_O, Z_O) defines the spacecraft's attitude, represented by the pitch, roll, and yaw angles. The angular velocity of the orbital frame with respect to the inertial frame (X_I, Y_I, Z_I) located at the Earth's centre, is denoted by Ω.

In Figure 2.1 the orbital and system frames are located at the spacecraft's centre of mass C_S. This is because, in practice, it is the trajectory of the mother spacecraft,

rather than that of the system's centre of mass, that is maintained. However, the problem of orbit maintenance is not considered here. In any case, due to the fact that the mother spacecraft usually has the most substantial contribution to the total mass of the system, the centre of mass of the system is very close to that of the mother spacecraft C_S.

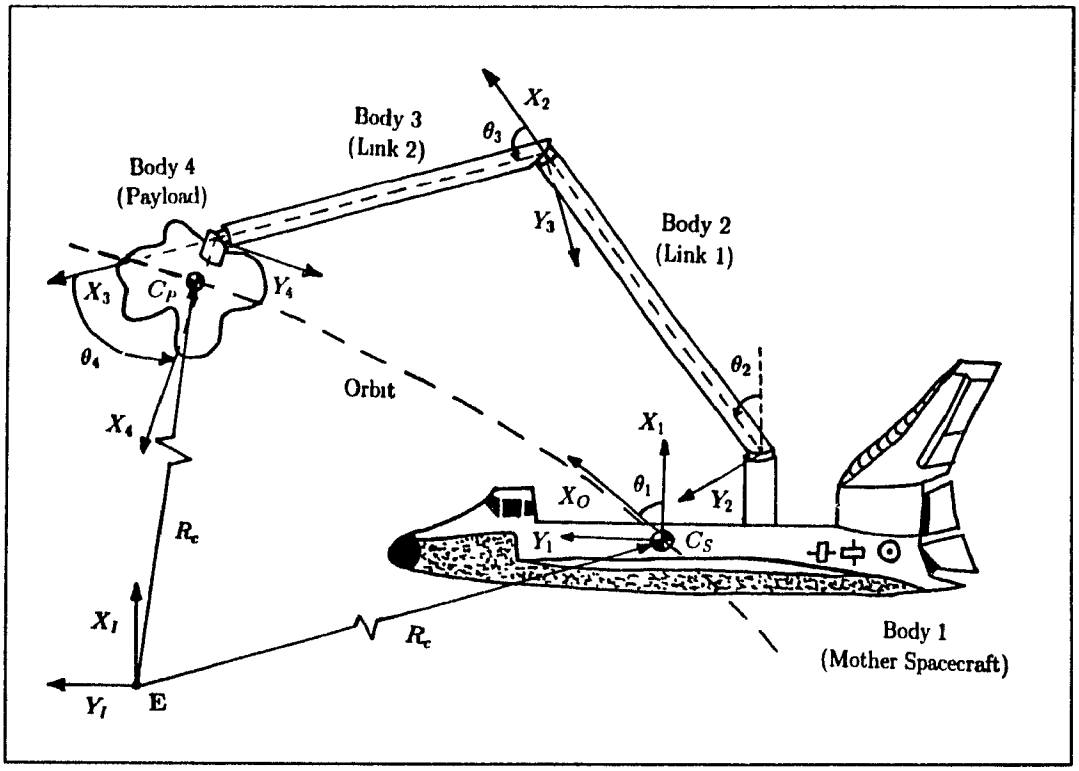

Figure 2.1: System under study

Both the platform and the payload are modelled as *rigid* in this study. However, the manipulator's links are modelled as *flexible* and the effect of the flexibility on the spacecraft/manipulator system is investigated. On the other hand, the joints of the manipulator are modelled as *rigid* and they are all chosen to be revolute for simplicity.

At first, the kinematics of an individual body, say body i, will be discussed and then the kinematics of the entire system will be presented in terms of rotation matrices and recursive relations. A suitable set of coordinates that describes the motion of a

rigid body will be described next. For the case of a *flexible* body, the flexibility is modelled by using either a finite-element model or beam eigenfunctions and the *flexible* body motion will be simply superimposed on the *rigid* body motion.

2.2 Generalized Coordinates

The vector ψ contains the independent generalized coordinates for an N-body system. It is defined as follows:

$$\psi = [\psi_1^T, \psi_2^T, \ldots, \psi_N^T]^T \tag{2.1}$$

where the vector ψ_1 represents the spacecraft's attitude degrees of freedom, namely, pitch, yaw, and roll. It can be written as :

$$\psi_1 = [\alpha, \beta, \gamma]^T \tag{2.2}$$

These angles will be modelled as the angular rotation of three separate joints. The actual formulation will use the quaternions discussed in section 2.3, however, for physical interpretation of the results quaternions will be converted into pitch, yaw, and roll angles because they are more easily interpreted in flight mechanics. In the planar case, α would be the same as θ_1 while β and γ are both zero.

For the remaining $(N-1)$ bodies, the generalized coordinates, which will depend on whether the body involved is *rigid* or *flexible*, could be written as follows:

$$\psi_i = \begin{cases} [\theta_i] & \text{if body } i \text{ is } rigid \\ [\theta_i, \mathbf{b}_i{}^T]^T, & \text{if body } i \text{ is } flexible \end{cases} \tag{2.3}$$

where,

$$\mathbf{b}_i = [b_{i1}, b_{i2}, \ldots, b_{im}]^T \tag{2.4}$$

contains the m generalized coordinates associated with bending in link i, and θ_i (Figure 2.2) is the angular rotation of joint i as a result of the actuator. For a

rigid link it represents the angle between X_i and X_{i-1}, measured along the positive direction of Z_i. For a *flexible* link the angle between X_i and X_{i-1} is the sum of θ_i and the angle of rotation of the tip of link $i-1$ which results from the structural flexibility.

2.3 Coordinates of a Rigid Body

The motion of a *rigid* body i, could be fully described by the position and orientation of its body-fixed frame (X_i, Y_i, Z_i) with respect to the orbital frame (X_O, Y_O, Z_O) . The position of the origin of (X_i, Y_i, Z_i) can be described by the position vector $\tilde{\mathbf{p}}_i$, while the rotation can be described by the rotation tensor $\mathbf{Q}_i$. The nine elements of the matrix $\mathbf{Q}_i$ are the direction cosines which describe the orientation of the body-fixed frame (X_i, Y_i, Z_i) in (X_O, Y_O, Z_O) coordinates. There exist only three independent parameters within the nine elements, i.e., there exist six constraint equations, which are due to the orthogonality property of $\mathbf{Q}_i$, i.e.,

$$\mathbf{Q}_i^T \mathbf{Q}_i = \mathbf{1}_{33} \tag{2.5}$$

where $\mathbf{1}_{33}$ is the 3x3 identity matrix. The independent parameters could be represented by either the Euler angles or by a four-parameter set such as the Euler parameters or linear invariants. The four-parameter sets, of course, will be subjected to a constraint. A more detailed description of these two four-parameter sets could be found in (Cyril 1988). Cyril has shown that the choice of Euler parameters or linear invariants is immaterial because they do not appear in the final dynamical equations of the system.

The 7-dimensional extended position vector, $\mathbf{q}_i$, contains the position vector of any point on a *rigid* body i and the orientation of the body. Meanwhile, the 6-dimensional

extended velocity vector, $\mathbf{w}_i$, contains the velocity of any point on a *rigid* i and the angular velocity of the body. This could be written as follows:

$$\mathbf{q}_i = [\tilde{\mathbf{p}}_i^T, \hat{\mathbf{q}}_i^T]^T \tag{2.6}$$

$$\mathbf{w}_i = [\tilde{\mathbf{v}}_i^T, \boldsymbol{\omega}_i^T]^T \tag{2.7}$$

where $\hat{\mathbf{q}}_i$ represents the quaternion formed by either the Euler parameters or the linear invariants which are extensively discussed by Cyril (1988).

2.4 Coordinates of a Flexible Body

The motion of a *flexible* body comprises of two components:

i) The *rigid* body motion described in Section 2.3.

ii) The *flexible* motion resulting from the structural elasticity inherent in the links.

The *flexible* motion of body i could be represented by m generalized coordinates $\mathbf{b}_i$, where m is the number of modes chosen to discretize the beam. Hence, the $(7+m)$-dimensional extended position vector and the $(6+m)$-dimensional extended velocity vector, $\mathbf{q}_i$ and $\mathbf{v}_i$, respectively, could be written as:

$$\mathbf{q}_i = [\tilde{\mathbf{p}}_i^T, \hat{\mathbf{q}}_i^T, \mathbf{b}_i]^T \tag{2.8}$$

$$\mathbf{w}_i = [\tilde{\mathbf{v}}_i^T, \boldsymbol{\omega}_i^T, \dot{\mathbf{b}}_i]^T \tag{2.9}$$

where $\mathbf{q}_i$ and $\mathbf{w}_i$ contain, in addition to the components of a *rigid* body described in the previous section, the vectors $\mathbf{b}_i$ and $\dot{\mathbf{b}}_i$ containing the elastic coordinates and their rates, respectively.

2.5 Modal Discretization

The displacement of any point on body i is a continuous function of both the location and time. In order for the Lagrangian formulation to be applicable, the displacements are discretized so as to obtain generalized coordinates that are functions of time only.

The motion of link i can be expressed in terms of two components:

i) a *rigid* body component describing the motion of a line that is tangent to the beam at the joint (which is considered to be clamped to a rotating hub) which is referred to as *nominal motion*,

ii) a *flexible* body component describing the elastic deflection of the body from this tangent line sshow in Figure 2.2, which depicts the planar case for clarity, which can essentially be superimposed over the *nominal motion*.

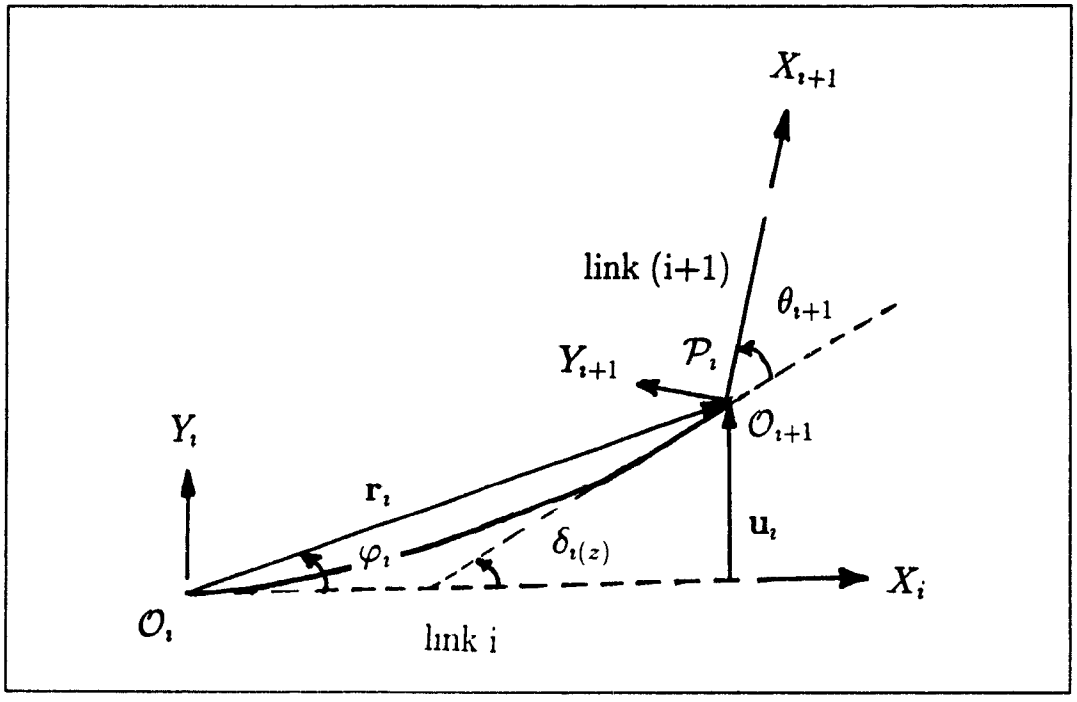

Figure 2.2: Motion of a flexible link

Let $\mathbf{r}_i$ be the position vector of any point $\mathcal{P}$ on the *flexible* body with respect to (X_i, Y_i, Z_i) axes. A set of unit vectors $\mathbf{x}_i, \mathbf{y}_i, \mathbf{z}_i$ are chosen to be parallel to (X_i, Y_i, Z_i) axes, respectively and x_i, y_i, z_i are the coordinates of a point in the frame. Vector $\mathbf{r}_i$ could be written as:

$$\mathbf{r}_i = x_i\mathbf{x}_i + \boldsymbol{\mu}_i(x_i, t) \tag{2.10}$$

where $\boldsymbol{\mu}_i$ represents the deflection of the beam due to bending, shear, and axial shortening. The components of $\boldsymbol{\mu}_i$ projected on X_i, Y_i, and Z_i axis respectively, are $\mu_{i(1)}, \mu_{i(2)}$, and $\mu_{i(3)}$. The component $\mu_{i(1)}$ results from an axial shortening effect, which is also referred to as centrifugal stiffening. Meirovitch (1967) relates $\mu_{i(1)}$ to $\mu_{i(2)}$ and $\mu_{i(3)}$ as:

$$\mu_{i(1)} \approx -\frac{1}{2}\int_{j=1}^{x_i}[(\frac{\partial\mu_{i(2)}}{\partial x})^2 + (\frac{\partial\mu_{i(3)}}{\partial x})^2]dx \tag{2.11}$$

the in-plane and out-of-plane deflections. The negative sign in equation (2.11) is a result of the shortening of the link. In this thesis the shortening effect will be ignored because the links will be moved at low speeds with rates that are considerably smaller than their first natural frequencies. On the other hand, if the links are operating at high speeds, the centrifugal stiffening has to be accommodated for in the model as done by Likins (1974).

The two other components of $\boldsymbol{\mu}$, namely, $\mu_{i(2)}$ and $\mu_{i(3)}$, are given in their discretized form as:

$$\mu_{i(2)} = \sum_{j=1}^{\bar{m}} \phi_{ij}(x_i)\mathrm{b}_{ij}(t) \tag{2.12}$$

$$\mu_{i(3)} = \sum_{j=1}^{\bar{m}} \phi_{ij}(x_i)\mathrm{b}_{i(\bar{m}+j)}(t) \tag{2.13}$$

where $\phi_{ij}(x_i)$ are the shape functions used for discretization, corresponding to body i with $j = 1, \ldots, \bar{m}$ and $m = 2\bar{m}$.

Effect of Shear

When *shear* effect is included in beam vibration, the flexibility of the beam is increased, consequently, the generalized stiffness is decreased.

Effects of Rotary Inertia

Rotary Inertia is the inertia associated with the angular acceleration of the beam sections. In the absence of shear, these sections, always remain plane and perpendicular to the longitudinal axis of the beam.

If shear is present then the above does not apply and the slope of the beam's axis has to be re-defined as follows:

$$\frac{\partial \mu_{i(3)}(x_i,t)}{\partial x} = -\xi_{i(2)} + \eta_{i(2)} \tag{2.14}$$

$$\frac{\partial \mu_{i(2)}(x_i,t)}{\partial x} = \xi_{i(3)} + \eta_{i(3)} \tag{2.15}$$

where $\frac{\partial \mu_{i(2)}}{\partial x}$, $\frac{\partial \mu_{i(3)}}{\partial x}$, $\xi_{i(2)}$, $\xi_{i(3)}$, $\eta_{i(2)}$, and $\eta_{i(3)}$ are the total angle of rotation about the Y_i-axis, the total angle of rotation about the Z_i-axis, the angle of rotation about the Y_i-axis due to bending, the angle of rotation about the Z_i-axis to bending, the angle of distortion about the Y_i-axis due to shear, and the angle of distortion about the Z_i-axis due to shear, respectively.

The displacement vector $\boldsymbol{\mu}_i$ can be written in the compact form:

$$\boldsymbol{\mu}_i(x_i,t) = \mathbf{B}_i(x_i)\mathbf{b}_i(t) \tag{2.16}$$

where $\mathbf{B}_i(x_i)$ is a $3\text{x}m$ matrix of shape functions associated with bending of link i and is defined as:

$$\mathbf{B}_i(x_i) = \begin{bmatrix} 0 & \dots & 0 & 0 & \dots & 0 \\ \phi_{i1} & \dots & \phi_{i\bar{m}} & 0 & \dots & 0 \\ 0 & \dots & 0 & \phi_{i1} & \dots & \phi_{i\bar{m}} \end{bmatrix} \tag{2.17}$$

As mentioned earlier, the *Euler-Bernoulli* beam theory will be used to model the structural flexibility in the beams. Hence, the total rotation of the beam will only depend on bending resulting from the flexibility. The rotation of the tip of link i with respect to (X_i, Y_i, Z_i) is denoted by δ_i (Figure 2.2) and is defined as:

$$\delta_i \equiv \begin{bmatrix} \delta_{i(1)} \\ \delta_{i(2)} \\ \delta_{i(3)} \end{bmatrix} = \mathbf{D}_i(l_i)\mathbf{b}_i \tag{2.18}$$

where,

$$\mathbf{D}_i(l_i) = \begin{bmatrix} 0 & \dots & 0 & 0 & \dots & 0 \\ 0 & \dots & 0 & -\phi'_{i1}(l_i) & \dots & -\phi'_{i\bar{m}}(l_i) \\ \phi'_{i1} & \dots & \phi'_{i\bar{m}} & 0 & \dots & 0 \end{bmatrix} \tag{2.19}$$

and $(\,)'$ represents differentiation with respect to x_i, while $\delta_{i(1)}$, $\delta_{i(2)}$, and $\delta_{i(3)}$ represent the x, y, and z components of δ_i, respectively.

2.6 Rotation Matrices

The rotation matrix describing the orientation of body i- fixed axes (X_i, Y_i, Z_i) with respect to the orbital frame (X_O, Y_O, Z_O) is defined as follows:

$$\mathbf{Q}_i \equiv \mathbf{R}_1\mathbf{R}_2 \dots \mathbf{R}_{i-1}\mathbf{R}_i \; ; \; i = 1, \dots, N \tag{2.20}$$

where, $\mathbf{R}_i$ describes the orientation of body i-fixed axes (X_i, Y_i, Z_i) , with respect to body $(i-1)$ fixed axes $(X_{i-1}, Y_{i-1}, Z_{i-1})$. The rotation matrices $\mathbf{R}_1$ and $\mathbf{R}_{i+1}$ are respectively defined by:

$$\mathbf{R}_1 = \begin{bmatrix} 1 & 0 & 0 \\ 0 & cos\beta & -sin\beta \\ 0 & sin\beta & cos\beta \end{bmatrix} \begin{bmatrix} cos\gamma & 0 & -sin\gamma \\ 0 & 1 & 0 \\ sin\gamma & 0 & cos\gamma \end{bmatrix} \begin{bmatrix} cos\alpha & sin\alpha & 0 \\ -sin\alpha & cos\alpha & 0 \\ 0 & 0 & 1 \end{bmatrix} \tag{2.21}$$

and

$$\mathbf{R}_{i+1} = \begin{bmatrix} 1 & 0 & 0 \\ 0 & cos\delta_{i(1)} & -sin\delta_{i(1)} \\ 0 & sin\delta_{i(1)} & cos\delta_{i(1)} \end{bmatrix} \begin{bmatrix} cos\delta_{i(2)} & 0 & -sin\delta_{i(2)} \\ 0 & 1 & 0 \\ sin\delta_{i(2)} & 0 & cos\delta_{i(2)} \end{bmatrix} \begin{bmatrix} cos\delta_{i(3)} & sin\delta_{i(3)} & 0 \\ -sin\delta_{i(3)} & cos\delta_{i(3)} & 0 \\ 0 & 0 & 1 \end{bmatrix} \begin{bmatrix} cos\theta_{i+1} & -sin\theta_{i+1} & 0 \\ sin\theta_{i+1} & cos\theta_{i+1} & 0 \\ 0 & 0 & 1 \end{bmatrix} \tag{2.22}$$

for $i = 1, \ldots, N-1$, where (α, β, γ) are the pitch, yaw, and roll of the mother spacecraft (body 1) described earlier.

All deformations resulting from the flexibility of the links are small enough so that their trigonometric functions could be linearized. Therefore, the rotation matrix $\mathbf{R}_{i+1}$ could be re-written in a simpler form as:

$$\mathbf{R}_{i+1} = \begin{bmatrix} 1 & -\delta_{i(3)} & -\delta_{i(2)} \\ \delta_{i(3)} & 1 & -\delta_{i(1)} \\ \delta_{i(2)} & \delta_{i(1)} & 1 \end{bmatrix} \begin{bmatrix} cos\theta_{i+1} & -sin\theta_{i+1} & 0 \\ sin\theta_{i-1} & cos\theta_{i+1} & 0 \\ 0 & 0 & 1 \end{bmatrix} \tag{2.23}$$

for $i = 1, \ldots, N-1$.

2.7 Recursive Relations

The position of the origin of (X_i, Y_i, Z_i) with respect to that of (X_O, Y_O, Z_O) is defined by the following recursive relation:

$$\tilde{\mathbf{p}}_i \equiv \tilde{\mathbf{p}}_{i-1} + \mathbf{r}_{i-1}(l_{i-1}) \tag{2.24}$$

for $i = 2, \ldots, N$. It is obvious that $\tilde{\mathbf{p}}_1$ is equal to zero, because it is defined as the distance between the origins of the orbital and system frames.

Differentiating equation (2.24) with respect to time, the inertial velocity of the frame (X_i, Y_i, Z_i) would be readily obtained as:

$$\tilde{\mathbf{v}}_i = \tilde{\mathbf{v}}_{i-1} + \boldsymbol{\omega}_{i-1} \times \mathbf{r}_{i-1}(l_{i-1}) + \dot{\boldsymbol{\mu}}_{i-1}, \quad i = 2, \ldots, N \tag{2.25}$$

Similarly, the acceleration vector can be obtained by differentiating equation (2.25) with respect to time as follows:

$$\dot{\tilde{\mathbf{v}}}_i = \dot{\tilde{\mathbf{v}}}_{i-1} + \boldsymbol{\omega}_{i-1} \times \boldsymbol{\omega}_{i-1} \times \mathbf{r}_{i-1}(l_{i-1}) + \dot{\boldsymbol{\omega}}_{i-1} \times \mathbf{r}_{i-1}(l_{i-1})$$
$$+2\boldsymbol{\omega}_{i-1} \times \dot{\boldsymbol{\mu}}_{i-1} + \ddot{\boldsymbol{\mu}}_{i-1}, \quad i = 2, \ldots, N \tag{2.26}$$

The angular velocity of the system frame (X_1, Y_1, Z_1) with respect to the orbital frame (X_O, Y_O, Z_O) in terms of the orbital rate Ω and the angles describing the attitude of the platform could be obtained as follows:

$$\boldsymbol{\omega}_1 = \begin{bmatrix} cos\gamma & 0 & -sin\gamma cos\beta \\ 0 & 1 & sin\beta \\ sin\gamma & 0 & cos\gamma cos\beta \end{bmatrix} \begin{Bmatrix} \dot{\beta} \\ \dot{\gamma} \\ \Omega + \dot{\alpha} \end{Bmatrix} \tag{2.27}$$

The angular velocity of (X_i, Y_i, Z_i) with respect to (X_O, Y_O, Z_O) is defined as follows:

$$\boldsymbol{\omega}_i \equiv \boldsymbol{\omega}_{i-1} + \dot{\boldsymbol{\delta}}_{i-1} + \dot{\theta}_i \mathbf{z}_i \tag{2.28}$$

where $i = 2, \ldots, N$. Differentiating equation (2.28) with respect to time, an expression for the angular velocity of body i is obtained as follows:

$$\dot{\boldsymbol{\omega}}_i = \dot{\boldsymbol{\omega}}_{i-1} + \ddot{\boldsymbol{\delta}}_{i-1} + \boldsymbol{\omega}_{i-1} \times \dot{\boldsymbol{\delta}}_{i-1} + \ddot{\theta}_i \mathbf{z}_i$$
$$+(\boldsymbol{\omega}_{i-1} + \dot{\boldsymbol{\delta}}_{i-1}) \times \dot{\boldsymbol{\theta}}_i \tag{2.29}$$

Chapter 3

Dynamical Equations of Motion

3.1 Introduction

In this chapter the unconstrained equations of motion of an $N(=n+2)$-body dynamical system (refer to Figure 2.1) composed of an n-link robot manipulator, a mother spacecraft, and a payload, will be derived. The Lagrangian formulation rather than the Newton-Euler formulation will be used, because the former is simple to implement and is directly applicable to systems with kinematic loops and flexible bodies. This will no doubt make the derivation straight forward, however one has to pay the price of lengthy partial differentiations.

The usual practice in Lagrangian Dynamics is to consider the dynamical system as a whole, i.e., expressions for the system's potential and kinetic energies are obtained and are used to derive the equations of motion for the whole system. In this thesis, however, the formulation is carried out by writing the Lagrange equations governing the motion of each individual body. The individual equations will then be assembled and re-arranged to obtain the *constrained* dynamical equation of the whole system. This procedure makes the derivation much simpler, however, it introduces the non-

working constraint forces and moments as in the case of the Newtonian approach. These constraint forces and moments, which are not relevant to the computations done in this thesis, complicate the dynamical system by introducing additional variables to the equations of motion. Hence, a novel technique that involves the *natural orthogonal complement*, described by Cyril (1988), will be used to eliminate those non-working constraint forces to produce a set of independent dynamical equations of motion.

In order to obtain the individual equations of motion of each body, expressions for both the potential and kinetic energies have to be obtained first. These are presented in the following two sections.

3.2 Kinetic Energy

For all practical purposes, the orbital and the attitude motions of a body in space could be studied separately. Hence, expressions for the kinetic energy resulting from the orbital motion and that from the attitude motion could be obtained independently. It is worth mentioning that the attitude motion of the body could perturb its orbital motion, however this perturbation is negligible and thus, it is assumed here that the orbital motion of the mother spacecraft is prescribed. From now on, the phrase kinetic energy would imply kinetic energy associated with attitude and structural dynamics.

The kinetic energy of an individual body i, denoted by T_i, can be written in terms of its extended velocity vector, $\mathbf{w}_i$, and its extended mass matrix, $\mathbf{M}_i$, as follows:

$$T_i = \frac{1}{2}\mathbf{w}_i^T \mathbf{M}_i(\mathbf{q}_i, t)\mathbf{w}_i \quad i = 1, \ldots, N \tag{3.1}$$

The derivation is carried out by obtaining an expression for the velocity of a point

$\mathcal{P}_i$ on body i as follows:

$$\mathbf{v}_i(x) = \begin{cases} \tilde{\mathbf{v}}_i + \boldsymbol{\omega}_i \times \mathbf{r}_i, & \text{if body } i \text{ is } \textit{rigid} \\ \tilde{\mathbf{v}}_i + \boldsymbol{\omega}_i \times \mathbf{r}_i + \dot{\mathbf{r}}_i, & \text{if body } i \text{ is } \textit{flexible} \end{cases} \tag{3.2}$$

In the following subsections, expressions for the kinetic energy of each body of the system, i.e., the mother spacecraft, the 2-link robot manipulator, and the captured satellite will be derived. These expressions will then be used in the Lagrangian formulation to obtain the individual equations of motion.

3.2.1 Kinetic Energy of the Mother Spacecraft

The mother spacecraft (body 1), which serves as a platform for the robot manipulator, will be modelled as a *rigid* body for simplicity. Its kinetic energy, T_1 could then be written as:

$$T_1 = \frac{1}{2} \int_{m_1} \mathbf{v}_1^T \mathbf{v}_1 \, dm_1 \tag{3.3}$$

where,

$$\mathbf{v}_1(x) = \tilde{\mathbf{v}}_1 + \boldsymbol{\omega}_1 \times \mathbf{r}_1 \tag{3.4}$$

Where $\boldsymbol{\omega}_1$ represents the angular velocity of the mother spacecraft and includes the orbital angular velocity Ω.

Now, equation (3.3) could be rewritten as (its detailed derivation is in appendix A):

$$T_1 = \frac{1}{2} m_1 \tilde{\mathbf{v}}_1^T \tilde{\mathbf{v}}_1 + \frac{1}{2} \boldsymbol{\omega}_1^T \left[\mathbf{I}_1 \right] \boldsymbol{\omega}_1 \tag{3.5}$$

where $\mathbf{I}_1$ is the inertia tensor of the spacecraft about its centre of mass. Also, $\tilde{\mathbf{v}}_1$ represents the velocity of the origin of the system frame relative to the orbital frame, which is zero in the present case.

The extended mass matrix of the spacecraft $\mathbf{M}_1$ could be readily obtained from

equation (3.5) as:

$$\mathbf{M}_1 = \begin{bmatrix} (m_1)\mathbf{1} & \mathbf{0}_{3x3} \\ \mathbf{0}_{3x3} & \mathbf{I}_1 \end{bmatrix}_{6x6} \tag{3.6}$$

3.2.2 Kinetic Energy of the Links

In this thesis, a flexible body i will be modelled as a beam. The kinetic energy of a beam, in general, can be written as follows (Timoshenko 1955):

$$\begin{aligned} T = &\frac{1}{2}\int_0^l \rho(x)\mathbf{v}^T(x)\mathbf{v}(x)dx + \frac{1}{2}M\mathbf{v}^T(l)\mathbf{v}(l) + \frac{1}{2}\omega^T\mathbf{I}_H\omega \\ &+\frac{1}{2}\int_0^l \rho(x)\kappa_2^2(x)\dot{\xi}_2^2(x,t)dx + \frac{1}{2}\int_0^{l_t} \rho(x)\kappa_3^2(x)\dot{\xi}_3^2(x,t)dx \end{aligned} \tag{3.7}$$

where the subscript i was and will be dropped from now on for brevity and ρ, κ, $\mathbf{I}_H$, and M are the mass per unit length, the radius of gyration of the cross-section taken about the neutral axis of bending, the hub moment of inertia, and the concentrated mass (if any) at the tip of body i, respectively. The first term in equation (3.7) corresponds to the *rigid* body motion of link i, the second term represents the kinetic energy of mass M located at the end of body i, the third term is the kinetic energy of the hub, and the last two terms are associated with the inertia due to the angular acceleration of the beam sections due to bending in the in-plane and out-of-plane directions, respectively. The links considered in this thesis are long and slender, i.e., their cross-sectional dimensions are small compared with their lengths. Therefore, the effect of the rotary inertia can be neglected as suggested by Timoshenko (1955). This allows the use of *Euler-Bernoulli* beam theory to model the elastic behaviour of the links. In the event that the beam is shorter or thicker, Timoshenko beam theory, which accounts for the transverse shear and the rotary inertia effects in the model, has to be used. Another assumption in this thesis is that the geometric and physical properties of the links remain constant along its length and that its neutral

axis coincides with the centroidal axis. Also, the effects of centrifugal stiffening could be neglected because the links will be rotated at relatively low speeds.

Next, starting from equation (3.7), a more convenient expression for the kinetic energy of each flexible body i will be derived, from which the extended mass matrix corresponding to that body will be extracted. The terms $\mathbf{v}_i^2(x)$ and $\mathbf{v}_i^2(l)$ in equation (3.7) can be easily evaluated from equation (3.2) (subscript i has been dropped for convenience), and are found to be as follows:

$$\begin{aligned}\mathbf{v}^2(x) = \tilde{\mathbf{v}}^2 + 2\tilde{\mathbf{v}}^T(\boldsymbol{\omega}\mathbf{x}\mathbf{r}) + (\boldsymbol{\omega}\mathbf{x}\mathbf{r})^T(\boldsymbol{\omega}\mathbf{x}\mathbf{r}) \\ +2\tilde{\mathbf{v}}^T\dot{\mathbf{r}} + 2(\boldsymbol{\omega}\mathbf{x}\mathbf{r})^T\dot{\mathbf{r}} + \dot{\mathbf{r}}^2 \end{aligned} \tag{3.8}$$

Equation (3.8) can be re-written in terms of $\mathbf{X}$ and $\mathbf{U}$, the cross-product tensor of $\mathbf{x}$ and $\boldsymbol{\mu}$, respectively. The resulting equation, whose detailed derivation is given in Appendix A, is as follows:

$$\begin{aligned}\mathbf{v}^2 = \tilde{\mathbf{v}}^2 - \tilde{\mathbf{v}}^T(2x\mathbf{X} + 2\mathbf{U})\boldsymbol{\omega} + 2\tilde{\mathbf{v}}^T\boldsymbol{\mu} + \dot{\boldsymbol{\mu}}^2 \\ +\boldsymbol{\omega}^T(x^2(\mathbf{1} - \mathbf{x}\otimes\mathbf{x}) - x(\mathbf{x}\otimes\boldsymbol{\mu} + \boldsymbol{\mu}\otimes\mathbf{x}) \\ +(\boldsymbol{\mu}^2\mathbf{1} - \boldsymbol{\mu}\otimes\boldsymbol{\mu})]\boldsymbol{\omega} + \boldsymbol{\omega}^T(2x\mathbf{X} + 2\mathbf{U})\dot{\boldsymbol{\mu}} \end{aligned} \tag{3.9}$$

Similarly, an expression for $\mathbf{v}^2(l)$ can be obtained as:

$$\begin{aligned}\mathbf{v}^2(l) = \tilde{\mathbf{v}}^2 - \tilde{\mathbf{v}}^T(2l\mathbf{X} + 2\mathbf{U}(\mathbf{l}))\boldsymbol{\omega} + 2\tilde{\mathbf{v}}^T\boldsymbol{\mu}(l) + \dot{\boldsymbol{\mu}}^2(l) \\ +\boldsymbol{\omega}^T(l^2(\mathbf{1} - \mathbf{x}\otimes\mathbf{x}) - l(\mathbf{x}\otimes\boldsymbol{\mu} + \boldsymbol{\mu}(l)\otimes\mathbf{x}) \\ +(\boldsymbol{\mu}^2(l)\mathbf{1} - \boldsymbol{\mu}(l)\otimes\boldsymbol{\mu}(l))]\boldsymbol{\omega} + \boldsymbol{\omega}^T(2l\mathbf{X} + 2\mathbf{U}(\mathbf{l}))\dot{\boldsymbol{\mu}}(l) \end{aligned} \tag{3.10}$$

The symbol $\otimes$ used in the above equations denotes the tensor product of two vectors.

Upon the substitution of equations (2.16), (3.9) and (3.10) into equation (3.7) and integrating, the kinetic energy for a *flexible* link i, could be written as (refer to

Appendix A for the detailed derivation):

$$
\begin{aligned}
2T = {} & \tilde{\mathbf{v}}^T[m+M]\tilde{\mathbf{v}} - \tilde{\mathbf{v}}^T[\rho(2\mathbf{T}_2 + l^2\mathbf{X}) + 2M(\mathbf{U}(l) + l\mathbf{X}]\boldsymbol{\omega} \\
& + 2\tilde{\mathbf{v}}^T[\rho\mathbf{T}_1 + M\mathbf{B}(l)]\dot{\mathbf{b}} + \boldsymbol{\omega}^T[2\rho(\mathbf{T}_4 + \mathbf{X}\mathbf{T}_5) + 2M(\mathbf{U}(l)\mathbf{B}(l) + l\mathbf{X}\mathbf{B}(l))]\dot{\mathbf{b}} \\
& + \boldsymbol{\omega}^T[\rho(\frac{l^3}{3}\mathbf{T}_{10} + 2\mathbf{x}^T\mathbf{T}_5\boldsymbol{\mu}\mathbf{1} + \mathbf{I}_{\mathrm{H}} - \mathbf{T}_6 - \mathbf{T}_7 + \mathbf{T}_8) \\
& + M(l^2\mathbf{T}_{10} + 2l\mathbf{x}^T\mathbf{B}(l)\boldsymbol{\mu}\mathbf{1} - l(\mathbf{x}\otimes\boldsymbol{\mu}(l) + \boldsymbol{\mu}(l)\otimes\mathbf{x}) - \boldsymbol{\mu}(l)\otimes\boldsymbol{\mu}(l) + \mathbf{T}_9)]\boldsymbol{\omega} \\
& + \dot{\mathbf{b}}^T[\rho\mathbf{T}_3 + M\mathbf{B}^T(l)\mathbf{B}(l)]\dot{\mathbf{b}}
\end{aligned}
\tag{3.11}
$$

In equation (3.11) the terms $\mathbf{x}^T\mathbf{T}_5$ and $\mathbf{x}^T\mathbf{B}(l)$ could be set to zero if the axial shortening effect is ignored, i.e. $u_1 = 0$. The terms $\mathbf{T}_1$, $\mathbf{T}_3$, $\mathbf{T}_4$, $\mathbf{T}_5$, $\mathbf{T}_6$, $\mathbf{T}_7$, $\mathbf{T}_8$, $\mathbf{T}_9$, and $\mathbf{T}_{10}$ are defined as follows:

$$
\begin{aligned}
\mathbf{T}_1 &= \int_0^l \mathbf{B}dx \\
\mathbf{T}_3 &= \int_0^l \mathbf{B}^T\mathbf{B}dx \\
\mathbf{T}_4 &= \int_0^l \mathbf{U}\mathbf{B}dx \\
\mathbf{T}_5 &= \int_0^l x\mathbf{B}dx \\
\mathbf{T}_6 &= \int_0^l x(\mathbf{x}\otimes\boldsymbol{\mu} + \boldsymbol{\mu}\otimes\mathbf{x})dx \\
\mathbf{T}_7 &= \int_0^l (\boldsymbol{\mu}\otimes\boldsymbol{\mu})dx \\
\mathbf{T}_8 &= \boldsymbol{\mu}^T\mathbf{T}_3\boldsymbol{\mu}\mathbf{1} \\
\mathbf{T}_9 &= \boldsymbol{\mu}^T\mathbf{b}^T(l)\mathbf{B}\boldsymbol{\mu}\mathbf{1} \\
\mathbf{T}_{10} &= \mathbf{1} - (\mathbf{x}\otimes\mathbf{x}) = -\mathbf{X}^2
\end{aligned}
\tag{3.12}
$$

and $\mathbf{T}_2$ represents the cross product tensor corresponding to $\mathbf{T}_1\mathbf{b}$.

The extended mass matrix, M, can be extracted from equation (3.11) and is given by:

$$\mathbf{M} = \begin{bmatrix} \mathbf{M}_{dd} & \mathbf{M}_{d\theta} & \mathbf{M}_{db} \\ \mathbf{M}_{\theta d} & \mathbf{M}_{\theta\theta} & \mathbf{M}_{\theta b} \\ \mathbf{M}_{bd} & \mathbf{M}_{b\theta} & \mathbf{M}_{bb} \end{bmatrix}_{(6+m)x(6+m)} \tag{3.13}$$

where the components of M are as follows:

$$\begin{aligned}
\mathbf{M}_{dd} &= (M+m)\mathbf{1} \\
\mathbf{M}_{d\theta} &= -\rho(\mathbf{T}_2 + \frac{l^2}{2}\mathbf{X}) + M(\mathbf{U}(l) + l\mathbf{X}) \\
\mathbf{M}_{db} &= \rho\mathbf{T}_1 + M\mathbf{B}(l) \\
\mathbf{M}_{\theta\theta} &= \rho(\frac{l^3}{3}\mathbf{T}_{10} + 2\mathbf{x}^T\mathbf{T}_5\boldsymbol{\mu}\mathbf{1} + \mathbf{I}_H - \mathbf{T}_6 - \mathbf{T}_7 + \mathbf{T}_8) \\
&\quad + M(l^2\mathbf{T}_{10} + 2l\mathbf{x}^T\mathbf{B}(l)\boldsymbol{\mu}\mathbf{1} - l(\mathbf{x}\otimes\boldsymbol{\mu}(l) + \boldsymbol{\mu}(l)\otimes\mathbf{x}) \\
&\quad - \boldsymbol{\mu}(l)\otimes\boldsymbol{\mu}(l) + \mathbf{T}_9) \\
\mathbf{M}_{\theta b} &= \rho(\mathbf{T}_4 + \mathbf{X}\mathbf{T}_5) + M(\mathbf{U}(l)\mathbf{B}(l) + l\mathbf{X}\mathbf{B}(l)) \\
\mathbf{M}_{bb} &= \rho\mathbf{T}_3 + M\mathbf{B}(l)^T\mathbf{B}(l) \\
\mathbf{M}_{\theta d} &= \mathbf{M}_{d\theta}^T \\
\mathbf{M}_{bd} &= \mathbf{M}_{db}^T \\
\mathbf{M}_{b\theta} &= \mathbf{M}_{\theta b}^T
\end{aligned} \tag{3.14}$$

and the subscripts d, θ, and b correspond to the displacement, rotation, and bending, of the body, respectively.

3.2.3 Kinetic Energy of the Captured Payload

The spacecraft/manipulator system has the capability of capturing a payload as mentioned earlier in Chapter 2. For such a case, the extended mass matrix of the captured

payload will be derived in this section. The payload was assumed to have an an initial spin rate of ω_n about its axis of symmetry and was modelled as a *rigid* body for simplicity. The position of any point, $\mathcal{P}_n$ on the payload could be written as:

$$\mathbf{p}_n = \mathbf{p}_{c_n} + \mathbf{r}_n \tag{3.15}$$

where $\mathbf{r}_n$ is the position of any point $\mathcal{P}_n$ on the payload measured from the centre of mass and $\mathbf{p}_{c_n}$ is the position vector of the payload's centre of mass measured from the orbital frame and is defined as follows (subscript n will be dropped for brevity):

$$\mathbf{p}_c = \tilde{\mathbf{p}} + \mathbf{r}_{bc} \tag{3.16}$$

where $\mathbf{r}_{bc}$ is the position vector of the payload's centre of mass $\mathcal{C}$ measured from the origin of its body-fixed frame $\mathcal{B}$ which coincides with the tip of the last link of the manipulator (see Figure 4.1). An expression for the velocity of any point on the payload could be readily obtained from equation (3.15) as:

$$\mathbf{v} = \mathbf{v}_c + \boldsymbol{\omega}\mathbf{x}\mathbf{r} \tag{3.17}$$

and,

$$\mathbf{v}^2 = \mathbf{v}_c^2 + 2\mathbf{v}_c^T(\boldsymbol{\omega}\mathbf{x}\mathbf{r}) + (\boldsymbol{\omega}\mathbf{x}\mathbf{r})^T(\boldsymbol{\omega}\mathbf{x}\mathbf{r}) \tag{3.18}$$

After performing the integration and re-arranging, the kinetic energy of the payload is obtained as follows (please refer to appendix A for its detailed derivation):

$$2T = \tilde{\mathbf{v}}^T[(m)\mathbf{1}]\tilde{\mathbf{v}} - \tilde{\mathbf{v}}^T[2m\mathbf{R}_{bc}]\boldsymbol{\omega} + \boldsymbol{\omega}^T[\mathbf{I}_b]\boldsymbol{\omega} \tag{3.19}$$

where $\mathbf{I}_b$ is the inertia tensor of the payload about the origin of its body-fixed frame and $\tilde{\mathbf{v}}$ represents the velocity of the payload's body-fixed axes relative to the mother spacecraft.

The extended mass matrix M of the payload could be readily extracted from equation (3.19) and could be written as follows:

$$\mathbf{M} = \begin{bmatrix} \mathbf{M}_{dd} & \mathbf{M}_{d\theta} \\ \mathbf{M}_{\theta d} & \mathbf{M}_{\theta\theta} \end{bmatrix}_{6x6} \tag{3.20}$$

where,

$$\mathbf{M}_{dd} = (m)\mathbf{1}$$

$$\mathbf{M}_{d\theta} = -m\mathbf{R}_{bc}$$

$$\mathbf{M}_{\theta d} = \mathbf{M}_{d\theta}^{T}$$

$$\mathbf{M}_{\theta\theta} = \mathbf{I}_{b}$$

3.3 Potential energy

The potential energy corresponding to body i, denoted by U_i, is a function of the extended position vector $\mathbf{q}_i$ alone. It consists of two parts; one due to the gravity gradient and the other due to the elastic strain energy stored in the *flexible* body. The effect of the former is much smaller than the latter and is neglected here. Hence the potential energy for a *rigid* body is equal to zero. The potential energy for a *flexible* body could be written as:

$$\begin{aligned} U = &\frac{1}{2}\int_0^l EI\left(\frac{\partial \xi_{(2)}}{\partial x}\right)^2 dx + \frac{1}{2}\int_0^l EI\left(\frac{\partial \xi_{(3)}}{\partial x}\right)^2 dx \\ &+ \frac{1}{2}\int_0^l KGA\eta_{(2)}^2 dx + \frac{1}{2}\int_0^l KGA\eta_{(3)}^2 dx \end{aligned} \tag{3.21}$$

where E, I, G and K are the modulus of elasticity, the area moment of inertia, the shear modulus, and the shear constant, respectively. Again, the subscript i has been dropped for convenience. The first two terms on the right hand side of equation (3.21) are the strain energy of the link due to bending, and the last two terms are the

strain energy due to shear deformation. As mentioned earlier the links considered in this thesis are long and slender, therefore the effect of shear deformations could be neglected without losing generality. After dropping the terms related to shear and performing the integration in equation (3.21), the potential energy could be re-written as (refer to Appendix A for a detailed derivation):

$$U = \frac{1}{2} EI \mathbf{b}^T \mathbf{T}_{11} \mathbf{b} \tag{3.22}$$

where,

$$\mathbf{T}_{11} = \int_0^l (\mathbf{B}'')^T \mathbf{B}'' dx \tag{3.23}$$

and

$$\mathbf{B}'' = \begin{bmatrix} 0 & \dots & 0 & 0 & \dots & 0 \\ \phi''_{i1} & \dots & \phi''_{i\bar{n}} & 0 & \dots & 0 \\ 0 & \dots & 0 & -\phi''_{i1} & \dots & -\phi''_{i\bar{n}} \end{bmatrix} \tag{3.24}$$

3.3.1 Structural Damping

The energy dissipation caused by cyclic stress and strain within a structural material is often referred to as structural damping. Experimental studies have shown that the energy dissipation per cycle for metals such as aluminum and steel, which are common structural materials, is approximately proportional to the square of the strain amplitude but is essentially independent of frequency (Kimball, 1929).

By incorporating structural damping in the model, the energy dissipated by the *flexible* links in the deformation process is accounted for. Structural damping could be modelled by replacing the modulus of elasticity, E, by the complex modulus of elasticity, E^* defined as follows:

$$E^* = E(1 + \nu \frac{\partial}{\partial t}) \tag{3.25}$$

where ν is a loss factor resulting from the normal strain lagging the normal stress during sinusoidal motion.

The new modulus of elasticity, E^*, is substituted in equation (3.22) replacing E and a new expression for the potential energy is obtained as follows:

$$U^* = U + EI\mathbf{b}^T\mathbf{T}_{11}\nu\dot{\mathbf{b}} \tag{3.26}$$

3.4 Equations of Motion of an Individual Body

The dynamical equations of motion of body i can be derived using the Lagrangian formulation, which is given by the following expression:

$$\frac{d}{dt}\left(\frac{\partial T_i}{\partial \dot{\mathbf{q}}_i}\right) - \frac{\partial T_i}{\partial \mathbf{q}_i} = \boldsymbol{\chi}_i - \frac{\partial U_i}{\partial \mathbf{q}_i} \quad i = 1, \ldots, N. \tag{3.27}$$

where $\boldsymbol{\chi}_i$ is a vector containing all the non-conservative generalized forces (dissipative, external, and constraint forces) acting on body i.

The kinetic and potential energy expressions obtained in sections (3.2) and (3.3), respectively are substituted in equation (3.27). Due to the length of the derivations of the equations of motion for each individual body they will not be presented in this thesis. However, it could be found in Cyril (1988) where the body equations were expressed in terms of displacement, rotation, and bending dependent terms.

The general form of the individual equation of motion of body i is:

$$\mathbf{M}_i\dot{\mathbf{w}}_i = \boldsymbol{\phi}_i^E + \boldsymbol{\phi}_i^S + \boldsymbol{\phi}_i^C \tag{3.28}$$

where vector $\boldsymbol{\phi}_i^E$ contains all the generalized external forces and moments acting on body i such as the ones arising due to the applied joint torques, vector $\boldsymbol{\phi}_i^S$ contains all the position and velocity dependent generalized forces and moments in addition to the dissipative forces, and vector $\boldsymbol{\phi}_i^C$ contains the generalized constraint forces vector arising due to the kinematic velocity constraints.

3.5 Equations of Motion of the System

Upon assembling the equations of motion for each body, the system's constrained equations of motion can be written in the form :

$$\mathbf{M}\dot{\mathbf{w}} = \boldsymbol{\phi}^E + \boldsymbol{\phi}^S + \boldsymbol{\phi}^C \tag{3.29}$$

where,

$$\mathbf{M} = \text{diag}(\mathbf{M}_1, \mathbf{M}_2, ..., \mathbf{M}_N)$$

is the generalized extended inertia matrix of the system. Vectors $\dot{\mathbf{w}}$, $\boldsymbol{\phi}^E$, $\boldsymbol{\phi}^S$, and $\boldsymbol{\phi}^C$ represent the the generalized extended acceleration vector, the generalized extended external, system, and constraint forces, respectively and are defined as follows:

$$\dot{\mathbf{w}} = \begin{bmatrix} \dot{\mathbf{w}}_1 \\ \dot{\mathbf{w}}_2 \\ \vdots \\ \dot{\mathbf{w}}_N \end{bmatrix} \quad \boldsymbol{\phi}^E = \begin{bmatrix} \boldsymbol{\phi}_1^E \\ \boldsymbol{\phi}_2^E \\ \vdots \\ \boldsymbol{\phi}_N^E \end{bmatrix} \quad \boldsymbol{\phi}^S = \begin{bmatrix} \boldsymbol{\phi}_1^S \\ \boldsymbol{\phi}_2^S \\ \vdots \\ \boldsymbol{\phi}_N^S \end{bmatrix} \quad \boldsymbol{\phi}^C = \begin{bmatrix} \boldsymbol{\phi}_1^C \\ \boldsymbol{\phi}_2^C \\ \vdots \\ \boldsymbol{\phi}_N^C \end{bmatrix} \tag{3.30}$$

3.5.1 Elimination of the Constraint Forces and Moments

The system's dynamical equations of motion given by equation (3.29) contain the non-working constraint forces and moments vector, $\boldsymbol{\phi}^C$, that is a result of the coupling between the adjacent components of the system. That vector introduces additional variables to the dynamical equations, and hence makes the simulation more complicated. Therefore, a method has to be implemented in order to eliminate the vector $\boldsymbol{\phi}^C$ from the equations of motion and will be presented next.

The linear kinematic velocity constraints of the system and the *natural orthogonal complement* associated with the matrix of constraint coefficients will be derived first.

An expression relating the *natural orthogonal complement* N, the generalized extended velocity vector, $\dot{\mathbf{w}}$, and the generalized coordinates of the system can be obtained (Cyril et al. 1989) as follows:

$$\mathbf{w} = \mathbf{N}(\dot{\psi} + \dot{\psi}_0) \tag{3.31}$$

and

$$\dot{\psi}_0 = [\Omega, 0, ..., 0]$$

where Ω is the orbital rate of the system and $\dot{\psi}$ is the vector containing the generalized velocities.

An expression for $\dot{\mathbf{w}}$ could be readily obtained as follows:

$$\dot{\mathbf{w}} = \mathbf{N}\ddot{\psi} + \dot{\mathbf{N}}(\dot{\psi} + \dot{\psi}_0) \tag{3.32}$$

It was shown by Cyril et al. (1989) that the result of pre-multiplying the constraint vector ϕ^C by $\mathbf{N}^T$ is zero, i.e.,

$$\mathbf{N}^T\phi^C = 0 \tag{3.33}$$

This is equivalent to saying that vector ϕ^C, which contains the constraint forces and moments, does no work, which is in accordance with the principle of virtual work. Hence, the *natural orthogonal complement* N will be used to eliminate ϕ^C.

Upon pre-multiplication of equation (3.29) by $\mathbf{N}^T$, substitution of equation (3.32), and utilization of equation (3.33) the independent dynamical equations of motion of the system become:

$$\tilde{\mathbf{M}}\ddot{\psi} = \mathbf{c}(\psi, \dot{\psi}, \dot{\psi}_0) + \mathbf{f} \tag{3.34}$$

where,

$$\tilde{\mathbf{M}} = \mathbf{N}^T\mathbf{M}\mathbf{N}$$

$$\mathbf{c} = \mathbf{N}^T[\phi^S - \mathbf{M}\dot{\mathbf{N}}(\dot{\psi} + \dot{\psi}_0)]$$

$$\mathbf{f} = \mathbf{N}^T\phi^E$$

Let N' be defined as $N + nm$. In the above equation, the $(N'\text{x}N')$-dimensional $\tilde{\mathbf{M}}$ is the generalized extended mass matrix of the system, which is symmetric and positive definite. Vector $\mathbf{f}$ represents the *actual* external forces and moments applied, and vector $\mathbf{C}$ contains all the *nonlinear* Coriolis, damping, and centrifugal terms.

It is more convenient, for simulation and control purposes, to partition equation (3.34) into rotational and elastic coordinates-dependent matrices and vectors, denoted by the subscripts θ and b, respectively, as follows:

$$\begin{bmatrix} \tilde{\mathbf{M}}_{\theta\theta} & \tilde{\mathbf{M}}_{\theta b} \\ \tilde{\mathbf{M}}_{b\theta} & \tilde{\mathbf{M}}_{bb} \end{bmatrix} \begin{bmatrix} \ddot{\boldsymbol{\theta}} \\ \ddot{\mathbf{b}} \end{bmatrix} = \begin{bmatrix} \mathbf{c}_\theta \\ \mathbf{c}_b \end{bmatrix} + \begin{bmatrix} \boldsymbol{\tau} \\ 0 \end{bmatrix} \tag{3.35}$$

where,

$$\boldsymbol{\theta} = [\theta_1, \ldots, \theta_N]^T \tag{3.36}$$

and

$$\mathbf{b} = [\mathbf{b}_1, \ldots, \mathbf{b}_n]^T \tag{3.37}$$

where $\mathbf{b}_i$ was previously defined in equation 2.4. The upper part of the generalized external force vector is equal to $\boldsymbol{\tau}$ which corresponds to the nominal joint torques, i.e., the actual joint torques applied, and has the dimension of N. The (nm)-dimensional lower part, however, is noted to be equal to zero, which implies that actuators are only present at the joints and separate distributed generalized forces cannot be applied to explicitly control the *flexible* modes. It is important to note that the above equation and all subsequent ones only apply under the two following conditions:

i) The orbit of the spacecraft's centre of mass is maintained as was mentioned in the introduction of Chapter 2, i.e., the system frame is at the centre of mass of the spacecraft.

ii) Only motion in the orbital plane is allowed.

Chapter 4

Dynamics during the Capture of a Satellite

4.1 Introduction

One of the tasks space robots are designed for is the retrieval of satellites in orbit for either periodical maintenance or repair of a malfunction. Dynamics and control issues associated with the capture of a satellite have to be resolved, and an efficient methodology has to be devised for simulation purposes. There are three stages involved in the capture of a satellite, namely:

1. Approach Dynamics: which is the pre-capture stage and involves trajectory planning of the end-effector in order to chase and arrive at the target.

2. Contact Dynamics: the end-effector latches onto the payload and it rigidizes the connection.

3. Post-Impact Dynamics: which involves the behaviour of the system following the capture.

Researchers such as Umetani and Yoshida (1989b) have studied the approach dynamics, others such as Yoshida et al. (1992) presented the formulation of the collision dynamics using the Generalized Inertia Tensor and the virtual mass concept. However, none of the researchers whose work has been reviewed investigated the effect of the impact resulting from the capture of a payload on the post-capture behaviour of the system. Thus, a methodology will be presented in this chapter that properly accounts for the impact effects and obtains the pitch rate of the mother spacecraft and the joint rates, immediately after impact. These will then be used as initial conditions for the post-impact dynamical simulation.

4.2 Impact Dynamics

Let us suppose that a spacecraft-mounted robot manipulator is preparing to capture a payload by means of its end effector. It is assumed that the payload's mass, m_p, and inertia tensor about its centre of mass, $\mathbf{I}_p$, are known beforehand. Also, at the instant of capture, the payload is expected to have a linear velocity of its centre of mass $\mathbf{v}_p$ and angular velocity $\boldsymbol{\omega}_p$ (Figure 4.1).

Before a dynamical simulation of the post-capture system is carried out, the joint rates of the manipulator and the spacecraft's pitch rate just after capture have to be determined. In other words the effect of capturing a satellite on the spacecraft/manipulator system has to be evaluated. Hence, an expression that could be used to calculate the post-impact rates has to be derived. This is carried out by writing the equation of motion of the spacecraft/manipulator system and that of the payload prior to contact between them. In the derivations to follow, all the bodies involved will be modelled as *rigid* for simplicity. However, the post-impact joint rates

obtained by the method of this section would be used for the dynamical simulation of a system with *flexible* bodies; the initial rates of the elastic coordinates will be given some reasonable values, which implies that the pre-impact rates of the elastic coordinates are unspecified but in principle, can be calculated.

The equation of motion of the spacecraft/manipulator system can be obtained by setting all the elastic-dependent terms in equation (3.35) to zero, and adding the term $\mathbf{J}^T\mathbf{f}_I$ that represents a vector of forces and moments associated with the impact force. The resulting equation could be written as:

$$\tilde{\mathbf{M}}_{\theta\theta}\ddot{\boldsymbol{\theta}} = \mathbf{c}_\theta(\boldsymbol{\theta}, \dot{\boldsymbol{\theta}}) + \boldsymbol{\tau} + \mathbf{J}^T\mathbf{f}_I \tag{4.1}$$

where $\mathbf{J}$ represents the $(6\text{x}N)$ Jacobian of the system and could be written in the following form:

$$\mathbf{J} \equiv \begin{bmatrix} \mathbf{J}_1 \\ \\ \mathbf{J}_2 \end{bmatrix} \tag{4.2}$$

where

$$\mathbf{J}_1 \equiv [\mathbf{e}_1 \text{x} \tilde{\mathbf{r}}_1 \ldots \mathbf{e}_N \text{x} \tilde{\mathbf{r}}_N]_{3\text{x}N} \tag{4.3}$$

and

$$\mathbf{J}_2 \equiv [\mathbf{e}_1 \ldots \mathbf{e}_N]_{3\text{x}N} \tag{4.4}$$

Here $\tilde{\mathbf{r}}_i$ represents the distance from joint i to point $\mathcal{B}$ on the end effector of the robot manipulator, and $\mathbf{e}_i$ is a unit vector along the axis of rotation of joint i.

Similarly the equation of motion of the impacting body, which is modelled as *rigid*, during collision could be written in the following form:

$$\mathbf{M}_p\dot{\mathbf{w}}_p = \mathbf{c}_p(\mathbf{v}_p) - \mathbf{A}\mathbf{f}_I \tag{4.5}$$

where $\mathbf{w}_p$ and $\mathbf{c}_p$ represent the extended velocity vector of the payload, and a vector containing the non-linear Coriolis, damping, and centrifugal terms, respectively. Also,

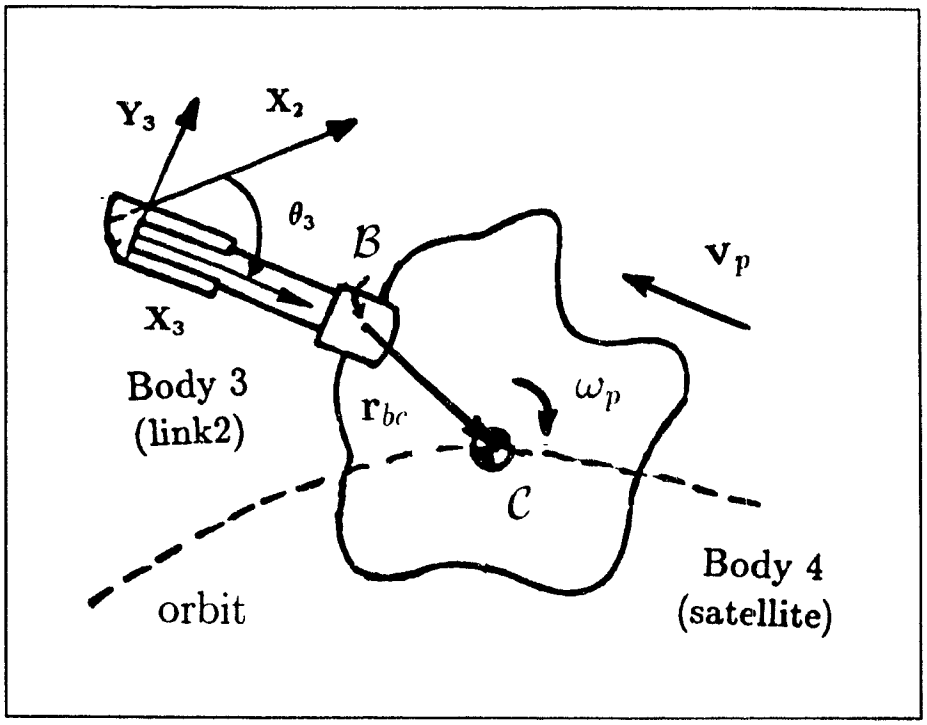

Figure 4.1: Capture of a payload.

$\mathbf{M}_p$ represents the generalized mass matrix of the payload, and is defined as follows:

$$\mathbf{M}_p \equiv \begin{bmatrix} (m_p)\mathbf{1} & \mathbf{0} \\ \mathbf{0} & \mathbf{I}_p \end{bmatrix} \tag{4.6}$$

The term $\mathbf{AF}_I$ on the right hand side of equation (4.5), represents a vector containing the forces and moment acting at the payload's centre of mass, associated with the impact force $\mathbf{f}_I$. Finally $\mathbf{A}$ is a non-singular transformation matrix defined as follows:

$$\mathbf{A} \equiv \begin{bmatrix} \mathbf{1} & \mathbf{0} \\ -\mathbf{R}_{bc} & \mathbf{1} \end{bmatrix} \tag{4.7}$$

where $\mathbf{R}_{bc}$ is the cross-product tensor of $\mathbf{r}_{bc}$ which represents the position vector of the payload's centre of mass $\mathcal{C}$ as measured from the point of contact $\mathcal{B}$, and is defined

as follows:

$$\mathbf{R}_{bc} \equiv \begin{bmatrix} 0 & -z & y \\ z & 0 & -x \\ -y & x & 0 \end{bmatrix} \tag{4.8}$$

The impacting force $\mathbf{f}_I$ resulting from the collision could be easily eliminated from the two equations of motion, i.e., this formulation will only consider the velocities before and after impact without the need for sensing the actual impact force. $\mathbf{f}_I$ could be eliminated upon the pre-multiplication of equation (4.5) by $\mathbf{J}^T\mathbf{A}^{-1}$ and adding the result to equation (4.1), the equations of motion could then be re-written as follows:

$$\mathbf{J}^T\mathbf{A}^{-1}\mathbf{M}_p\dot{\mathbf{w}}_p + \tilde{\mathbf{M}}_{\theta\theta}\ddot{\boldsymbol{\theta}} = \mathbf{c}_\theta + \mathbf{J}^T\mathbf{A}^{-1}\mathbf{c}_p + \boldsymbol{\tau} \tag{4.9}$$

Note that $\mathbf{A}$ is non-singular and $\mathbf{A}^{-1}$ exists.

Next, equation (4.9) is integrated over the period of the impact τ_I, with the assumption that there are no joint torques $\boldsymbol{\tau}$ applied during the impact. The resulting equation after integration is as follows:

$$\mathbf{J}^T\mathbf{A}^{-1}\mathbf{M}_p(\mathbf{w}_{p_f} - \mathbf{w}_{p_i}) + \tilde{\mathbf{M}}_{\theta\theta}(\dot{\boldsymbol{\theta}}_f - \dot{\boldsymbol{\theta}}_i) = \int_0^{\tau_I} (\mathbf{C} + \mathbf{J}^T\mathbf{A}^{-1}\mathbf{c}_p)dt \tag{4.10}$$

where the subscripts i and f signify pre-impact and post-impact values, respectively.

The impact force $\mathbf{f}_I$ during a collision between two bodies is usually very large and acts for a very short impact time of τ_I . Thus, one can say that:

$$\begin{aligned} \tau_I &\equiv O(\epsilon), \epsilon << 1 \\ \dot{\boldsymbol{\theta}}, \mathbf{w}_p, \boldsymbol{\theta}, \mathbf{r}_{bc} &\equiv O(1), \\ \ddot{\boldsymbol{\theta}}, \dot{\mathbf{w}}_p &\equiv O(\frac{1}{\epsilon}) \end{aligned} \tag{4.11}$$

Clearly, the left hand side of equation (4.10) is O(1). The integrand $(\mathbf{C}+\mathbf{J}\mathbf{A}^{-1}\mathbf{c}_p)$ on the right hand side is also O(1); however, the value of the integral is $O(\epsilon)$ and

therefore could be neglected. Thus, equation (4.10) could be re-written as:

$$\mathbf{J}^T\mathbf{A}^{-1}\mathbf{M}_p(\mathbf{w}_{p_f} - \mathbf{w}_{p_i}) + \tilde{\mathbf{M}}_{\theta\theta}(\dot{\boldsymbol{\theta}}_f - \dot{\boldsymbol{\theta}}_i) = 0 \tag{4.12}$$

Equation (4.12) could be applied to all kinds of collisions ranging from plastic ones, where the payload is rigidly attached to the end effector of the robot manipulator after impact, to the elastic ones, where the payload rebounds with no loss of energy. However, of interest here is the case where the payload is successfully captured (plastic case) and the consequent behaviour of the spacecraft/manipulator system. In such a case the extended velocity vector of the payload after impact, $\mathbf{w}_{p_f}$, could be written in terms of $\mathbf{J}$, $\mathbf{R}_{bc}$, and $\dot{\boldsymbol{\theta}}_f$ as follows:

$$\mathbf{w}_{p_f} \equiv \tilde{\mathbf{J}}\dot{\boldsymbol{\theta}}_f \tag{4.13}$$

where,

$$\tilde{\mathbf{J}} \equiv \begin{bmatrix} \mathbf{J}_1 - \mathbf{R}_{bc}\mathbf{J}_2 \\ \mathbf{J}_2 \end{bmatrix} \tag{4.14}$$

By substituting equations (4.13) and (4.14) into equation (4.12) and re-arranging, the following is obtained:

$$\dot{\boldsymbol{\theta}}_f = \mathbf{G}^{-1}\mathbf{H} \tag{4.15}$$

where

$$\mathbf{G} = \mathbf{J}^T\mathbf{A}^{-1}\mathbf{M}_p\tilde{\mathbf{J}} + \tilde{\mathbf{M}}_{\theta\theta} \tag{4.16}$$

$$\mathbf{H} = \mathbf{J}^T\mathbf{A}^{-1}\mathbf{M}_p\mathbf{w}_{p_i} + \tilde{\mathbf{M}}_{\theta\theta}\dot{\boldsymbol{\theta}}_i \tag{4.17}$$

from which, for the planar case, the pitch rate of the mother spacecraft as well as the joint rates of the manipulator just after impact could be solved for in terms of the pre-impact extended velocity vector of the payload, and the joint rates of the manipulator, $\mathbf{w}_{p_i}$ and $\dot{\boldsymbol{\theta}}_i$, respectively. These rates could then be used as the initial conditions for the post-impact dynamical simulation of the system.

Chapter 5

Control Design

5.1 Introduction

There are generally two objectives of the control of a robot manipulator system. The first involves trajectory planning of the arm where it is moved via an actuator torque, calculated using a PID control law, to a desired configuration. The other objective is simply to maintain stability following a disturbance by applying appropriate control torques; e.g., capture of a spinning satellite. The captured satellite in this thesis is considered to be a deterministic disturbance; i.e., the inertia and dynamic properties are presumed to be known beforehand. However, in a realistic situation there could be some parameter uncertainties and some noise in the system which might complicate the control design and undermine its effectiveness.

In this thesis, the control scheme developed will only be concerned with the post-capture behaviour of the system, i.e., appropriate joint torques will be calculated and applied to achieve the desired final values. The *computed torque method*, which will be used to calculate to control torques, is presented next.

5.2 Computed Torque Method

This method will be used to calculate the appropriate control torques needed to achieve the specified final values of the rotation-dependent coordinates of the system. Due to the highly non-linear nature of the equations of motion in this thesis in particular and in multi-body dynamics in general, they are first linearized via appropriate feedback. Therefore, this control method is sometimes referred to as feedback linearization control. The torque calculations are carried out by first obtaining the values of the spacecraft attitude, the the joint angles, the tip deflections, and their rates which are measured by collocated sensors at the joints and possibly at the end-effector. The required torques that achieve control could then be calculated based on these sensors' measurements. This control method assumes that all the state variables are available. The actuators needed to apply the torques, which are generally motors, are located at the joints, except for the spacecraft where the control is achieved by means of jet thrusters or reaction wheels.

In the following subsections the feedback linearization control torques will be calculated by first assuming that the manipulator is *rigid*. Next, the effects of flexibility will be evaluated and they will be included in the control design.

5.2.1 Control of the Rigid System

For *rigid* link manipulators, the joint angles and their rates are obtained from the measurements of collocated sensors at the joints. By setting all the flexibility related matrices in equation (3.35) to zero, the equation of motion for the *rigid* system can be written as:

$$\tilde{\mathbf{M}}_{\theta\theta}\ddot{\boldsymbol{\theta}} = \mathbf{c}_\theta + \boldsymbol{\tau} \tag{5.1}$$

The actuator torques required to suppress the disturbance resulting from the capture of a payload can be calculated using the following:

$$\tau = -\tilde{\mathbf{M}}_{\theta\theta}[\mathbf{D}_1\dot{\theta} + \mathbf{D}_2(\theta - \theta_d)] - \mathbf{c}_\theta \tag{5.2}$$

where,

$$\mathbf{D}_1 = \text{diag}(2\zeta_1\omega_1, 2\zeta_2\omega_2, ..., 2\zeta_N\omega_N)$$

$$\mathbf{D}_2 = \text{diag}(\omega_1^2, \omega_2^2, ..., \omega_N^2)$$

are diagonal matrices containing the control gains, and θ_d contains the desired final values of the joint angles. It must be noted that vector $\mathbf{c}_\theta$ in equation (5.2) represents the nonlinear compensation term.

By substituting equation (5.2) into equation (5.1), a set of linearized, uncoupled, and homogeneous equations of motion are obtained and could be written as

$$\ddot{\theta} + \mathbf{D}_1\dot{\theta} + \mathbf{D}_2(\theta - \theta_d) = 0 \tag{5.3}$$

5.2.2 Control of the Flexible System

Control of *flexible* manipulator systems is far more complex than the *rigid* case. This is a result of the coupling between the rotation and bending coordinates. A different control strategy altogether has to be followed in order to attain the desired results. Another complication in the control of *flexible* manipulators arises due to the more involved measurement of the joint rotation angle. The angle between two consecutive links represents the sum of the joint rotation due to the actuator of the current link and the deflection due to flexibility of the previous one (see Figure 2.2).

There can be basically three possible approaches used for *flexible* system control, they are as follows :

1) The elastic effects are ignored; i.e., the equation of motion is assumed to be as in equation (5.1). By this method the *flexible* system is treated as a *rigid one*. The

computed torque by this model would give good results only if the elastic effects due to the links' flexibility are negligible, otherwise it may result in gross inaccuracies in the positioning of the end-effector.

2) The elastic effects are included in the mathematical model, and their amplitudes could be determined from the sensor readings by means of an estimator. This model accounts for the *flexible* degrees of freedom in the calculation of the torques and treats them as known disturbances but does not explicitly control them. Therefore, some residual oscillations in the tip deflections of the links are expected before they are damped to zero as a result of structural damping inherent in the material of the links.

3) Active control of both the rotational and bending coordinates, which is achieved by applying both torques and generalized forces. Such control is only possible if actuators capable of applying transverse forces to the links are present.

The approach presented in (3) is still in the experimental stages and has not been used in an actual situation. Therefore, the only feasible model that could be implemented at the present time is the one that treats the elastic deformations as known disturbances, but does not explicitly control them, namely (2).

The bending coordinates can be solved for in terms of the rotational coordinates and equation (3.35) could be re-arranged as:

$$\hat{\mathbf{M}}\ddot{\boldsymbol{\theta}} = \hat{\mathbf{c}}(\boldsymbol{\psi}, \dot{\boldsymbol{\psi}}) + \boldsymbol{\tau} \tag{5.4}$$

where,

$$\hat{\mathbf{M}} = \tilde{\mathbf{M}}_{\theta\theta} - \tilde{\mathbf{M}}_{\theta b}\tilde{\mathbf{M}}_{bb}^{-1}\tilde{\mathbf{M}}_{b\theta}$$

$$\hat{\mathbf{c}} = \mathbf{c}_{\theta} - \tilde{\mathbf{M}}_{\theta b}\tilde{\mathbf{M}}_{bb}^{-1}\mathbf{c}_{b}$$

The feedback linearization control torque that produces an equation of controlled motion similar to equation (5.3) is given by:

$$\boldsymbol{\tau} = -\hat{\mathbf{M}}[\mathbf{D}_1\dot{\boldsymbol{\theta}} + \mathbf{D}_2(\boldsymbol{\theta} - \boldsymbol{\theta}_d)] - \hat{\mathbf{c}} \tag{5.5}$$

The above torque calculations are based on the true parameters of the system. Hence, it is assumed that $\mathbf{b}$ and $\dot{\mathbf{b}}$ could be estimated, possibly by means of an accelerometer located at a point close to the tip of the link. This will obtain $\ddot{\mathbf{b}}$ which could be easily integrated to obtain the values $\mathbf{b}$ and $\dot{\mathbf{b}}$. The robustness of the controller has not been evaluated because it is beyond the scope of this thesis.

The control torque vector τ in equation (5.5) is of the same order as the *rigid*-body degrees of freedom, consequently a control strategy similar to that used for the *rigid* manipulator, can be used for the *flexible* manipulator as well.

5.3 Modified Control for Improved Positioning of the End Effector

The control method described in the previous section controls the joint angles and would produce good position control of the end effector provided that the tip deflections of the links, due to structural flexibility, are small. For those systems where the elastic deformations and their rates are not small, a modified control law, that accounts for their effects, has to be designed and implemented if a better accuracy in the positioning of the end-effector is sought. Otherwise, the deflections will cause the end-effector to oscillate and the accuracy in its positioning will be substantially affected, possibly causing it to miss its target.

By incorporating the rotations of the links resulting from the structural flexibility into the control law a better positioning of the end-effector, without having to explicitly control the elastic coordinates and their rates, is expected. This could be explained by recalling that the vector θ, used in the control algorithm of the previous section, contains the angles θ_i's. For a body i, θ_i is defined as the angular rotation

of its X-axis, X_i, relative to the X-axis of the previous body, namely X_{i-1}, measured along the positive direction of Z_i. Those axes, which were defined in section 2.5, correspond to the *rigid* body motion only. Thus, they do not account for the *flexible* motion resulting from the elastic deformations. Therefore, vector $\boldsymbol{\theta}$ in equation (5.5) could be replaced by $\hat{\boldsymbol{\theta}} = \boldsymbol{\theta} + \Delta\boldsymbol{\theta}$ where, $\Delta\boldsymbol{\theta}$ is given in the following table:

Body(i-1) \ Body(i)	Rigid	Flexible
Rigid	0	φ_i
Flexible	$-\varphi_{i-1}$	$\varphi_i - \varphi_{i-1}$

Table 5.1: Adjustments needed for θ_i

Here φ_i, which is the slope of the line joining the origin of link i's body-fixed frame to its tip (see Figure 2.2), is defined as:

$$\varphi_i = tan^{-1}(\frac{\mu_{i(2)}}{l_i}) \tag{5.6}$$

where $\mu_{i(2)}$ represents the in-plane tip deflection of link i and l_i represents the length of link i. Hence, it could be seen from table 5.1 that the proper adjustment of θ_i will depend on whether the current and the previous bodies are *rigid* or *flexible*. A similar adjustment has to be done to $\dot{\boldsymbol{\theta}}$.

Finally, the modified vectors $\hat{\boldsymbol{\theta}}$ and $\dot{\hat{\boldsymbol{\theta}}}$, obtained by applying the proper adjustments, according to table 5.1, to vectors $\boldsymbol{\theta}$ and $\dot{\boldsymbol{\theta}}$, could be used to achieve position control of the end effector. The modified control torque to be implemented could be written as:

$$\boldsymbol{\tau} = -\hat{\mathbf{M}}[\mathbf{D}_1\dot{\hat{\boldsymbol{\theta}}} + \mathbf{D}_2(\hat{\boldsymbol{\theta}} - \boldsymbol{\theta}_d)] - \hat{\mathbf{c}} \tag{5.7}$$

5.4 Attitude Control of the Mother Spacecraft

The objective of this scheme is to control only the *attitude* of the mother spacecraft following a disturbance, e.g. capture of a satellite, without controlling the manipulator joint angles and their rates. The attitude of the mother spacecraft must be maintained, otherwise it will affect the orbit maintenance manoeuvres, since the thrusters will fire along incorrect directions.

Before calculating the torque required for such control, one has to obtain an equation of motion of the mother spacecraft that does not contain any coupling terms with the joint accelerations. This is achieved by the pre-multiplication of equation 3.34 by $I_1\tilde{\mathbf{M}}^{-1}$ and considering only the first equation. The following uncoupled equation can be obtained:

$$I_1\ddot{\theta}_1 = \bar{c}(\psi, \dot{\psi}, \dot{\psi}_0) + \tau_1 \tag{5.8}$$

where I_1 represents the moment of inertia of the spacecraft about its centre of mass, and $\bar{c}$ is a linear combination of the components of vector $\mathbf{c}$, which contains the non-linear terms and is dependent on $\boldsymbol{\theta}$, $\mathbf{b}$, and their derivatives.

A **PD** control torque, which linearizes the equation of motion, can be applied to achieve spacecraft attitude control. It could be presented as: as:

$$\tau_1 = -I_1(2\zeta_1\omega_1\dot{\theta}_1 + \omega_1^2\theta_1) - \bar{c} \tag{5.9}$$

where ζ_1 and ω_1 are appropriate control gains.

By substituting equation (5.9) into equation (5.8) the feedback-linearized equation of motion of the spacecraft can be written as:

$$\ddot{\theta}_1 + 2\zeta_1\omega_1\dot{\theta}_1 + \omega_1^2\theta_1 = 0 \tag{5.10}$$

which is a linear, uncoupled, homogeneous equation whose response will depend on the values of the gains ζ_1 and ω_1.

Chapter 6

Simulation Results and Discussion

6.1 Introduction

In this chapter some simulation results are presented with the purpose of demonstrating the effects of capturing a satellite by a spacecraft/manipulator system. The effect of flexibility on the system is also investigated and its effects on the performance of the system are evaluated by comparing the results that model the links as *rigid* with those that model the links as *flexible*.

In the dynamical simulation carried out, the shape functions used for modelling the elasticity of the links were assumed in advance, hence they are referred to as the *assumed modes method* (Meirovitch 1987). That method usually involves choosing a set of admissible functions that adequately represent the link shapes and satisfy at least the geometric boundary conditions. The admissible functions could be chosen from any of the following: polynomials, harmonic functions, splines, or eigenfunctions. In this model eigenfunctions of a clamped-free beam are chosen as admissible functions because of their orthogonal properties. Cetinkunt and Book (1987) concluded after thorough experimental and theoretical investigations that the choice of eigenfunctions

of a clamped-free beam provides the best approximations possible of a flexible link.

The initial-value problem to be solved involves a set of highly non-linear, coupled, stiff, ordinary differential equations It may be noted here that a system is considered stiff if the ratio between its largest and smallest eigenvalue is large (Gear 1971). Therefore, the numerical integration method used should be able to handle stiff systems that have slowly and rapidly changing components at the same time. One of the best available multi-step scheme, that is based on Gear's method, is the IMSL subroutine DIVPAG and was used in this thesis to integrate the differential equations of motion.

6.2 Data Used in the Simulation

The simulation of a spacecraft-manipulator system as it captures a payload (Figure 2.1) was carried out for the planar case only. The relevant parameters of the various components of the system are shown in Table 6.1.

Body	l (m)	m (kg)	EI (Nm^2)	I_{zz} (kgm^2)
1	N/A	10000	N/A	40000
2	8.13	20	$8.81x10^3$	440.65
3	8.13	20	$8.81x10^3$	440.65
4	N/A	1000	N/A	500

Table 6.1: Parameters of a 4-Body System

The moment of inertia I_{zz} for bodies 1 and 4 is about the body's centre of mass, and that for bodies 2 and 3, which are links, is about the joint of that link. As was mentioned earlier, the payload was assumed to be initially spinning about an axis normal to the plane of orbit, better known as the orbit normal.

The flexibility in the robot's links is modelled by one mode. It was found, through simulation results, that the contribution of the higher modes was negligible and using two modes yielded results that are very close to those using one mode only. Hence, the total number of degrees of freedom of the system to be simulated is 6, of which 4 are rotation-dependent and 2 are flexibility-dependent. Finally, the tolerance input, which reflects on the magnitude of the simulation errors, is of the order of 10^{-8}, and the integration step size is equal to 10^{-4}.

6.3 Calculation of the Initial Conditions

When a payload is captured by a spacecraft-mounted robot with an impact, the generalized velocities will be affected. Hence, the post-capture values are ought to be calculated and are subsequently used as initial conditions for a dynamical simulation of the system. It is assumed that the effect of capturing a payload on the spacecraft pitch and joint angles is negligible due to the small impact duration, hence their pre-capture values could be directly used for the post-capture simulation. On the other hand, the spacecraft's pitch rate, and joint rates of the manipulator's links will be substantially affected and are solved for using equation (4.15). The values calculated here are crucial because they will govern the subsequent behaviour of the system, hence they should be fairly accurate in order for the simulation results to be realistic.

The calculations of the post-impact initial conditions, as seen in equation (4.15),

will depend on the inertial (mass and inertia) and dynamical (linear and angular velocity) of the payload, the initial configuration of the system, and joint rates of the robot manipulator prior to berthing. In order to proceed with the calculations, the pre-impact linear and angular velocities of the payload must be accurately known beforehand. These values are used in order to calculate the velocity of the manipulator's hand at the point of contact. One would like to achieve a smooth capture, i.e., at the instant of capture there is no impact, or in other words there is no relative motion, at the point of contact, between the body to be captured and the manipulator's hand. In a realistic situation, however, a velocity mismatch between the end effector and the payload is bound to occur because one could only estimate approximately the magnitude and direction of the payload's velocity. Hence, the resulting capture will not be smooth. The effects of a velocity mismatch on the system will be investigated by comparing the corresponding results to those associated with a smooth capture.

After the extended velocity vector of the hand, $\mathbf{w}_{h_i}$, which contains its linear and angular velocities, is determined, the pitch rate of the mother spacecraft and the joint rates of the manipulator's links, represented by vector $\dot{\boldsymbol{\theta}}_i$, could be calculated. This is carried out by solving the inverse kinematics problem of the manipulator according to the following relation:

$$\mathbf{w}_{h_i} = \mathbf{J}\dot{\boldsymbol{\theta}}_i \tag{6.1}$$

where $\mathbf{J}$, which is defined in equations (4.2-4.4), represents the Jacobian of the system and subscript i signifies the pre-capture parameters. Finally, the vector containing the mother spacecraft's pitch rate as well as the joint rates of the links, $\dot{\boldsymbol{\theta}}_f$, just after capture is calculated by solving equation (4.15). Those rates will then be used as the initial conditions for the post-capture simulation of the system.

6.4 Results for the Uncontrolled Case

6.4.1 Smooth Capture

A dynamical simulation of the uncontrolled system after a smooth capture, was first carried out. The payload is assumed to be cylindrical in shape with a radius and length of 1 m each. Its initial angular velocity, ω_p, is $\frac{1}{2}$ rpm about the negative direction of the orbit normal, and linear velocity of its centre of mass relative to the mother spacecraft, $\mathbf{v}_p$, is assumed to be zero at the instant of contact. The velocity of the hand, $\mathbf{v}_h$, is taken as 0.052 m/sec in the direction shown in Figure 6.1, which matches the payload's velocity at the point of contact, $\mathbf{v}_B$, in both magnitude and direction, i.e., smooth capture is achieved. The corresponding rates of the manipulator are then calculated, as explained in section 6.3, and used as the initial conditions for the post-capture simulation. Material damping was incorporated in the model in order to make it more realistic; this also has the effect of damping out the oscillations resulting from structural flexibility as explained in subsection 3.3.1.

Figures (6.3 & 6.4) show the response of the spacecraft's pitch θ_1 and joint angles θ_2, θ_3, and θ_4 and their rates, respectively as a result of capturing a spinning satellite. It is found that, without any control, the spacecraft's pitch remains negligible until about 45 seconds, after which it suddenly starts to increase sharply at a rate of 0.05 deg /sec. At the same instant the end effector's joint angle, θ_4, reaches a maximum rotation of 120 deg, which is beyond the capability of the joint and would probably cause breakage, and its rate reverses direction. It is interesting to note that both behaviours coincides with the instant at which the joint angle θ_3 (corresponding to the rotation of the second link with respect to the first one) becomes zero, i.e., the two links of the manipulator become co-linear. The configurations of the post-

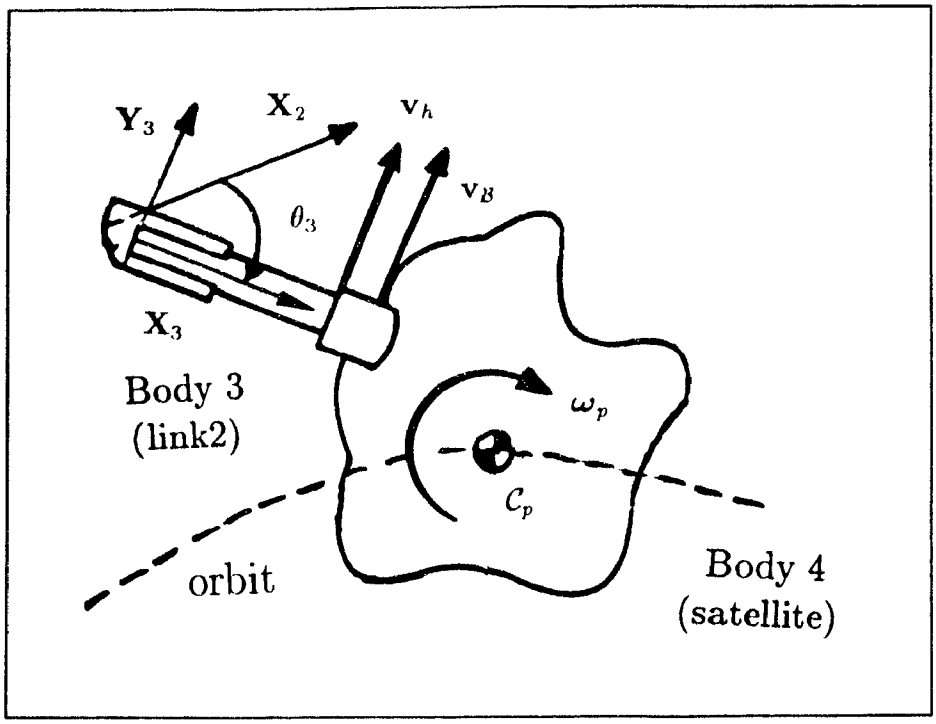

Figure 6.1: Velocities corresponding to smooth capture.

capture system, in which all bodies where modelled as *rigid*, are shown in Figure 6.8. One can see that, just after the manipulator's links become co-linear, the payload, whose trajectory is represented by the dashed line, starts to move towards the mother spacecraft. This result is quite significant because it implies that the captured payload could be retrieved to some extent without the application of any joint joint torques which can save some energy and extend the life of the joints and actuators.

The tip deflections of the links resulting from the elasticity, and their rates (Figure 6.5) are quite reasonable and the oscillations damp out fairly quickly due to the incorporation of a structural damping ratio η of 0.01 in the model. The incorporation of damping is very essential because it account for the energy lost in the links as they deform elastically. Otherwise, the tip deflections and their rates will have an oscillatory behaviour as shown in Figure 6.6.

In order to validate the model used and to show that the results obtained are

realistic, the total energy of the system was plotted versus time. As could be seen from Figure 6.7, the total energy is virtually constant with no noticeable variations.

6.4.2 Hard Impact (Velocity Mismatch)

As mentioned in section 6.3 in order to achieve a smooth capture the linear and angular velocities of the impacting body have to be accurately known beforehand. However, in a realistic situation the velocities could only be estimated and therefore a velocity mismatch between the payload and the manipulator's end effector is bound to occur. This in turn will result in a harder impact on the spacecraft/manipulator system. In this simulation, the parameters of the payload are the same as in the previous section. However, the velocity of the hand, $\mathbf{v}_h$ was chosen as 0.1 m/sec in the direction shown in Figure 6.2.

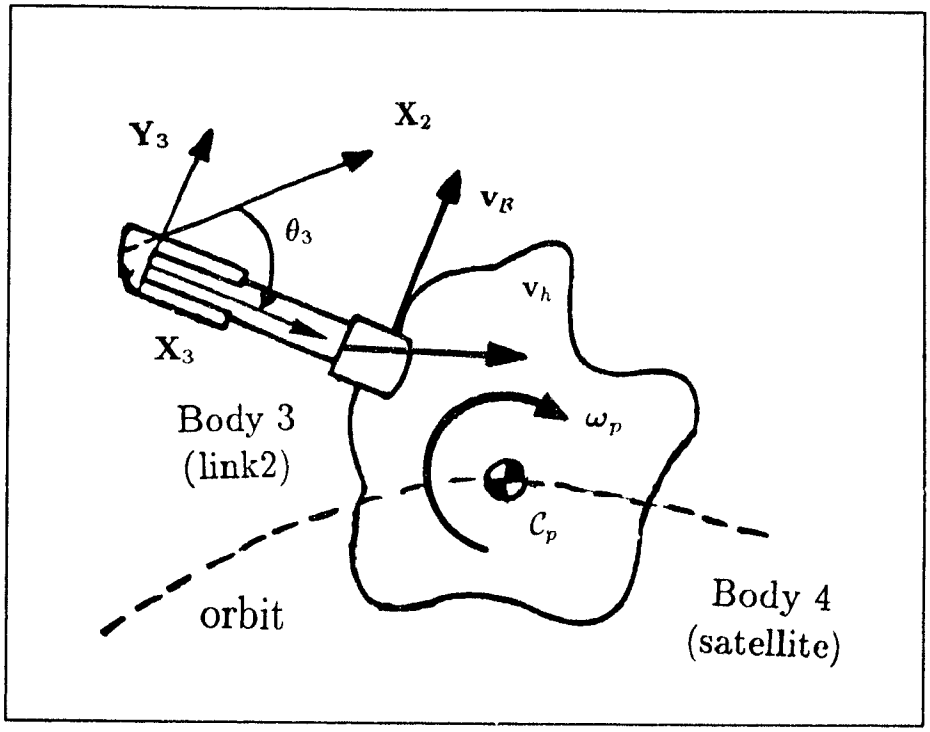

Figure 6.2: Velocities corresponding to a hard impact.

Figures (6.9-6.11) compare the effects of a soft and a hard impact on the post-capture behaviour of the system. It can be concluded from the obtained results that the type of impact could be quite crucial and that a soft impact will have the least adverse effects on the system. For the case of a velocity mismatch (hard impact) the spacecraft pitch angle at the end of the simulation period is 1 deg higher than that of the smooth capture case. Also, it is found, from the particular case studied, that the elastic deformations and their rates corresponding to a hard impact are almost double that of their counterparts for smooth capture. These results emphasize the importance of having a good estimate of the payload's velocity before impact in order for the capture to be as smooth as possible.

6.5 Results for the Controlled case

6.5.1 Feedback Linearization Control

In the absence of control, the mother spacecraft experiences an attitude drift, the links can undergo large rotations, and the payload rotates beyond the capacity of the end effector's joint. Thus, a control system is needed to prevent this. A control law is used based on feedback linearization in order to obtain a set of uncoupled, linear, and homogeneous equations of motion for the closed loop system, as was shown in Chapter 5. The control torque τ applied depends on whether the components of the system are treated as *rigid* or *flexible*. The torque applied in the case of a *rigid* system is presented in equation (5.2), and that for the *flexible* system could be found in equation (5.5). A simulation was carried out using the aforementioned joint torques and the results obtained are shown in Figures (6.12-6.15).

The nominal joint control torques and thrusters corresponding to the *rigid* sys-

tem (solid line) (Figure 6.12) are active for only about 20 seconds with a maximum magnitude of the order of 10 Nm. After that the joint torques approach zero, which means that the desired joint angles and rates were attained. On the other hand, the same figure shows that the applied torques for the *flexible* case are substantially different and have an oscillatory behaviour. This could be explained by recalling that those torques were designed to compensate for the nonlinear terms which, after the rotation coordinates are controlled, are dependent on the flexible coordinates only. Therefore, the oscillations in the control torques persist as long as the oscillations in the links are present. It may be recalled that the flexible modes were not controlled.

The response of the spacecraft's pitch, the joint angles, and their rates is very good and can be found in Figures 6.13 and 6.14 The spacecraft's pitch is maintained almost at zero throughout the simulation period, while the end-effector rotates a mere 7 deg before the rotation is reduced to zero. This compares with, in the absence of control, a total rotation of approximately 3 deg for the spacecraft and 120 deg for the payload. The links' joint angles and rates reach steady state fairly quickly, and the configuration of the system after control is identical to the pre-capture one, thanks to the position and velocity tracking available in the control algorithm. Figure 6.15 shows the oscillatory behaviour of the link tip deflections and their rates which were excited due to the application of the joint torques. The explanation behind this is that the flexible modes are only accounted for in the control algorithm but are not explicitly controlled. The links' oscillations take a while to die down because the only kind of damping incorporated in the model is the one inherent in the material of the links, which is quite small. In practice, the effective damping would be larger. Active control of the elastic generalized coordinates could only be achieved by applying transverse control forces along the links by means of distributed actuators or the

integration of piezoelectric materials within the links (e.g. van Poppel 1992).

The position of the robot's end effector relative to the mother spacecraft is plotted in Figure 6.16, where the circles and stars represent the position at each time step for the *rigid* and *flexible* controls, respectively. One can see that, if the links are *rigid*, the end-effector position is maintained after about 20 seconds. However, for the *flexible* case, the position is shown to be oscillating in a region represented by the framed box, for time greater than 20 seconds. These oscillations are undesirable because they render the manipulator inaccurate and might cause the end effector to miss its target. The figure also shows the importance of modelling a link as *flexible* in order to obtain realistic results. A *flexible* link could only be modelled as *rigid* if the elastic deformations are very small and neglecting them will have a negligible effect on the positioning of the end effector.

6.5.2 Modified Control for Better Positioning of the End Effector

In cases where the effect of the flexibility in the links is substantial, a modified joint control torque has to be applied in order to achieve better accuracy in the positioning of the end-effector. Details of the scheme are presented in section 5.3. The modified control torques, shown in Figure 6.17, implemented are found to be slightly higher than those needed to achieve joint control. Hence, the effect of the modified control torque on the link tip deflections and their rates is minimal as seen in Figure 6.20. The only substantial difference between the two control schemes can be seen in the response of the joint angles and their rates in Figures (6.18 & 6.19), respectively. They are found to demonstrate an oscillatory behaviour similar in nature to that of the link tip deflections, and their rates. This kind of response is expected because

the modified angles and their rates are designed to account for, in addition to the *rigid* rotations, the tip rotation of the links due to the structural flexibility. This ensures a better accuracy in the positioning of the end effector. The effectiveness of the modified control method is validated by Figure 6.21 where the position of the end effector relative to the mother spacecraft is plotted. After about 20 seconds the position, represented by the framed box, is shown to converge to a point very close to that prior to the capture (t=0).

6.5.3 Spacecraft Attitude Control

In some situations only the attitude of the mother spacecraft is needed to be controlled at all times in order to maintain its trajectory. Therefore, with that objective in mind, a simulation was carried out by implementing a control torque that can be calculated using equation (5.9). That control torque on the mother spacecraft required to maintain its pitch as close as possible to zero is presented in Figure 6.22. It is found that the spacecraft's torque is only active for about 15 seconds with a maximum value of 6 Nm, while no torques are applied to the manipulator's joints. The implementation of the control torque is very effective as seen in Figure 6.23 where the spacecraft drifts by a mere 0.07 deg compared to 3 deg for the uncontrolled case. It is also found from Figure 6.24 that the spacecraft's pitch rate responds quite well to the control torque where it only reaches a maximum of 0.01 deg/sec compared to a steady value of 0.06 deg/sec in the uncontrolled case. Due to the small magnitude of the control torque and its short duration, its effect on the joint angles, link tip deflections, and their rates is negligible. This can be seen by comparing Figures 6.23, 6.24, and 6.25 to Figures 6.3, 6.4, and 6.5, respectively.

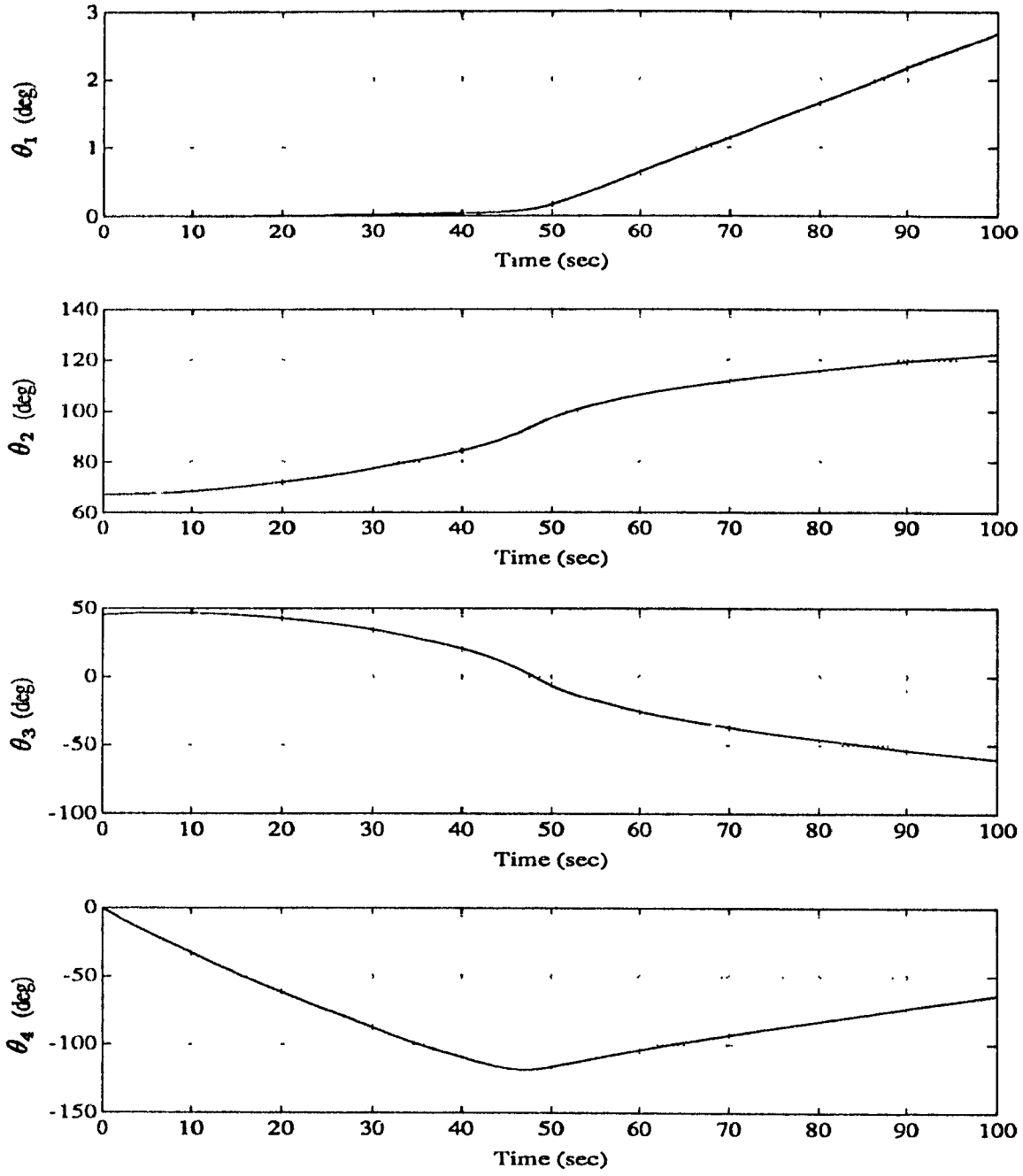

Figure 6.3: Spacecraft's pitch and joint angles corresponding to the uncontrolled system with material damping incorporated (— rigid .... flexible).

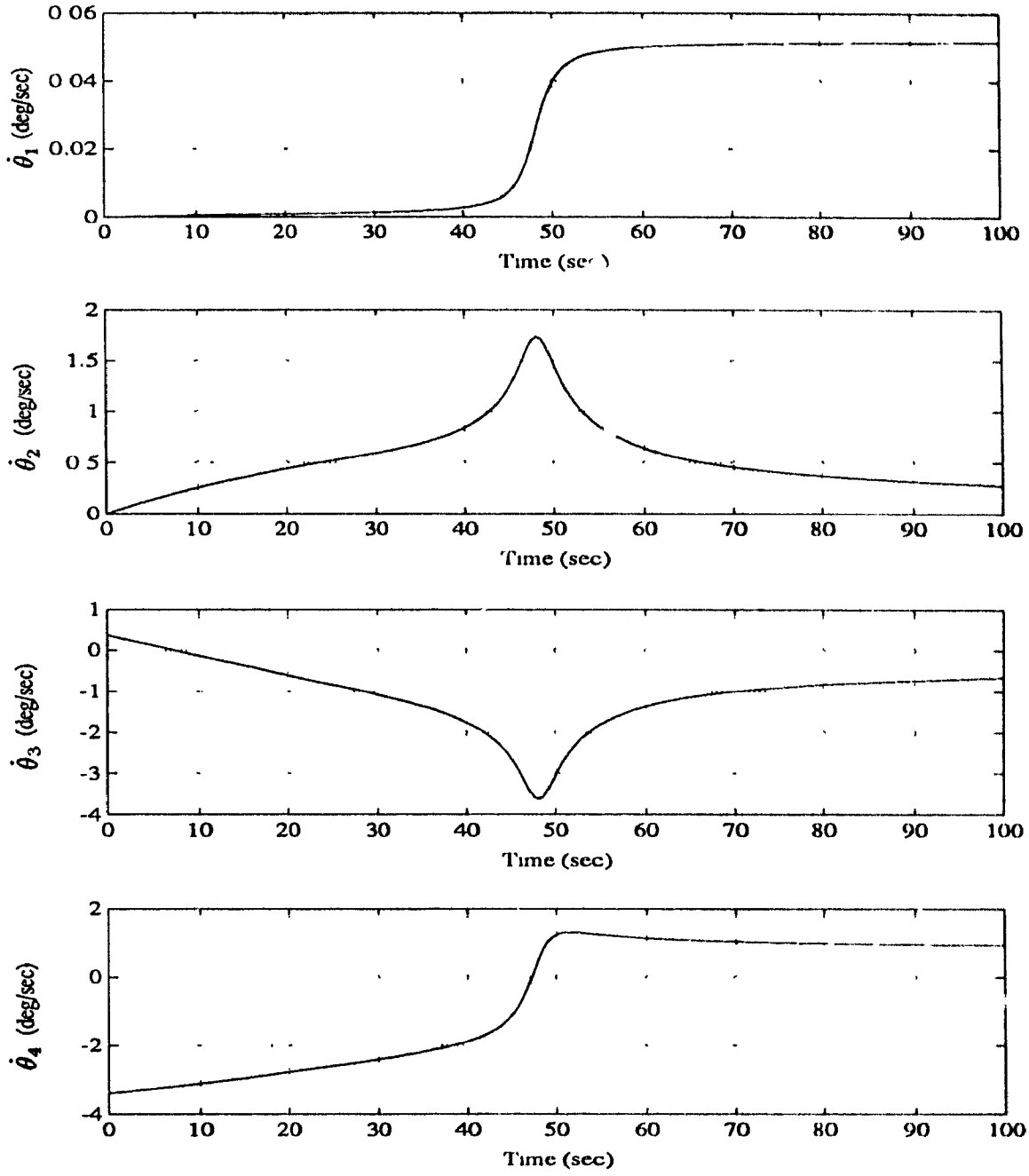

Figure 6.4: Spacecraft's pitch rate and joint rates corresponding to the uncontrolled system with material damping incorporated (– – rigid . .. flexible).

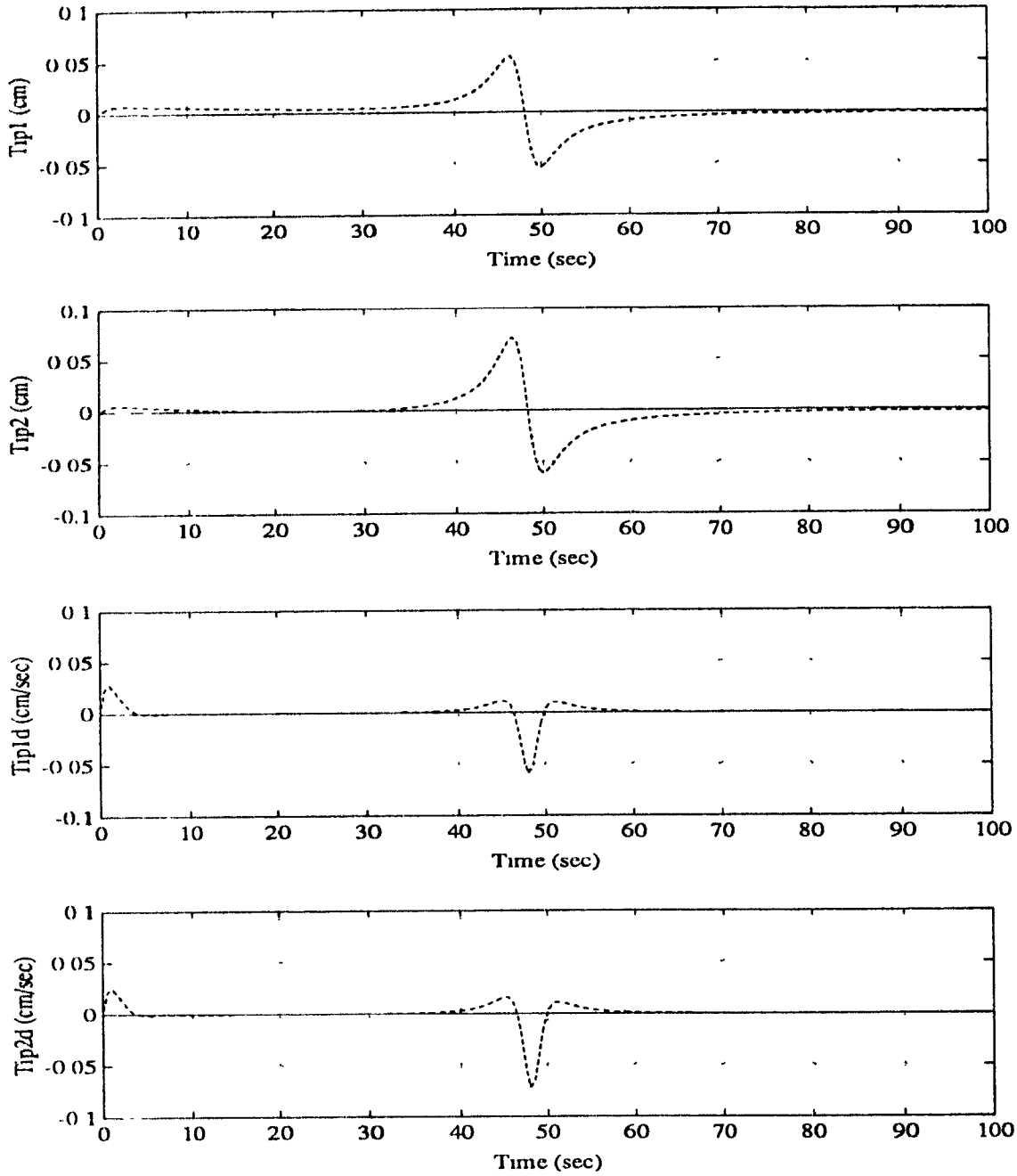

Figure 6.5: Link tip deflections and their rates corresponding to the uncontrolled system with material damping incorporated (— rigid .... flexible).

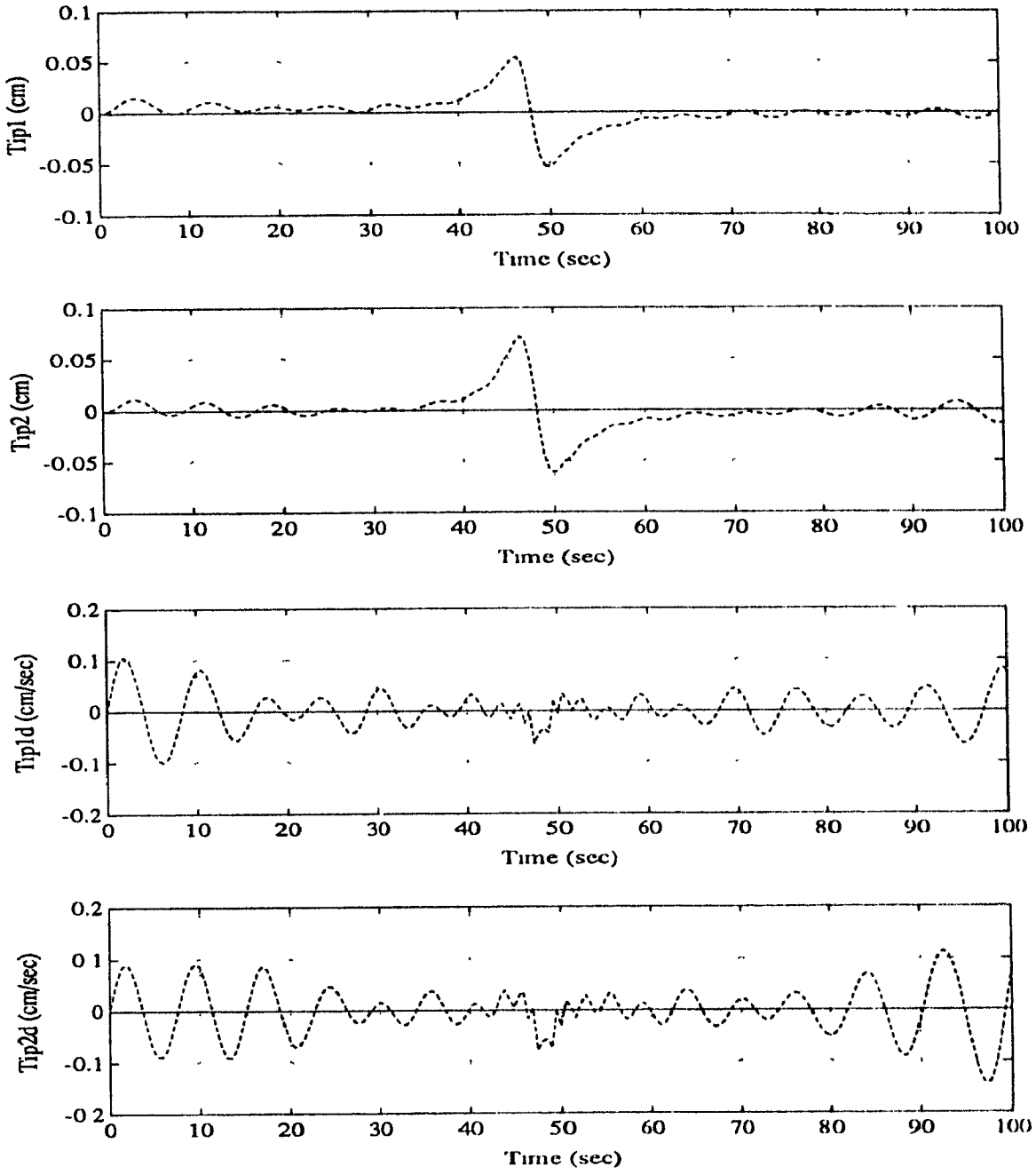

Figure 6.6: Link tip deflections and their rates corresponding to the uncontrolled system **without** material damping incorporated (- - rigid .... flexible)

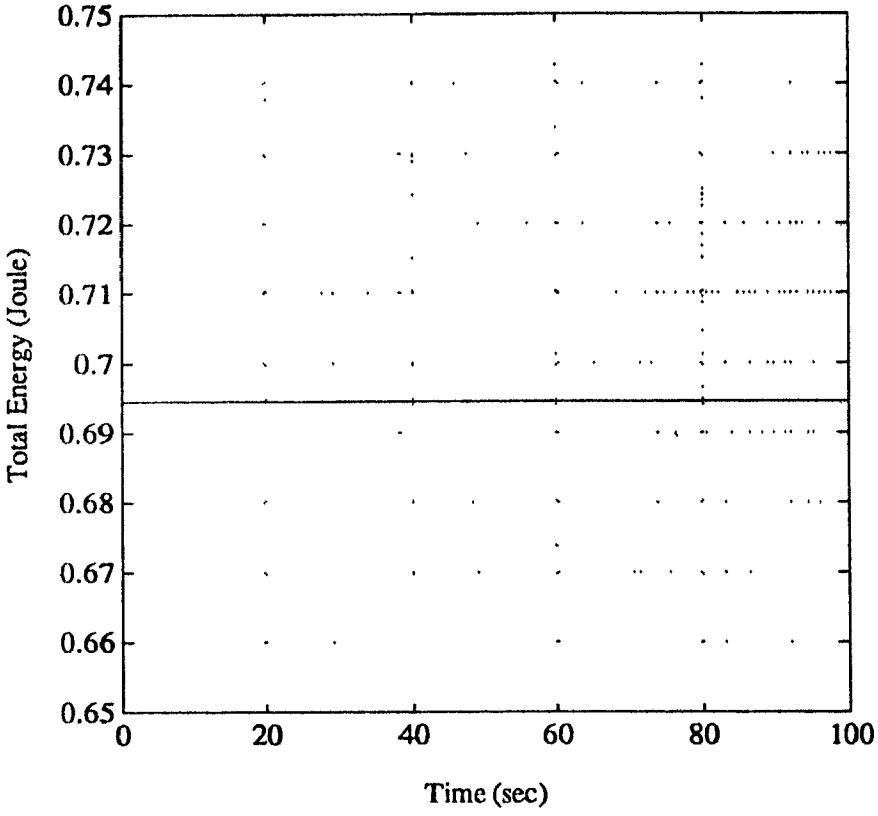

Figure 6.7: Total Energy of the System.

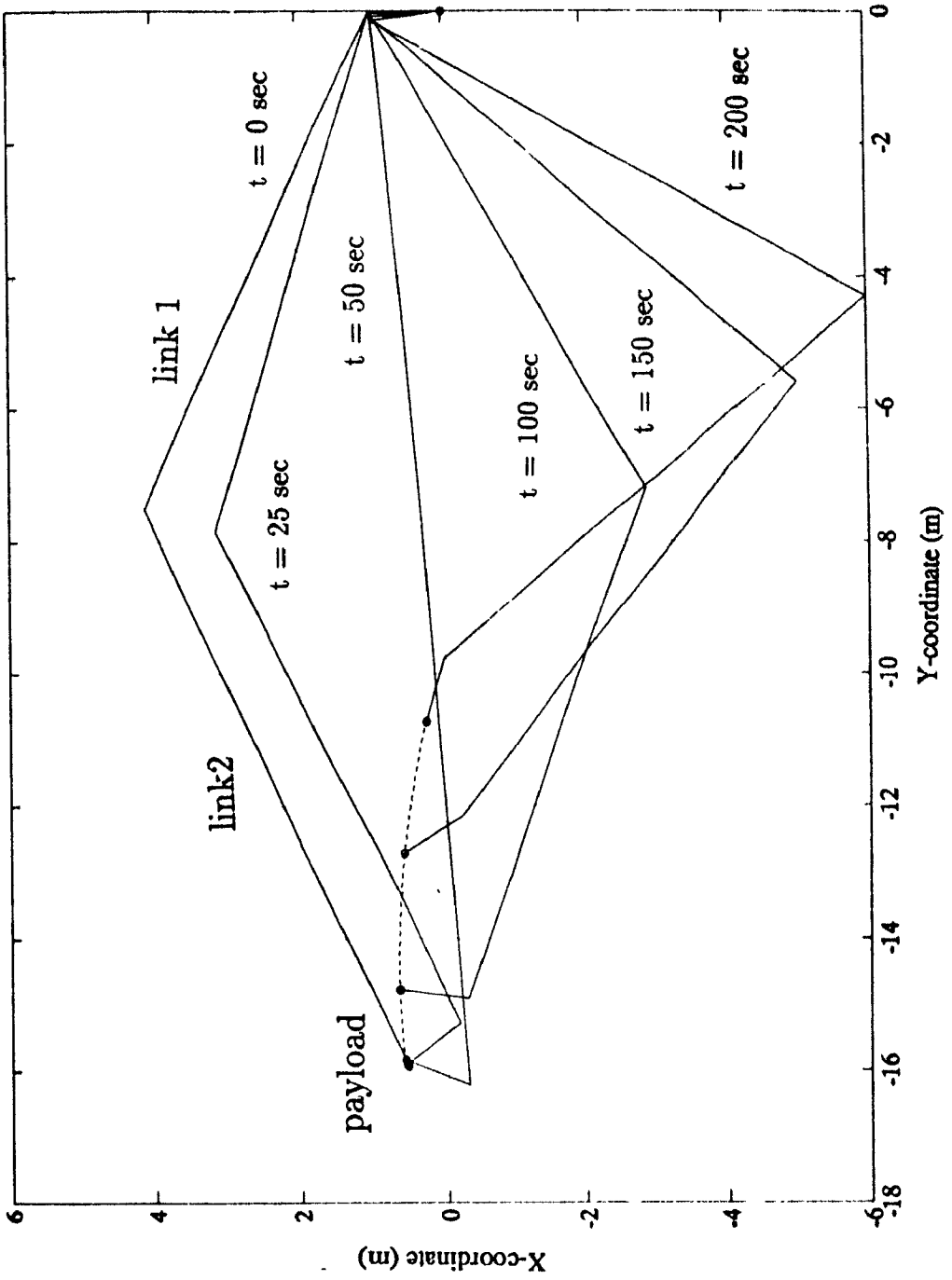

Figure 6.8: Configuration of the post-capture rigid uncontrolled system.

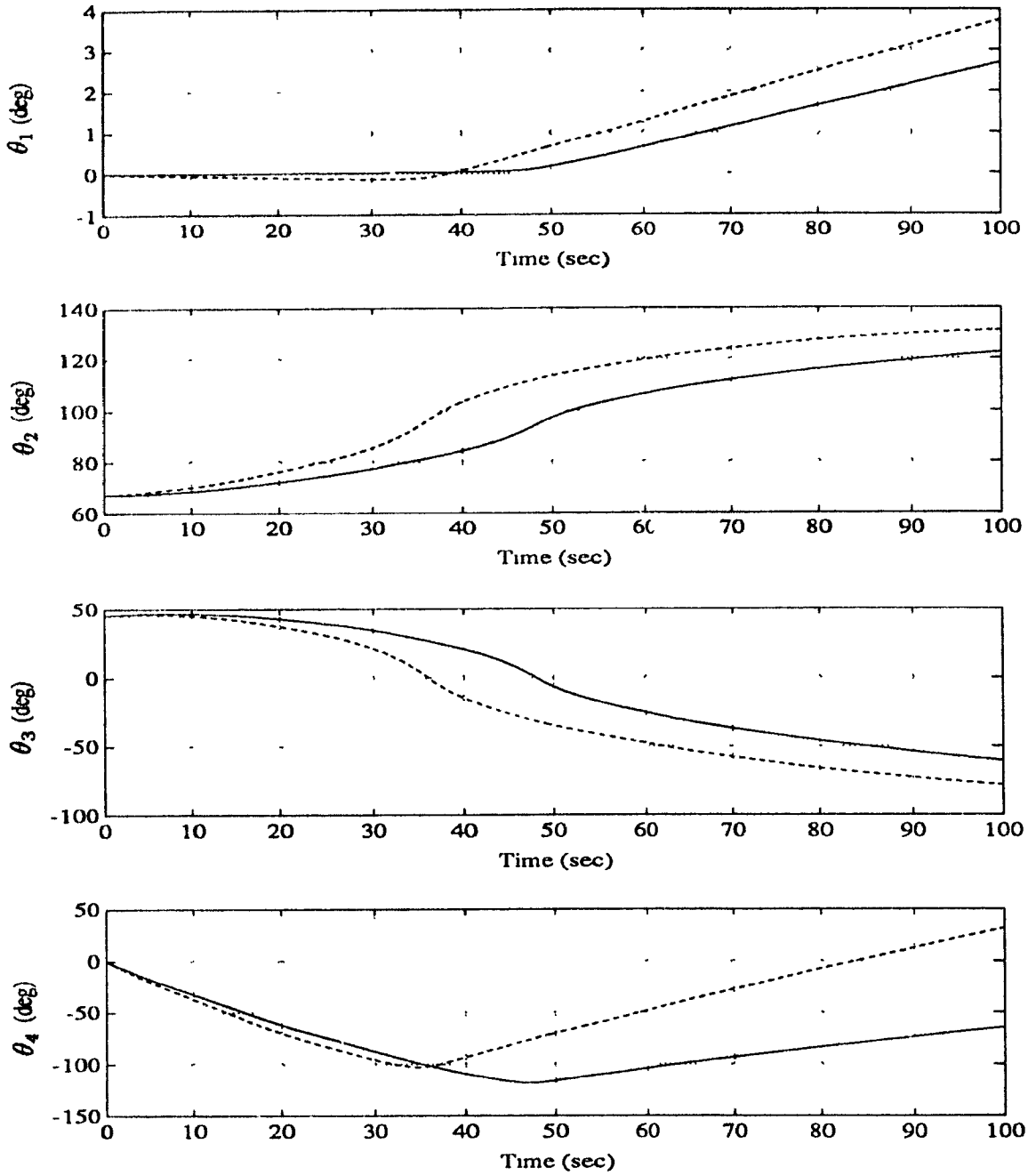

Figure 6.9: Effect of a hard impact on the spacecraft's pitch and joint angles corresponding to the uncontrolled system (— soft impact .... hard impact).

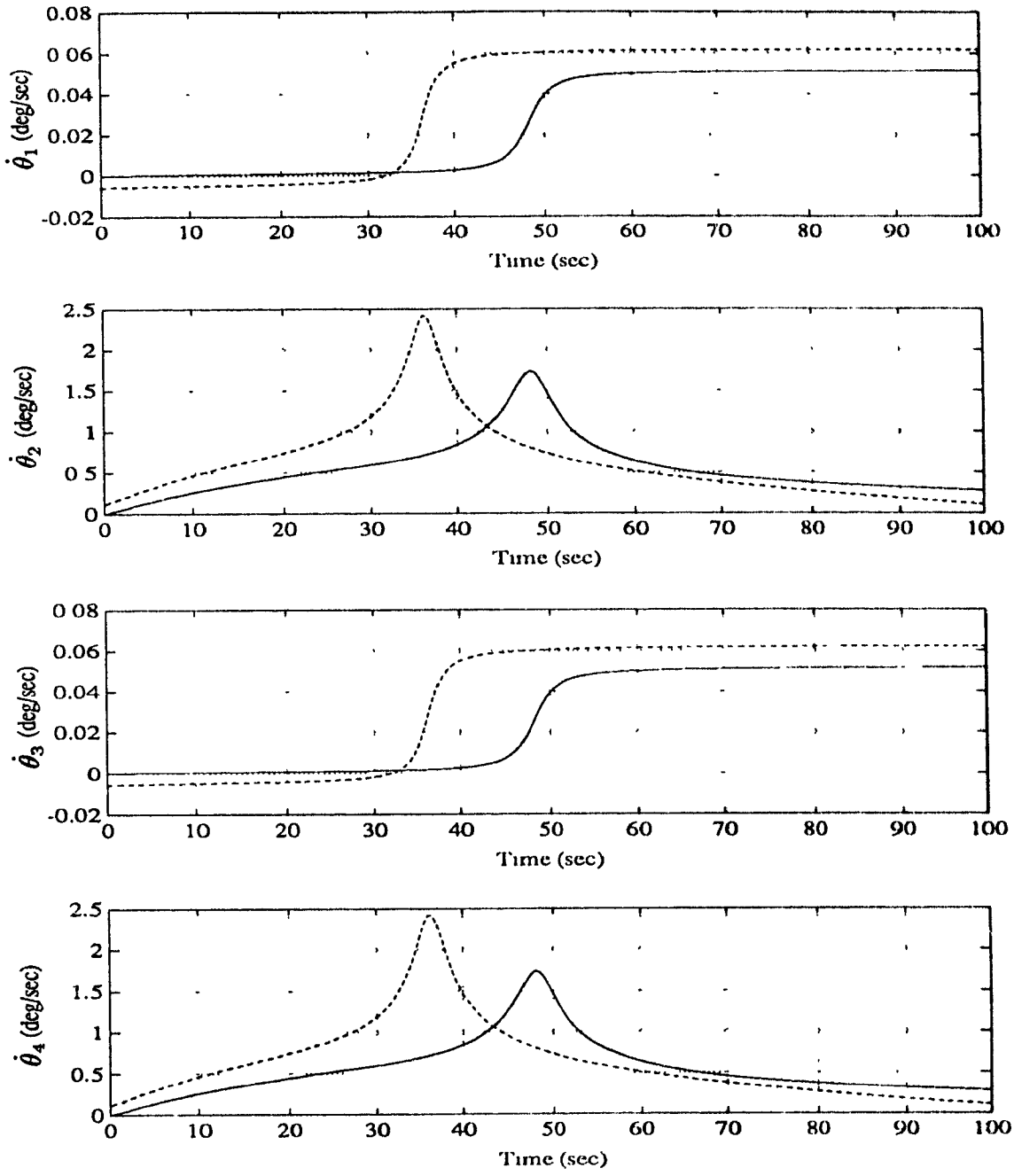

Figure 6.10: Effect of a hard impact on the spacecraft's pitch rate and joint rates corresponding to the uncontrolled system (- - soft impact .... hard impact).

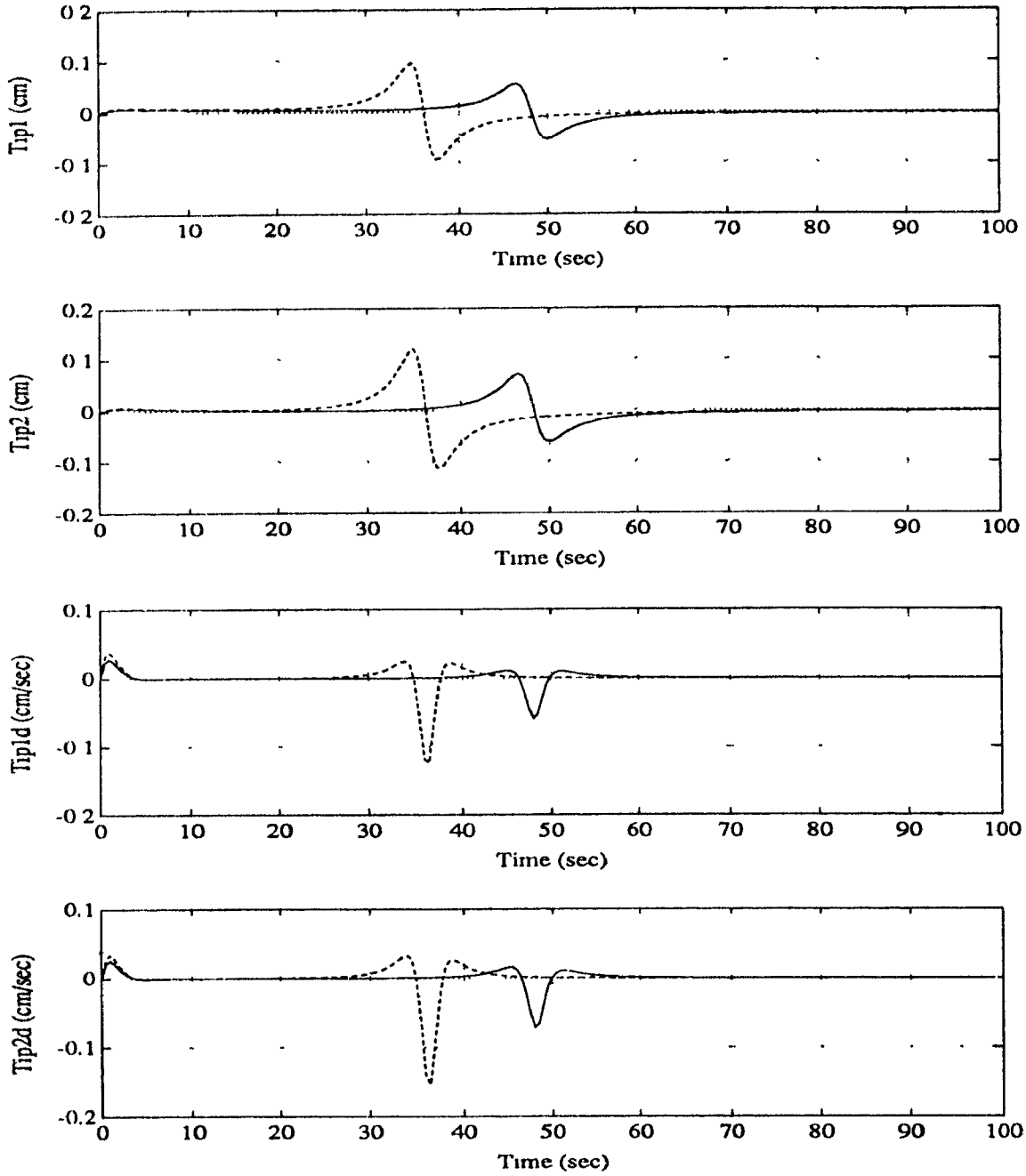

Figure 6.11: Effect of a hard impact on the link tip deflections and their rates corresponding to the uncontrolled system (-- soft impact .... hard impact).

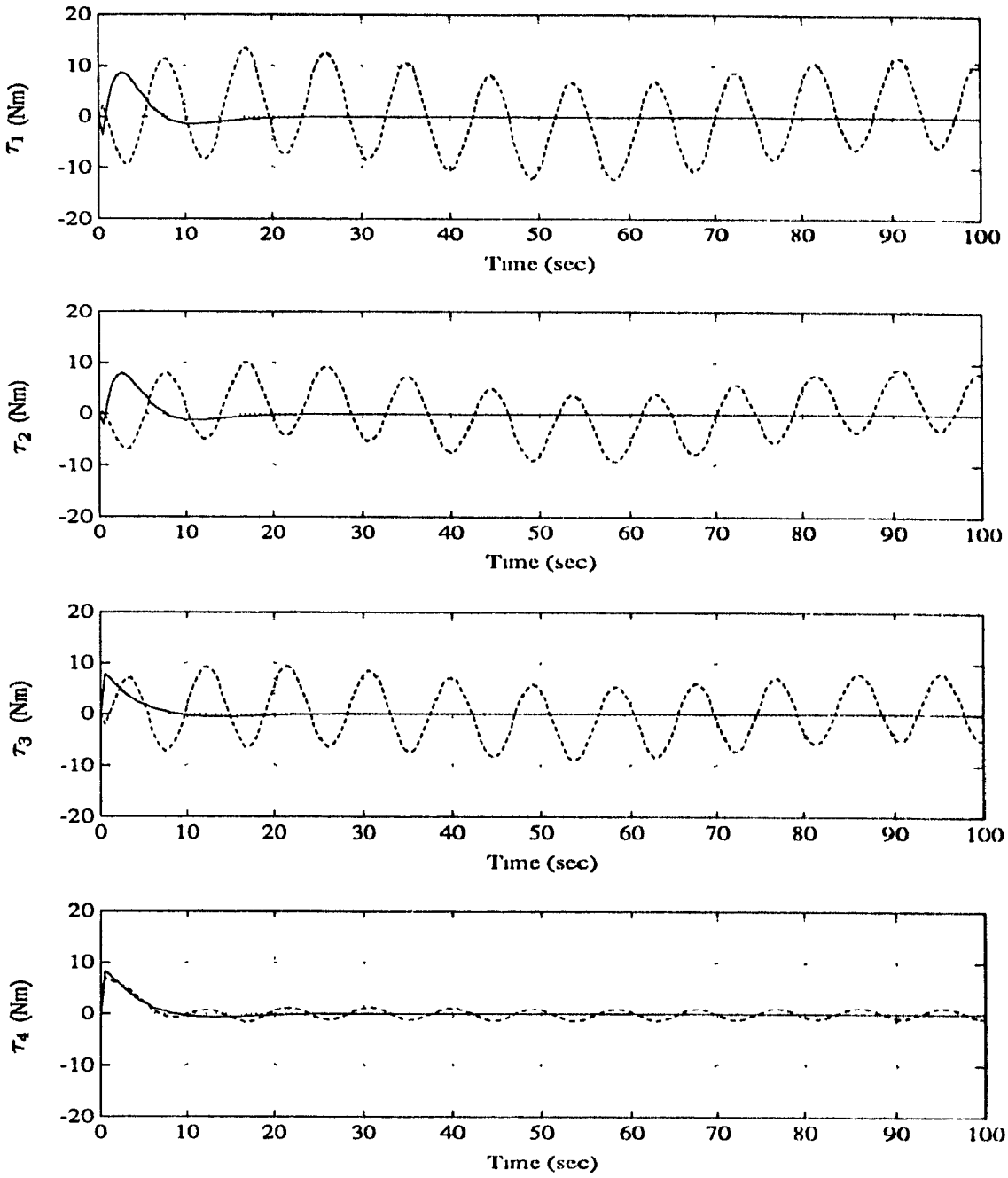

Figure 6.12: Joint control torques applied corresponding to the feedback linearization control (— rigid .... flexible).

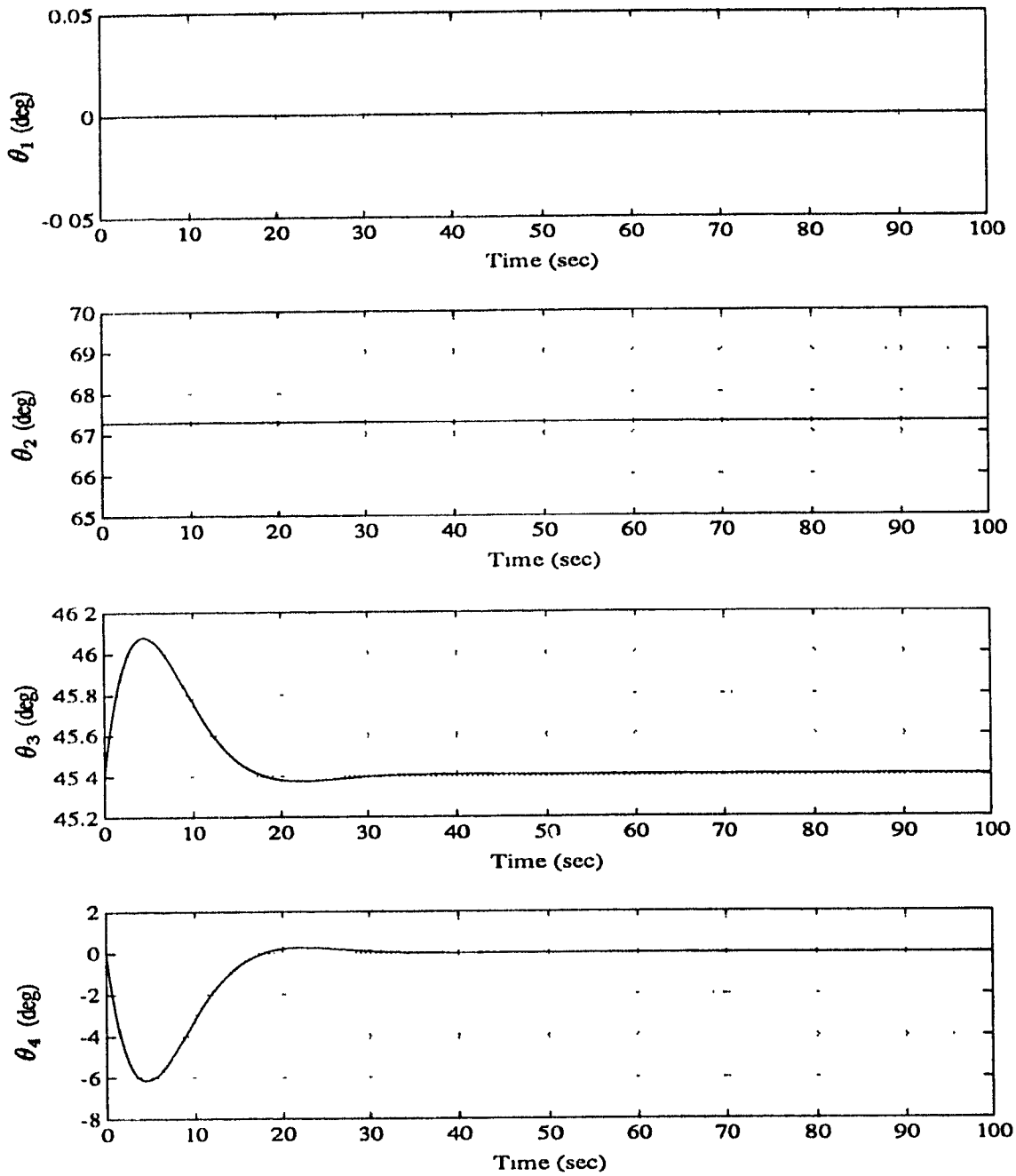

Figure 6.13: Spacecraft's pitch and joint angles response to the feedback linearization control torques (— rigid .... flexible).

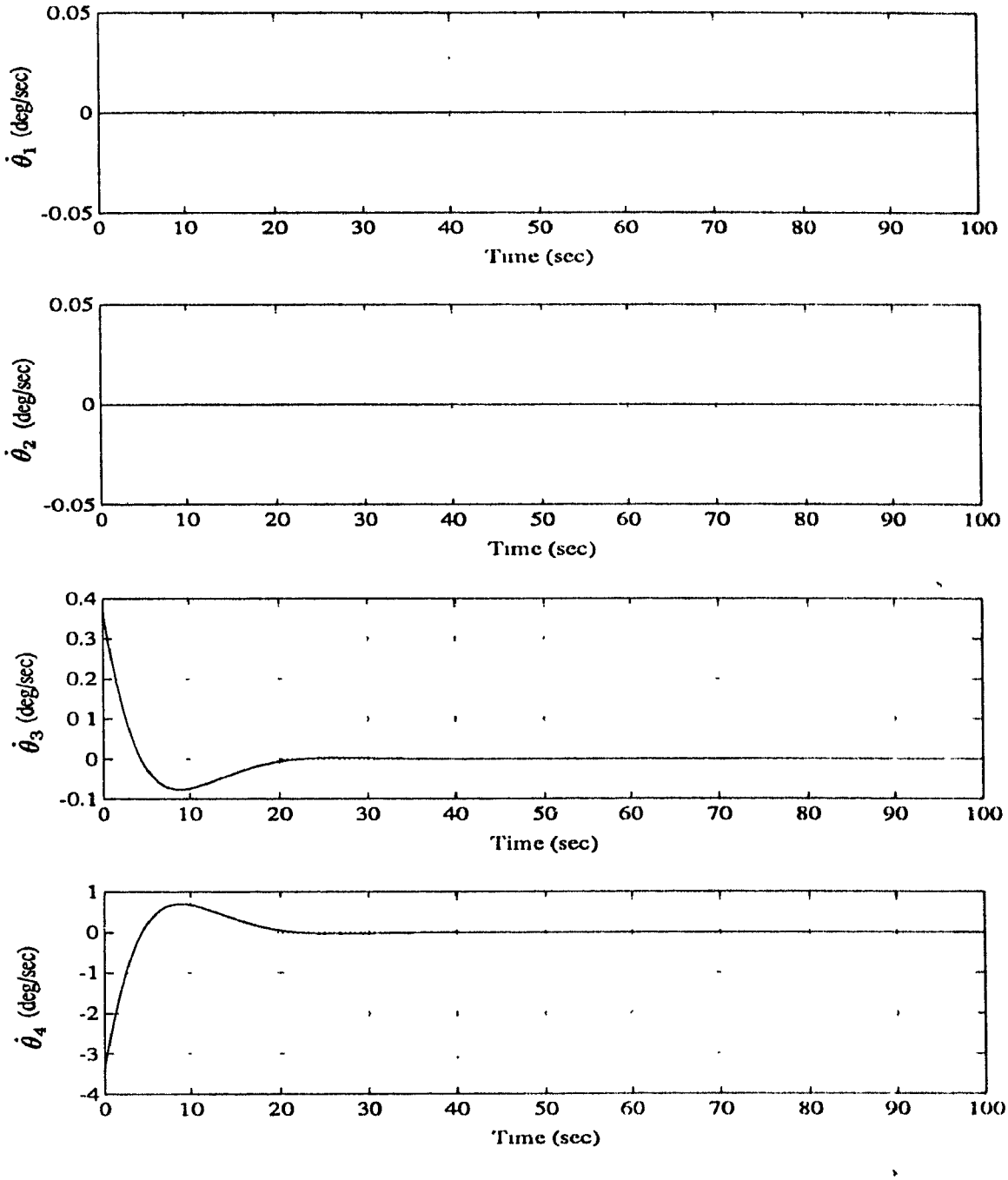

Figure 6.14: Spacecraft's pitch rate and joint rates response to the feedback linearization control torques (— rigid .... flexible).

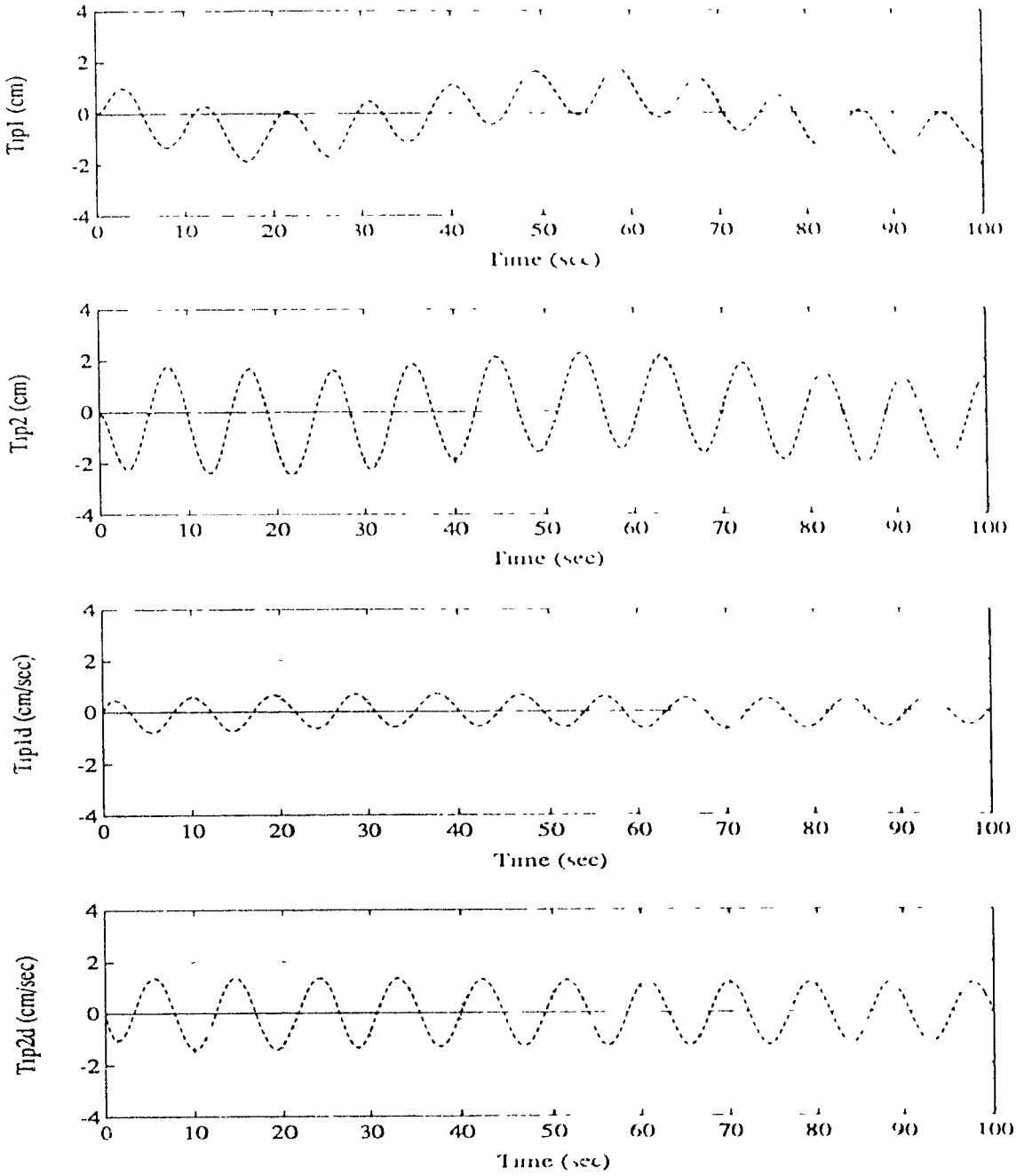

Figure 6.15. Link tip deflections and their rates induced by the application of the feedback linearization control torques (rigid flexible)

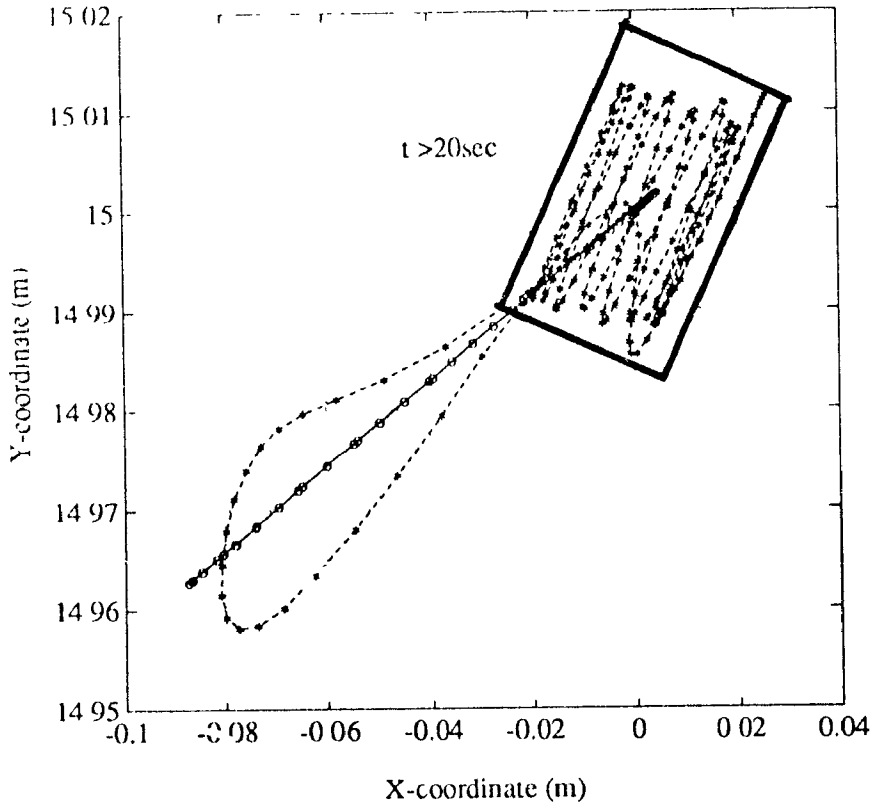

Figure 6.16. Position of the end effector corresponding to feedback linearization control (rigid flexible).

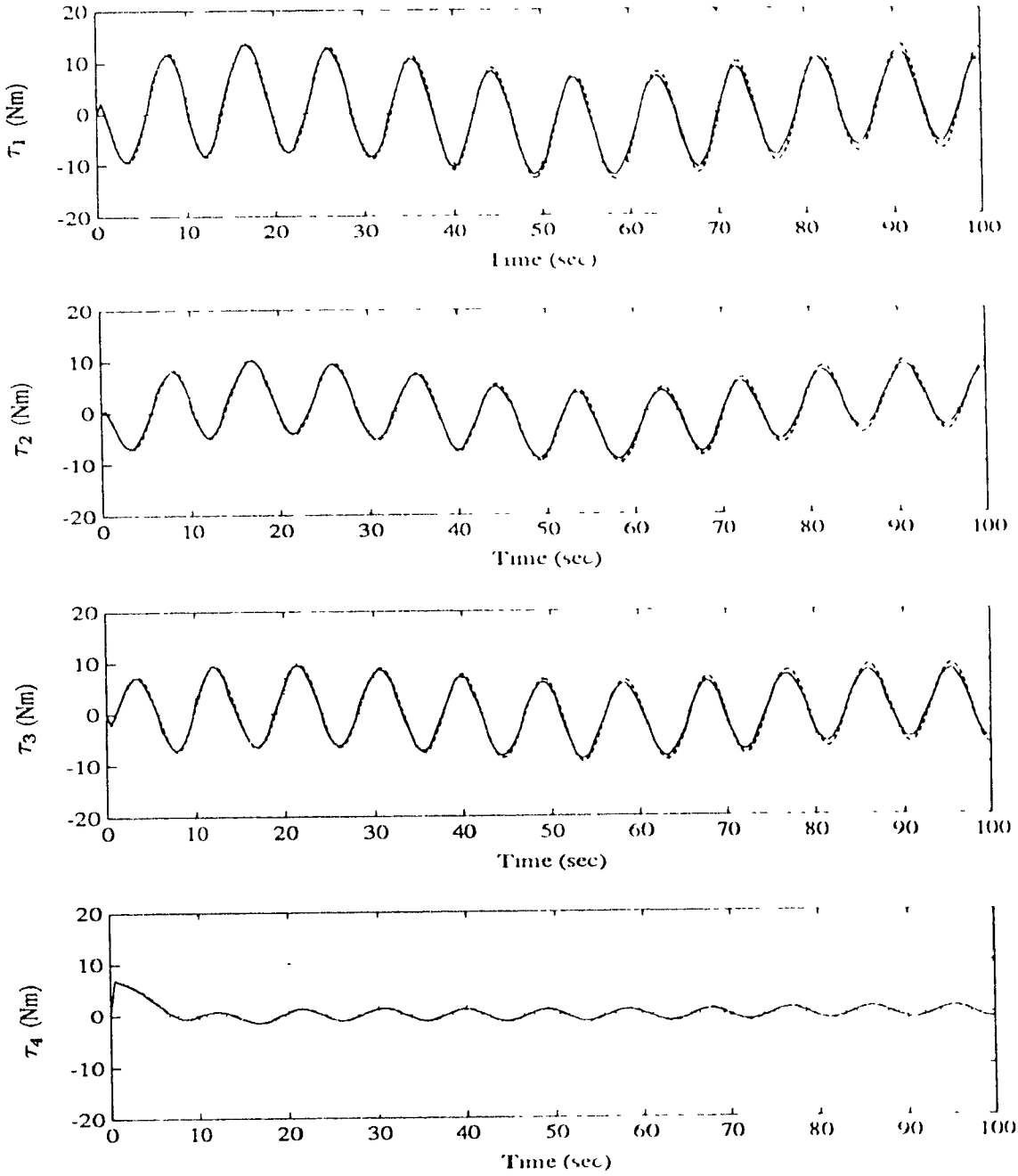

Figure 6.17: Modified joint control torques applied for better positioning of the end effector (- - joint control .... modified control).

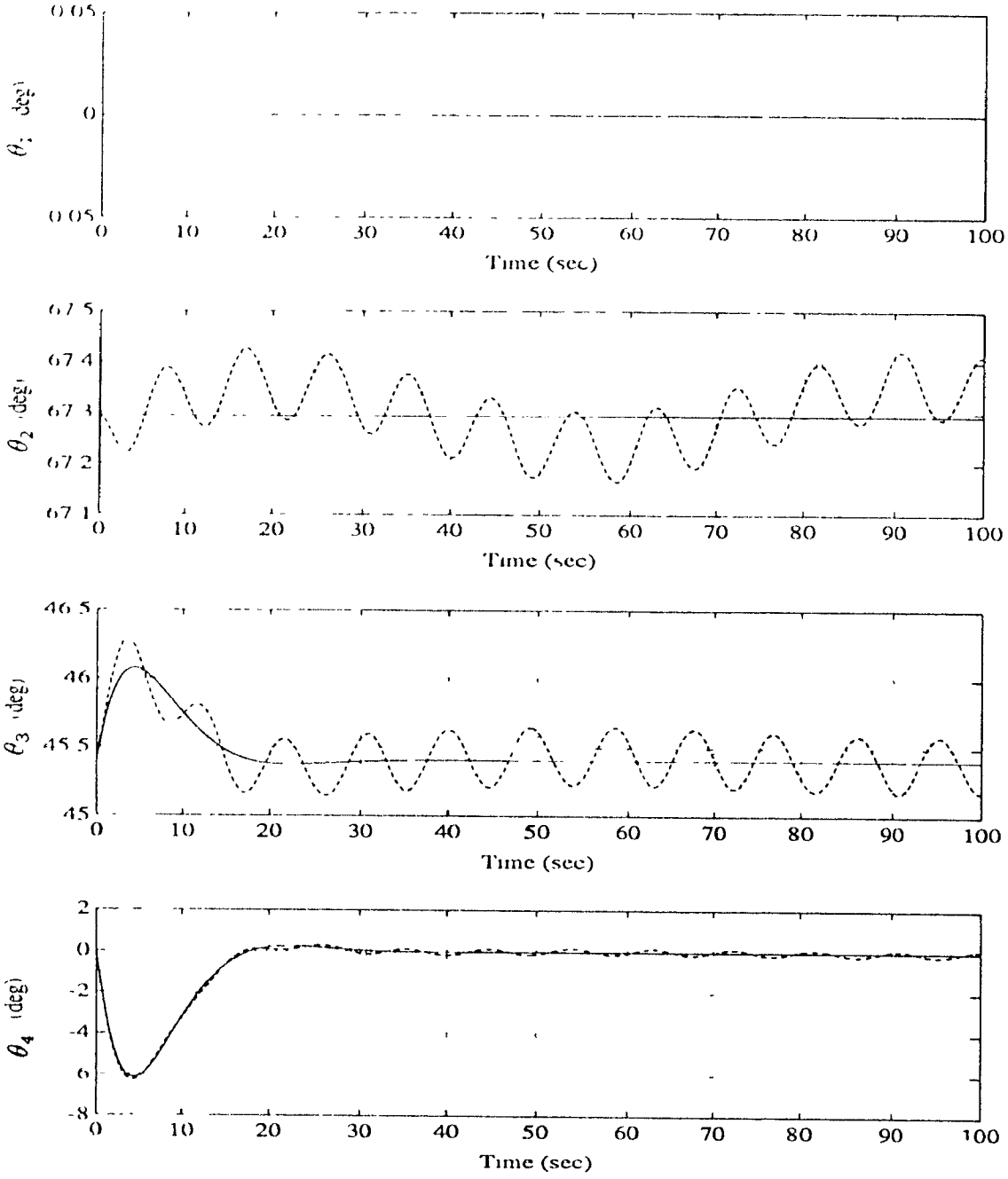

Figure 6.18: Spacecraft's pitch and joint angles response to the modified control torques (joint control ... modified control).

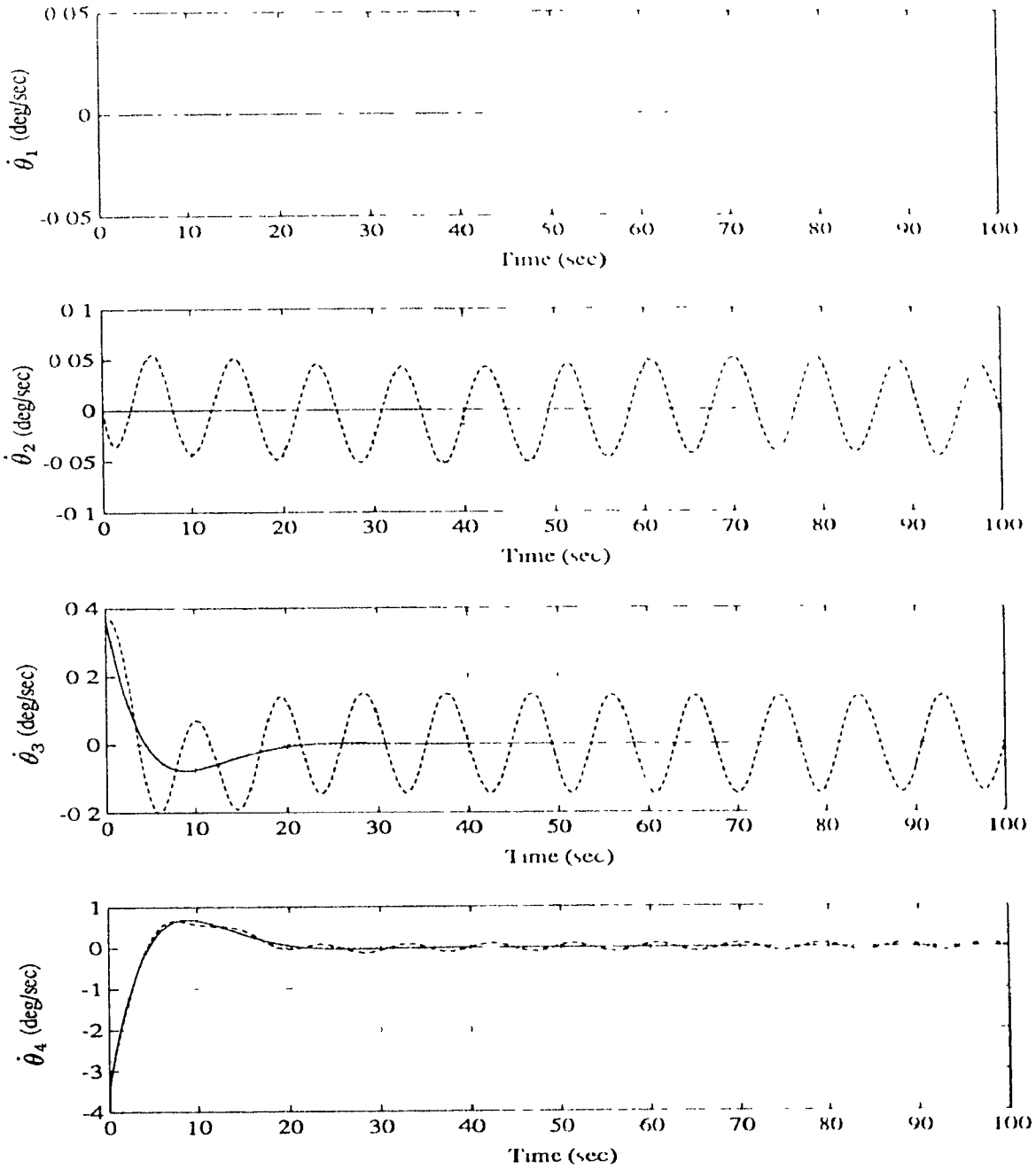

Figure 6.19: Spacecraft's pitch rate and joint rates response to the modified control torques (– joint control .... modified control)

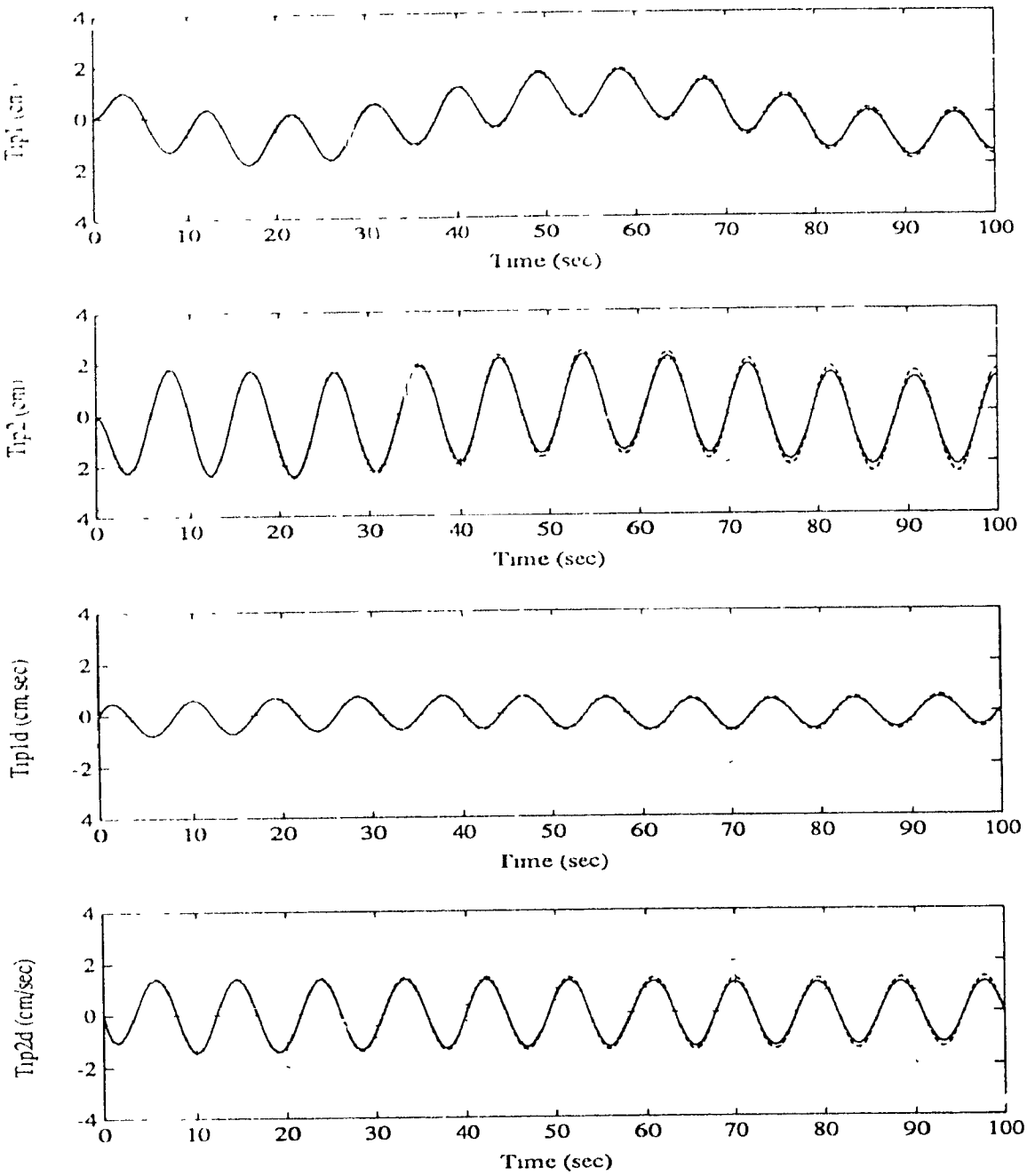

Figure 6.20 Link tip deflections and their rates induced by the application of the modified control torques. (— joint control . modified control).

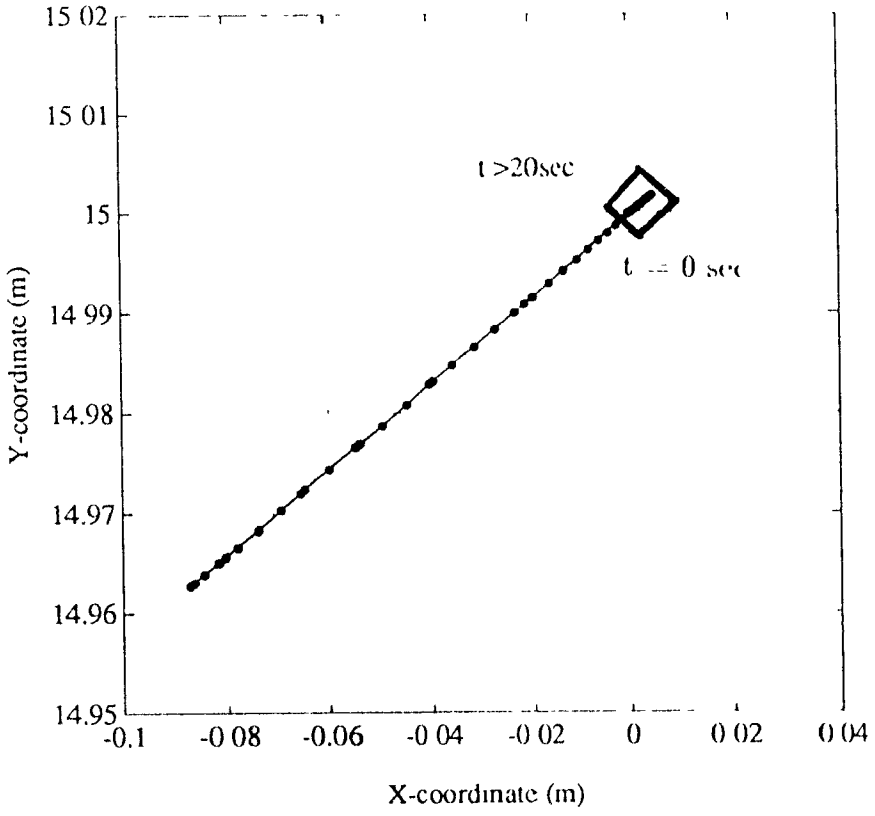

Figure 6.21: Position of the end effector corresponding to the modified control.

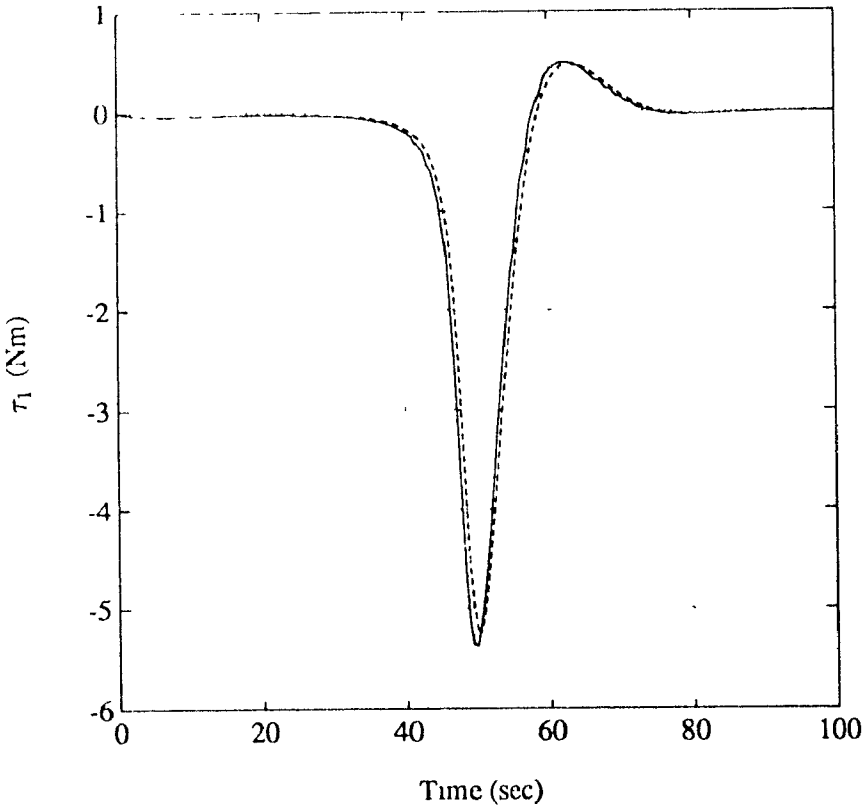

Figure 6.22 Applied torque that achieves attitude control of the mother spacecraft.

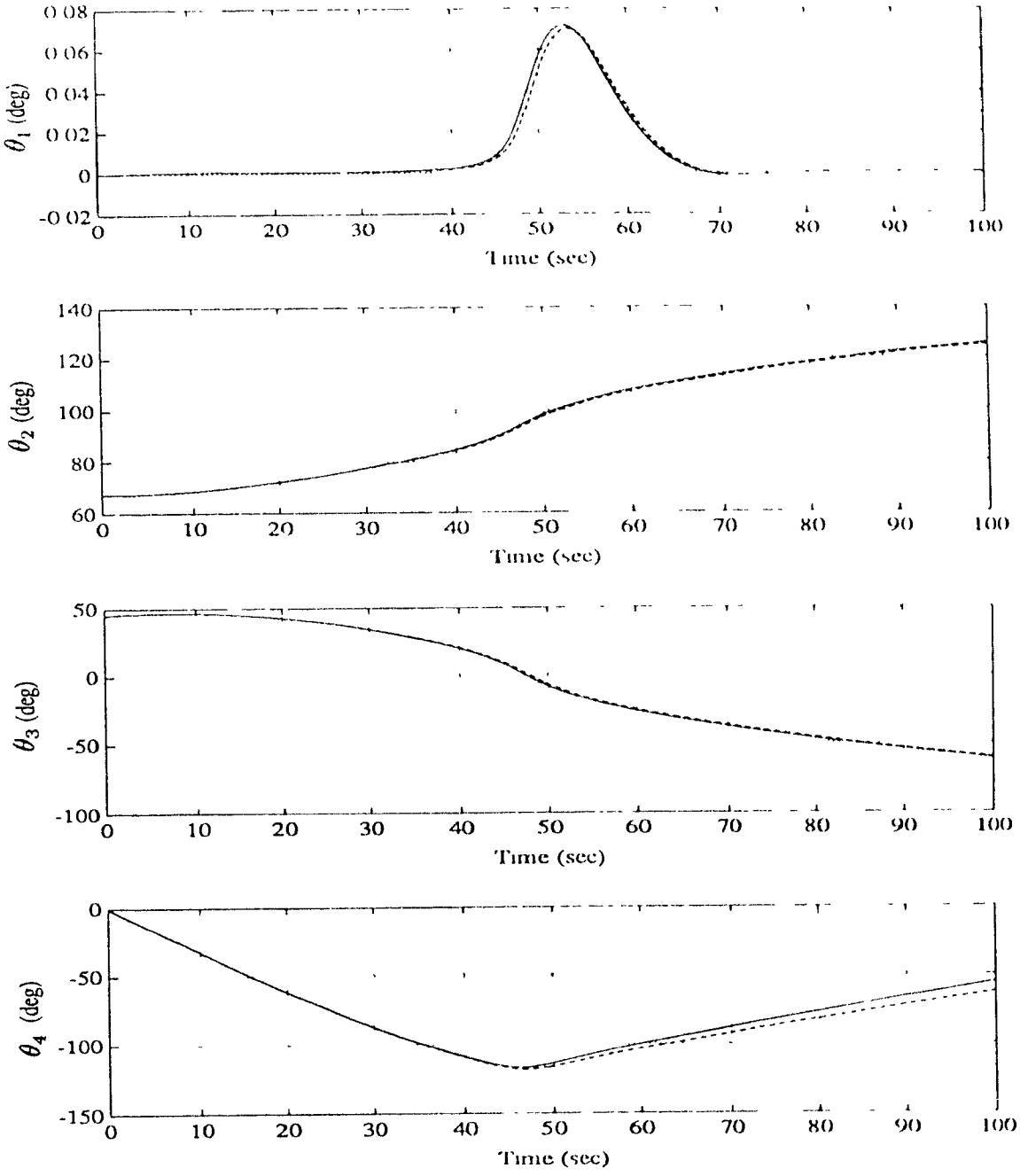

Figure 6.23: Spacecraft pitch and joint angles response to the attitude control torque (-- rigid .. flexible).

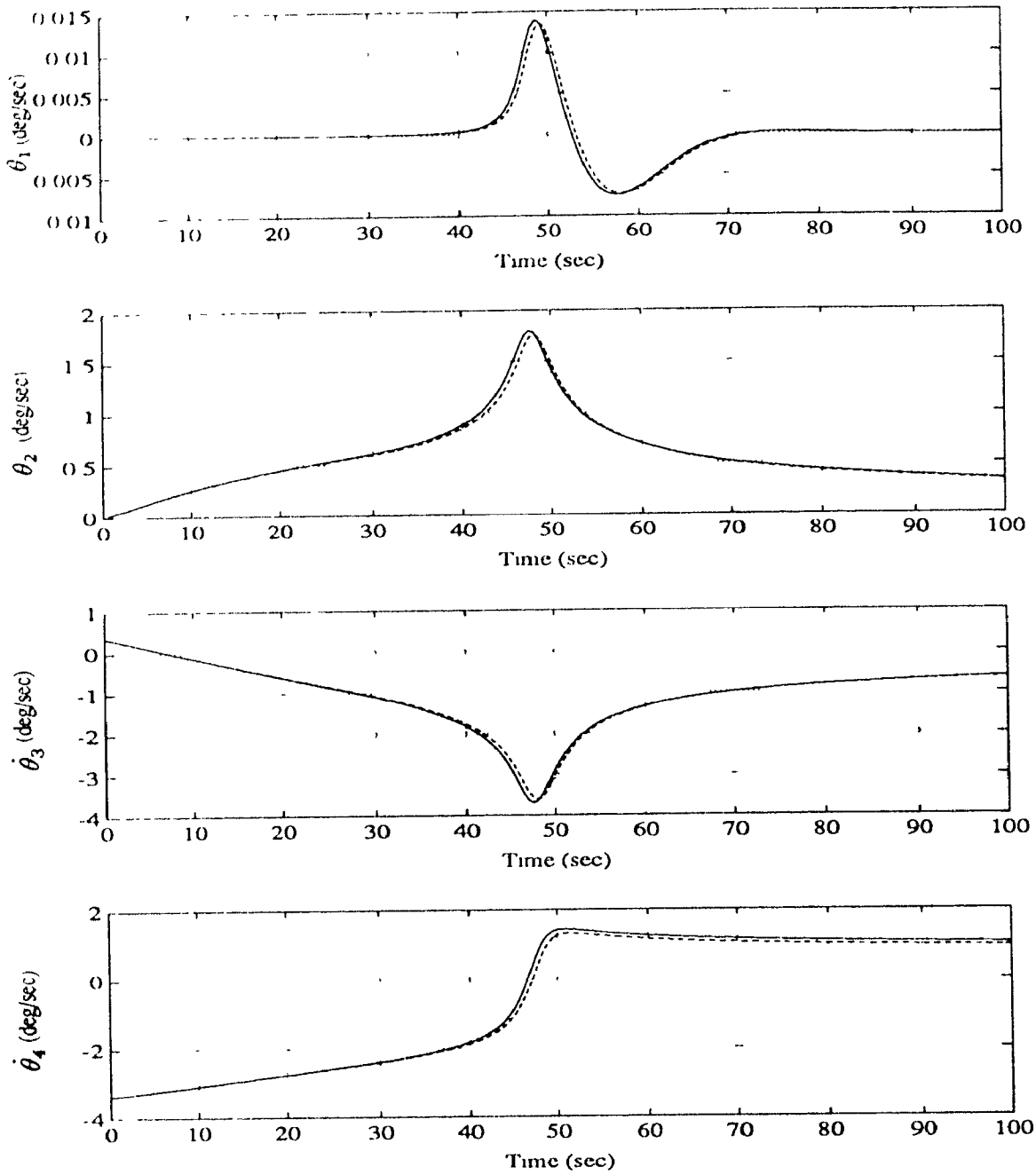

Figure 6.24: Spacecraft pitch rate and joint rates response to the attitude control torque (rigid .... flexible).

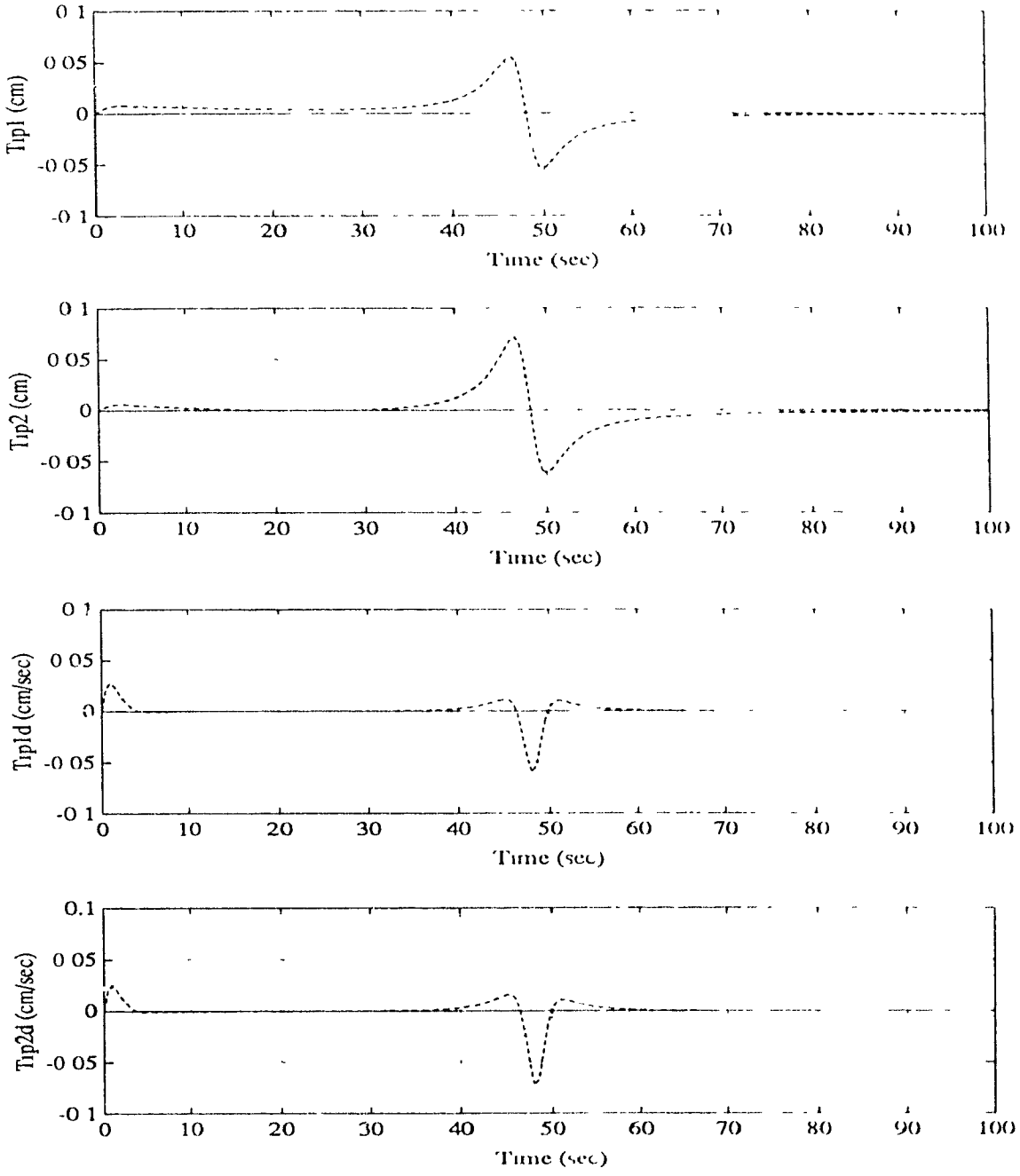

Figure 6 25: Link tip deflections and their rates induced by the attitude control torque (- - rigid ... flexible).

Chapter 7

Conclusions

7.1 Conclusion

This thesis was concerned with the behaviour of a spacecraft/manipulator system just after it captures a payload, in this case a satellite in orbit. The formulation was carried out by writing the *individual* equations of motion for each of the four bodies constituting the system, i e the mother spacecraft, the two-link robotic manipulator and the captured satellite These equations were then assembled and the equations of motion of the system as whole, which contained the constraint forces and moments, were obtained These were then eliminated by using the *natural orthogonal complement* of the velocity-constraint matrix This approach leads to computationally efficient algorithms for the dynamic simulation of both *rigid* and *flexible* bodies. The computations carried out in this thesis were in the local frame, therefore there was no need to transform vectors and matrices to the inertial frame which substantially simplified the derivations. A computer program was written using FORTRAN, and several dynamical simulations were performed using the IMSL subroutine DIVPAG, and the results were plotted using MATLAB.

A methodology was devised in order to calculate the values of the generalized coordinates and their rates of the system immediately following the impact with a satellite by the robot manipulator. Those were then used as the initial conditions for the post-capture simulation. It was found that the post impact behaviour of the system is highly affected by the pre-impact inertial and dynamical properties of the payload, i.e., whether the resulting impact is soft or hard, also the results have shown that the prescribed end-effector's velocity at the instant of impact is very crucial because it could substantially reduce the effect of impact on the system. Hence, a very good estimation of the payload's initial velocity has to be obtained beforehand.

The simulation results of the system following the capture of a satellite, without the application of any control torques, have shown that the effect of capturing a satellite on a spacecraft/manipulator system was quite substantial. The biggest concern was the attitude drift of the mother spacecraft which is undesirable. Also, the end effector joint rotation was found to be beyond the capability of the joint which in no doubt will cause breakage. Hence, a control algorithm had to be designed and implemented to maintain the attitude of the mother spacecraft, prevent the links from large rotations, and suppress any residual motion of the payload.

A **PD** feedback linearization control scheme was implemented and the results have shown that it was quite effective as far as the *rigid* system was concerned. The control torques applied were found to be small in magnitude and had a reasonably short duration; also the joint angles and rates achieved the prescribed values fairly quickly thanks to the position and velocity feedback in the control law. On the other hand, the control of the *flexible* system was complicated by the heavy coupling between the rotation and bending coordinates. Therefore, the control torques, which are highly dependent on the elastic coordinates and their rates, showed an oscillatory

behaviour. Those oscillations were found to be damping out quite slowly because the only damping available is that inherent in the material of the links, which is very small. The incorporation of joint friction in the model would probably eliminate the oscillations much quicker. The positioning of the end-effector could be improved by developing a control algorithm which will provide accurate end-effector trajectory tracking. Experiments, that use such a controller, were conducted at the University of Toronto (Carusone and D'Eleuterio 1991). The results have shown that such a control is superior to a PID controller and is less susceptible to the oscillations of the links. On the other hand, if an effective complete control is sought, the elastic coordinates and their rates have to be controlled explicitly by means of collocated sensors and actuators distributed along the flexible links and capable of the application of transverse forces to the links.

From the results obtained in this thesis, it could be concluded that the effect of the flexibility in the robot's links has to be accounted for in most dynamical simulations, otherwise gross inaccuracies in the positioning of the end effector will occur and will render the particular task the robot was set to do inefficient. Only in cases were the elastic deformations are found to be very small, the flexibility could be ignored and hence the links could be modelled as *rigid*.

7.2 Recommendations for Future Work

The material presented in this thesis covered only a small part of capture dynamics. There is a wide range of further investigations that could be done as an extension to this work; therefore some suggestions for future work are outlined next.

a) Incorporate joint friction and joint flexibility in the model.

b) Extend the simulation to a 3-dimensional case as opposed to a planar case considered here.

c) Consider the approach dynamics as the spacecraft/manipulator system goes to capture a payload.

d) Investigate the effects of capturing a payload which is flexible or contains flexible appendages.

e) Design and implement a control torque whose purpose is to retrieve the captured payload towards the mother spacecraft.

f) Conduct some robustness studies, and investigate the effect of noise on the system.

g) Explicit control of the elastic coordinates and their rates.

h) Implement a control algorithm for end-effector trajectory tracking.

Bibliography

[1] Baruh H. and S. S. K. Tadikunda, "Issues in the Dynamics and Control of Flexible Robot Manipulators", *AIAA Symposium on Dynamics and Control of Large Structures*, pp. 659-671, June 29-July 1, 1987.

[2] Bayo E., "Computed Torque for the Position Control of Open-Chain Flexible Robots", *Proceedings IEEE International Conference on Robotics and Automation*, pp. 316-321, April 1988.

[3] Buchan K. S., J. Carusone, and G. M. T. D'Eleuterio, "A Laboratory Facility for the Study of the Dynamics and Control of Structurally Flexible Manipulators", *Seventh VPI&SU/AIAA Symposium on Dynamics and Control of Large Structures*, Blacksburg, VA, May 8-10, 1989.

[4] Cannon R., and E. Schmitz, "Initial Experiments on End-Point Control of a Flexible One-Link Robot", *International Journal of Robotics Research*, Vol. 3, No. 3, pp 62-75, Fall 1984.

[5] Carton D. and J. P. Chrétien, "Dynamic Modelling and Control of a Flexible Arm Holding a Non-Rigid Payload", *Proceedings of the 2nd European In-Orbit Operations Technology Symposium*, Toulouse, France, September 12-14, 1989.

[6] Carusone J. and G. M. T. D'Eleuterio, "Experiments in the Control of Structurally Flexible Manipulators with the *Radius* Facility", *Proceedings of the Second Japan-USA Conference on Adaptive Structures*, Nagoya, Japan, November 12-14, 1991.

[7] Cetinkunt S., and W. J Book," Symbolic Modeling of Flexible Manipulators", *Proceedings of the 1987 IEEE Conference on Robotics and Automation*, Vol. 3, March 31-April 3, 1987, Raleigh, NC, pp. 2074-2080.

[8] Chan J. K. and V. J. Modi, "A Closed-Form Dynamical Analysis of an Orbiting Flexible Manipulator", *Acta Astronautica*, Vol. 25, No. 2, pp 67-75, 1991

[9] Chapnik B. V., G. R Heppler, and J.D. Aplevich, " Modeling Impact on a One-Link Flexible Robotic Arm", *IEEE Transactions on Robotics and Automation*, Vol. 7, No. 4, pp. 479-488, August 1991.

[10] Chiou B. C. and M. Shahimpoor, "Effect of Joint Stiffness on the Dynamic Stability of a One-Link Force-Controlled Manipulator", *Robotica*, Vol. 7, pp. 339-342, 1989.

[11] Craig J. J., *Introduction to Robotics : Mechanics & Control.* Addison-Wesly, Reading, Mass., 1986.

[12] Cyril X., "Dynamics of Flexible-Link Manipulators", *Ph.D Thesis*, 1988, Department of Mechanical Engineering, McGill University, Montréal, Canada.

[13] Cyril X., J. Angeles, and A. K Misra, "FLEXLINK A Software Package for the Dynamic Simulation of Flexible-Link Robotic Manipulators", *Proceedings 1989 ASME International Computers in Engineering Conference*, Anaheim, CA, pp. 453-459, July 30-August 3, 1989.

[14] Cyril X., J. Angeles, and A. K. Misra, "Dynamics of Flexible Multibody Mechanical Systems", *Transactions of the CSME*, Vol. 15, No. 3, pp. 235-256, 1991.

[15] Dubowsky S., E. Vance, and M. Torres, "The Control of Space Manipulators Subject to Spacecraft Attitude Control Saturation Limits", *Proceedings of the NASA Conference on Space Telerobotics*, JPL , Pasadena, CA, January 31-February 2, 1989.

[16] Gear C. W., *Numerical Initial Value Problems in Ordinary Differential Equations* Prentice-Hall, Englewood Cliffs, NJ, 1971.

[17] Gevarter W B., "Basic Relations for Control of Flexible Vehicles", *AIAA J.*, Vol. 8, No. 4, pp 666-672, April 1970.

[18] Goldsmith W., *Impact.* London : Edward Arnold Ltd., 1960.

[19] Hughes P C., "Dynamics of a Chain of Flexible Bodies", *The Journal of the Astronautical Sciences*, Vol. 27, No. 4, pp. 359-380.

[20] Hughes P. C., *Spacecraft Attitude Dynamics.* New York : Wiley, 1986.

[21] Hurty W. C. and M. Rubinstein. *Dynamics of Structures*, Prentice-Hall, NJ, 1964.

[22] Kane T. R., R. R. Ryan, and A. K. Banerjee, "Dynamics of a Cantilever Beam Attached to a Moving Base", *Journal of Guidance and Control*, Vol. 10, No. 2, pp. 139-151, 1987.

[23] Kaplan M. H , *Modern Spacecraft Dynamics & Control*, John Wiley & Sons, 1976

[24] Kimball A. L., "Vibration Damping Including the Case of Solid Friction", *Transactions of the ASME, APM*, Vol. 51, No. 21, 1929.

[25] Likins P. W., "Geometric Stiffness Characteristics of a Rotating Elastic Appendage", *International Journal of Solids and Structures*, Vol. 10, No. 2, pp. 161-167, 1974.

[26] Longman R. W., "Attitude Tumbling due to the Flexibility in Satellite-Mounted Robots", *The Journal of the Astronautical Sciences*, Vol. 38, No. 4, pp. 487-509, October - December 1990a.

[27] Longman R. W., "The Kinetics and Workspace of a Satellite-Mounted Robot", *The Journal of the Astronautical Sciences*, Vol. 38, No. 4, pp. 423-440, October - December 1990b.

[28] Longman R., R. Lindberg, and M. Zedd, "Satellite-Mounted Robot Manipulators - New Kinematics and Reaction Moment Compensation", *International Journal of Robotics Research*, Vol. 6, No. 3, pp. 87-103, 1987.

[29] R. Lindberg, R. Longman, and M. Zedd, "Kinematic and Dynamic Properties of an elbow Manipulator Mounted on a Satellite", *The Journal of the Astronautical Sciences*, Vol 38, No. 4, pp. 397-421, 1990.

[30] Meirovitch L., *Analytical Methods in Vibrations*. The Macmillan Company, New York, 1967.

[31] Murphy S H., J. Wen, and G N. Saridis, " Simulation of Cooperating Robot Manipulators on a mobile Platform", *IEEE Transactions on Robotics and Automation*, Vol. 7, No.4, August 1991.

[32] Nenchev D., Y Umetani, and K. Yoshida, " Analysis of a redundant Free-Flying Spacecraft/Manipulator System", *IEEE Transactions on Robotics and Automation*, Vol 8, No. 1, pp 1-6., February 1992.

[33] Papadopoulos E and S. Dubowsky, " On the Nature of Control Algorithms for Free-Floating Space Manipulators", *IEEE Transactions on Robotics and Automation*, Vol 7, No.6, pp. 750-758, December 1991.

[34] Paul, R. P. , *Robot Manipulators: Computer Interfacing and control*, The MIT Press, Cambridge, Mass., 1981.

[35] Sakaws I., F Matsuno, S. Fukushima, "Modelling and Feedback Control of a Flexible Arm", *Journal of Robotic Systems*, Vol. 2, pp. 453-472, 1985

[36] Timoshenko S , *Vibrations Problems in Engineering*. Princeton, NJ, 1955.

[37] Torres M and S. Dubowsky, "Path Planning for Space Manipulators to Minimize Spacecraft Attitude Disturbance", *Proceedings 1991 IEEE International Conference on Robotics and Automation*, Sacramento, CA, Vol. 3, pp. 2522-2528, April 1991

[38] Umetani Y. and K. Yoshida, "Experimental Study on Two Dimensional Free-Flying Robot Satellite Model", *Proceedings of The NASA Conference on Space Telerobotics*, JPL, January 31-February 2, 1989a.

[39] Umetani Y. and K. Yoshida, "Theoretical and Experimental Study on in-orbit Capture Operation with Satellite Mounted Manipulators", *Proceedings of the 11th IFAC Symposium on Automatic Control in Aerospace*, Tsukuba, Japan, pp. 137-142, 1989b.

[40] Vafa Z. and S. Dubowsky, "On the Dynamics of Manipulators in Space Using the Virtual Manipulator Approach", *Proceedings 1987 IEEE Conference on Robotics and Automation*, Rayleigh, NC, pp. 579-585, March 30-April 3, 1987

[41] Vafa Z. and S Dubowsky, " On the Dynamics of Space Manipulators Using the Virtual Manipulator, with Applications to Path Planning", *The Journal of the Astronautical Sciences*, Vol 38, No. 4, pp.441-472, October-December 1990

[42] van Poppel J. and A. K Misra, "Active Control of Space Structures Using Bonded Piezoelectric Film Actuators", *AIAA/AAS Astrodynamics Conference*, Hilton Head Island, SC, pp. 328-341, August 10-12, 1992

[43] van Woerkom P. Th. L. M, and A. de Boer, "Development of a Linear Recursive "Order-N" Algorithm for the Simulation of Flexible Space Manipulator Dynamics", *43rd Congress of the International Astronautical Federation*, Washington, DC, August 28-September 3, 1992.

[44] Yang G. and M. Donath, "Dynamic Model of a One-Link Robot Manipulator with Both Structural and Joint Flexibility", *IEEE International Conference on Robotics and Automation*, Philadelphia, PA, pp. 476-481, 1988

[45] Yoshida K., R Kurazume, N Sashida, and Y Umetani, " Modeling of Collision Dynamics for Space Free-Floating Links with Extended Generalized Inertia Tensor", *Proceedings 1992 IEEE Conference on Robotics and Automation*, Nice, France, May 1992.

[46] Yoshida K and Y Umetani, " Control of Space Free-Flying Robot", *Proceedings of the 29th IEEE Conference on Decision and Control*, pp 97-102, 1990.

Appendix A

Detailed Derivations of Various Equations

A.1 Derivation of Equation (3.5)

By substituting equation (3.4) into (3.3) the following is obtained:

$$T_1 = \frac{1}{2}\int_{m_1} \tilde{\mathbf{v}}_1^T \tilde{\mathbf{v}}_1 dm_1 + \frac{1}{2}\int_{m_1} (\boldsymbol{\omega}_1 \mathrm{x} \mathbf{r}_1)^T (\boldsymbol{\omega}_1 \mathrm{x} \mathbf{r}_1) dm_1 \tag{A.1}$$

By using the definition of the integrand, the equation is re-written as:

$$T_1 = \frac{1}{2} m_1 \tilde{\mathbf{v}}_1^T \tilde{\mathbf{v}}_1 + \frac{1}{2}\boldsymbol{\omega}_1^T \int_{m_1} (\mathbf{r}_1^2 \mathbf{1} - \mathbf{r}_1 \otimes \mathbf{r}_1) dm_1 \, \boldsymbol{\omega}_1 \tag{A.2}$$

The value of the integral represents the moment of inertia of the spacecraft, $\mathbf{I}_1$, about its centre of mass. Therefore, equation (A.2) could be re-written as:

$$T_1 = \frac{1}{2} m_1 \tilde{\mathbf{v}}_1^T \tilde{\mathbf{v}}_1 + \frac{1}{2}\boldsymbol{\omega}_1^T [\mathbf{I}_1] \boldsymbol{\omega}_1 \tag{A.3}$$

which is identical to equation (3.5).

A.2 Derivation of Equation (3.9)

Recall equation (3.8)

$$\mathbf{v}^2(x) = \tilde{\mathbf{v}}^2 + 2\tilde{\mathbf{v}}^T(\boldsymbol{\omega}\mathrm{x}\mathbf{r}) + (\boldsymbol{\omega}\mathrm{x}\mathbf{r})^T(\boldsymbol{\omega}\mathrm{x}\mathbf{r}) + 2\tilde{\mathbf{v}}^T\dot{\mathbf{r}} + 2(\boldsymbol{\omega}\mathrm{x}\mathbf{r})^T\dot{\mathbf{r}} + \dot{\mathbf{r}}^2 \tag{A.4}$$

which can be re-written as:

$$\mathbf{v}^2(x) = \tilde{\mathbf{v}}^2 + 2\tilde{\mathbf{v}}^T(\boldsymbol{\omega}\mathrm{x}\mathbf{r}) + \boldsymbol{\omega}^T(\mathbf{r}^2\mathbf{1} - \mathbf{r}\otimes\mathbf{r})\boldsymbol{\omega} + 2\tilde{\mathbf{v}}^T\dot{\mathbf{r}} + 2(\boldsymbol{\omega}\mathrm{x}\mathbf{r})^T\dot{\mathbf{r}} + \dot{\mathbf{r}}^2 \tag{A.5}$$

Substituting equation (2.10) into equation (A.5) and noting that

$$\dot{\mathbf{r}} = \dot{\boldsymbol{\mu}} \tag{A.6}$$

the following equation is obtained:

$$\begin{aligned}\mathbf{v}^2(x) = \tilde{\mathbf{v}}^2 &+ 2\tilde{\mathbf{v}}^T(\boldsymbol{\omega}\mathrm{x}\boldsymbol{\mu}) + 2x\tilde{\mathbf{v}}^T(\boldsymbol{\omega}\mathrm{x}\mathrm{x}) + \boldsymbol{\omega}^T[(\boldsymbol{\mu}^2\mathbf{1} + x^2\mathrm{x}^2\mathbf{1} + 2x\mathrm{x}^T\boldsymbol{\mu}\mathbf{1}) \\ &-(\boldsymbol{\mu}\otimes\boldsymbol{\mu} + x^2\mathrm{x}\otimes\mathrm{x} + x\mathrm{x}\otimes\boldsymbol{\mu} + x\boldsymbol{\mu}\otimes\mathrm{x})]\boldsymbol{\omega} + 2\tilde{\mathbf{v}}^T\dot{\boldsymbol{\mu}} \\ &+2x(\boldsymbol{\omega}\mathrm{x}\mathrm{x})^T\dot{\boldsymbol{\mu}} + 2(\boldsymbol{\omega}\mathrm{x}\boldsymbol{\mu})^T\dot{\boldsymbol{\mu}} + \dot{\boldsymbol{\mu}}^2\end{aligned} \tag{A.7}$$

Equation (A.7) could then be re-written in terms of the cross product tensors $\mathbf{X}$ and $\mathbf{U}$ associated with x and $\boldsymbol{\mu}$, respectively, to obtain:

$$\begin{aligned}\mathbf{v}^2(x) = \tilde{\mathbf{v}}^2 &- 2\tilde{\mathbf{v}}^T\mathbf{U}\boldsymbol{\omega} - 2x\tilde{\mathbf{v}}^T\mathbf{X}\boldsymbol{\omega} + \boldsymbol{\omega}^T[(\boldsymbol{\mu}^2\mathbf{1} + x^2\mathrm{x}^2\mathbf{1} + 2x\mathrm{x}^T\boldsymbol{\mu}\mathbf{1}) \\ &-(\boldsymbol{\mu}\otimes\boldsymbol{\mu} + x^2\mathrm{x}\otimes\mathrm{x} + x\mathrm{x}\otimes\boldsymbol{\mu} + x\boldsymbol{\mu}\otimes\mathrm{x})]\boldsymbol{\omega} + 2\tilde{\mathbf{v}}^T\dot{\boldsymbol{\mu}} \\ &+2x(\boldsymbol{\omega}\mathrm{x}\mathrm{x})^T\dot{\boldsymbol{\mu}} + 2(\boldsymbol{\omega}\mathrm{x}\boldsymbol{\mu})^T\dot{\boldsymbol{\mu}} + \dot{\boldsymbol{\mu}}^2\end{aligned} \tag{A.8}$$

It was assumed earlier that the axial shortening in the links is negligible, i.e. $u_1 = 0$, hence the term $\mathbf{x}^T\mathbf{u}$ in equation (A.8) vanishes. Also, since $\mathbf{x}$ is a unit vector, $\mathbf{x}^2$ is

set to 1. Equation (A.8) could be further simplified to obtain:

$$\begin{aligned}\mathbf{v}^2 = \tilde{\mathbf{v}}^2 &- \tilde{\mathbf{v}}^T(2x\mathbf{X} + 2\mathbf{U})\boldsymbol{\omega} + 2\tilde{\mathbf{v}}^T\boldsymbol{\mu} + \dot{\boldsymbol{\mu}}^2 \\ &+\boldsymbol{\omega}^T(x^2(\mathbf{1} - \mathbf{x} \oslash \mathbf{x}) - x(\mathbf{x} \oslash \boldsymbol{\mu} + \boldsymbol{\mu} \otimes \mathbf{x}) \\ &+(\boldsymbol{\mu}^2\mathbf{1} - \boldsymbol{\mu} \oslash \boldsymbol{\mu})]\boldsymbol{\omega} + \boldsymbol{\omega}^T(2x\mathbf{X} + 2\mathbf{U})\dot{\boldsymbol{\mu}} \end{aligned} \tag{A.9}$$

which is identical to equation (3.9).

A.3 Derivation of Equation (3.11)

The terms associated with the inertia due to the angular acceleration in equation (3.7) are ignored and the equation becomes:

$$T = \frac{1}{2}\int_0^l \rho(x)\mathbf{v}^T(x)\mathbf{v}(x)dx + \frac{1}{2}M\mathbf{v}^T(l)\mathbf{v}(l) + \frac{1}{2}\boldsymbol{\omega}^T\mathbf{I}_H\boldsymbol{\omega} \tag{A.10}$$

Substituting equations (3.9) and (3.10) into equation (A.10) the following is obtained:

$$\begin{aligned} 2T = \rho\int_0^l [&\tilde{\mathbf{v}}^2 - \tilde{\mathbf{v}}^T(2x\mathbf{X} + 2\mathbf{U})\boldsymbol{\omega} + 2\tilde{\mathbf{v}}^T\boldsymbol{\mu} + \dot{\boldsymbol{\mu}}^2 \\ &+\boldsymbol{\omega}^T(x^2(\mathbf{1} - \mathbf{x} \otimes \mathbf{x}) - x(\mathbf{x} \otimes \boldsymbol{\mu} + \boldsymbol{\mu} \otimes \mathbf{x}) \\ &+(\boldsymbol{\mu}^2 1 - \boldsymbol{\mu} \otimes \boldsymbol{\mu})]\boldsymbol{\omega} + \boldsymbol{\omega}^T(2x\mathbf{X} + 2\mathbf{U})\dot{\boldsymbol{\mu}}]\, dx \\ &+M[\tilde{\mathbf{v}}^2 - \tilde{\mathbf{v}}^T(2l\mathbf{X} + 2\mathbf{U}(\mathbf{l}))\boldsymbol{\omega} + 2\tilde{\mathbf{v}}^T\boldsymbol{\mu}(l) + \dot{\boldsymbol{\mu}}^2(l) \\ &+\boldsymbol{\omega}^T(l^2(\mathbf{1} - \mathbf{x} \otimes \mathbf{x}) - l(\mathbf{x} \otimes \boldsymbol{\mu} + \boldsymbol{\mu}(l) \otimes \mathbf{x}) \\ &+(\boldsymbol{\mu}^2(l)1 - \boldsymbol{\mu}(l) \otimes \boldsymbol{\mu}(l))]\boldsymbol{\omega} + \boldsymbol{\omega}^T(2l\mathbf{X} + 2\mathbf{U}(\mathbf{l}))\dot{\boldsymbol{\mu}}(l)] \end{aligned} \tag{A.11}$$

Substituting equation (2.16) into equation (A.11), performing the integration, and re-arranging, the equation becomes:

$$\begin{aligned}2T = {} & \tilde{\mathbf{v}}^T[m + M]\tilde{\mathbf{v}} - \tilde{\mathbf{v}}^T[\rho(2\mathbf{T}_2 + l^2\mathbf{X}) + 2M(\mathbf{U}(l) + l\mathbf{X}]\boldsymbol{\omega} \\ & + 2\tilde{\mathbf{v}}^T[\rho\mathbf{T}_1 + M\mathbf{B}(l)]\dot{\mathbf{b}} + \boldsymbol{\omega}^T[2\rho(\mathbf{T}_4 + \mathbf{X}\mathbf{T}_5) + 2M(\mathbf{U}(l)\mathbf{B}(l) + l\mathbf{X}\mathbf{B}(l))]\dot{\mathbf{b}} \\ & + \boldsymbol{\omega}^T[\rho(\frac{l^3}{3}\mathbf{T}_{10} + 2\mathbf{x}^T\mathbf{T}_5\boldsymbol{\mu}\mathbf{1} + \mathbf{I}_{\mathrm{II}} - \mathbf{T}_6 - \mathbf{T}_7 + \mathbf{T}_8) \\ & + M(l^2\mathbf{T}_{10} + 2l\mathbf{x}^T\mathbf{B}(l)\boldsymbol{\mu}\mathbf{1} - l(\mathbf{x} \otimes \boldsymbol{\mu}(l) + \boldsymbol{\mu}(l) \otimes \mathbf{x}) - \boldsymbol{\mu}(l) \otimes \boldsymbol{\mu}(l) + \mathbf{T}_9)]\boldsymbol{\omega} \\ & + \dot{\mathbf{b}}^T[\rho\mathbf{T}_3 + M\mathbf{B}^T(l)\mathbf{B}(l)]\dot{\mathbf{b}} \end{aligned} \tag{A.12}$$

which is identical to equation (3.11), and $\mathbf{T}_1$, $\mathbf{T}_2$, $\mathbf{T}_3$, $\mathbf{T}_4$, $\mathbf{T}_5$, $\mathbf{T}_6$, $\mathbf{T}_7$, $\mathbf{T}_8$, $\mathbf{T}_9$, and $\mathbf{T}_{10}$ are defined in chapter 3.

A.4 Derivation of Equation (3.19)

The kinetic energy of the payload is as follows:

$$2K = \int_m \mathbf{v}^2 \, dm \tag{A.13}$$

substituting equation (3.18) into equation (A.13) yields:

$$\begin{aligned} 2K = {} & m\mathbf{v}_c^2 + 2(\mathbf{v}_c \mathrm{x} \boldsymbol{\omega})^T \int_m \mathbf{r} \, dm \\ & + \boldsymbol{\omega}^T \int_m (\mathbf{r}^2\mathbf{1} - \mathbf{r} \otimes \mathbf{r}) \, dm \; \boldsymbol{\omega} \end{aligned} \tag{A.14}$$

by definition the integral of the second term vanishes and the integral of the last term represents the moment of inertia of the payload $\mathbf{I}_c$ about its centre of mass. Equation (A.14) then becomes:

$$2K = m\mathbf{v}_c^2 + \boldsymbol{\omega}^T [\mathbf{I}_c] \boldsymbol{\omega} \tag{A.15}$$

An expression for $\mathbf{v}_c$ is readily obtained from equation (3.16) as follows:

$$\mathbf{v}_c = \tilde{\mathbf{v}} + \boldsymbol{\omega}\mathrm{x}\mathbf{r}_{bc} + \mathbf{r}_{bc} \tag{A.16}$$

the last term of equation (A.16) is zero because it is assumed that the payload is *rigid*. An expression for $\mathbf{v}_c^2$ could now be obtained as:

$$\mathbf{v}_c^2 = \tilde{\mathbf{v}}^2 - 2\tilde{\mathbf{v}}^T\mathbf{R}_{bc}\boldsymbol{\omega} + \boldsymbol{\omega}^T\mathbf{R}_{bc}^T\mathbf{R}_{bc}\boldsymbol{\omega} \tag{A.17}$$

where $\mathbf{R}_{bc}$ represents the cross product tensor of $\mathbf{r}_{bc}$, and can be written as:

$$\mathbf{R}_{bc} \equiv \begin{bmatrix} 0 & -z & y \\ z & 0 & -x \\ -y & x & 0 \end{bmatrix} \tag{A.18}$$

Substituting equation (A.17) into equation (A.15) and re-arranging yields:

$$2T = \tilde{\mathbf{v}}^T[(m)\mathbf{1}]\tilde{\mathbf{v}} - \tilde{\mathbf{v}}^T[2m\mathbf{R}_{bc}]\boldsymbol{\omega} + \boldsymbol{\omega}^T[\mathbf{I}_b]\boldsymbol{\omega} \tag{A.19}$$

where

$$\mathbf{I}_b = m\mathbf{R}_{bc}^T\mathbf{R}_{bc} + \mathbf{I}_c \tag{A.20}$$

represents the moment of inertia of the payload about the origin of its body-fixed frame. It could be seen that equation (A 19) is identical to equation (3.19).

A.5 Derivation of Equation (3.22)

As discussed in chapter 3 the effects of shear could be ignored, hence equation (3.21) could be re-written as:

$$U = \frac{1}{2}\int_0^l EI\left(\frac{\partial\xi_{(2)}}{\partial x}\right)^2 dx + \frac{1}{2}\int_0^l EI\left(\frac{\partial\xi_{(3)}}{\partial x}\right)^2 dx \tag{A.21}$$

Since shear deformation was neglected, hence one can obtain the following from equations (2.14) and (2 15):

$$\xi_{(2)} = -\frac{\partial u_{(3)}}{\partial x} \equiv \sum_{j=1}^{\bar{m}} \phi_j' \mathbf{b}_{\bar{n}+j} \tag{A.22}$$

and

$$\xi_{(3)} = \frac{\partial u_{(2)}}{\partial x} \equiv \sum_{j=1}^{m} \phi_j' \mathbf{b}_j \tag{A 23}$$

Therefore,

$$\left(\frac{\partial \xi_{(2)}}{\partial x}\right)^2 + \left(\frac{\partial \xi_{(3)}}{\partial x}\right)^2 \equiv \mathbf{b}^T (\mathbf{B}'')^T \mathbf{B}'' \mathbf{b} \tag{A.24}$$

Substituting equation A.24 into A 21 yields.

$$U = \frac{1}{2} EI \mathbf{b}^T \mathbf{T}_{11} \mathbf{b} \tag{A 25}$$

which is identical to equation (3.22).